THESIS FOR THE DEGREE OF DOCTOR OF PHILOSOPHY

# Turbulence Modelling for Internal Cooling of Gas-Turbine Blades

JONAS BREDBERG

*Department of Thermo and Fluid Dynamics*
CHALMERS UNIVERSITY OF TECHNOLOGY
GÖTEBORG, SWEDEN, 2002

Turbulence Modelling for Internal Cooling of Gas-Turbine Blades
JONAS BREDBERG
ISBN 91-7291-181-66



Doktorsavhandlingar vid Chalmers tekniska högskola
Ny serie nr 1863
ISSN 0346-718X

Institutionen för termo- och fluiddynamik
Chalmers tekniska högskola
SE-412 96 Göteborg, Sweden
Phone +46-(0)31-7721400
Fax: +46-(0)31-180976

Printed at Chalmers reproservice
Göteborg, Sweden 2002

# Turbulence Modelling for Internal Cooling of Gas-Turbine Blades

by

JONAS BREDBERG

Department of Thermo and Fluid Dynamics
Chalmers University of Technology
SE-412 96 GÖTEBORG, SWEDEN

## Abstract

Numerical simulations of geometrical configurations similar to those present in the internal cooling ducts within gas turbine blades have been performed. The flow within these channels are characterized by heat transfer enhancing ribs, sharp bends, rotation and buoyancy effects. On the basis of investigations on rib-roughened channel it is concluded that the frequently employed two-equation turbulence models ($k-\varepsilon$, $k-\omega$) cannot predict heat transfer in separated regions with a correct Reynolds number dependency. Extensions to non-linear models, such as EARSM, do not alters this inaccurate tendency. The importance of the length-scale determining equation for this behaviour is discussed. A low-Reynolds number (LRN) $k-\omega$ turbulence model, with improved heat transfer predictions, is proposed. The new model includes cross-diffusion terms which enhances free-shear flow predictability. A new method to reduce the mesh sensitivity for LRN turbulence models is proposed. Within the concept of finite volume codes it is shown that through a carefully treatment of the integrations for the first interior control volume, minor modifications results in a significant reduced grid dependency for near-wall sensitive parameter. The latter modification in conjunction with the new $k-\omega$ turbulence model results in an accurate and robust method for simulating large and complex geometries within the frame of internal cooling of turbine blades.

**Keywords:** gas turbine blades, U-bend, rib-roughened channel, rotation, heat transfer, cooling, turbulence model, EARSM, $k-\varepsilon$, $k-\omega$

# List of Publications

This thesis is based on the work contained in the following papers:

I. J. Bredberg and L. Davidson
"Prediction of flow and heat transfer in a stationary two-dimensional rib roughened passage using low-Re turbulent models"
In *Proceedings of 3:rd European Conference on Turbomachinery: Fluid Dynamics and Thermodynamics*, pages 963-972, IMechE 1999.

II. J. Bredberg, L. Davidson and H. Iacovides
"Comparison of Near-wall Behavior and its Effect on Heat Transfer for $k-\omega$ and $k-\varepsilon$ Turbulence Models in Rib-roughened 2D Channels"
In *Proceedings of 3:rd Int. Symposium on Turbulence, Heat and Mass Transfer*, pages 381-388, eds. Y. Nagano and K. Hanjalić and T. Tsuji, Aichi Shuppan 2000.

III. J. Bredberg, S.-H. Peng and L. Davidson
"On the Wall Boundary Condition for Computing Turbulent Heat Transfer with $k-\omega$ Models"
In *Proceedings of the ASME Heat Transfer Division - 2000*, HTD-Vol. 366-5, pages 243-250, ed. J.H. Kim, ASME 2000.

IV. J. Bredberg
"On the Wall Boundary Condition for Turbulence Models"
*Report 00/4, Department of Thermo and Fluid Dynamics, Chalmers University of Technology*, 2000.

V. J. Bredberg
"On Two-equation Eddy-Viscosity Models"
*Report 01/8, Department of Thermo and Fluid Dynamics, Chalmers University of Technology*, 2001.

VI. J. Bredberg, S.-H. Peng and L. Davidson
"An improved $k-\omega$ turbulence model applied to recirculating flows"
Accepted for publication in *Int. J. Heat and Fluid Flow*, 2002.

VII. J. Bredberg and L. Davidson
"Prediction of turbulent heat transfer in stationary and rotating U-ducts with rib roughened walls"
Accepted to *5:th International Symposium on Engineering Turbulence Modelling and Measurements*, 2002.

VIII. J. Bredberg and L. Davidson
"Low-Reynolds Number Turbulence Models: An Approach for Reducing Mesh Sensitivity"
*Submitted for journal publication.*

Relevant scientific publications not included in this thesis:

9. J. Bredberg and L. Davidson
"Case 7.2: Two-Dimensional Flow and Heat Transfer over a Smooth Wall Roughened with Squared Ribs"
In *Proceedings of 7:th ERCOFTAC/IAHR Workshop on Refined Turbulence Modelling*, 1998.

10. J. Bredberg
"Prediction of Flow and Heat Transfer in 3-D Rib Roughened Passage using Low-Re Turbulent Models"
In *Proceedings of GTC annual meeting*, 1998.

11. J. Bredberg
"Prediction of Flow and Heat Transfer Inside Turbine Blades using EARSM, $k-\epsilon$, and $k-\omega$ Turbulence Models"
Thesis for the Degree of Licentiate of Engineering, *Report 99/3, Department of Thermo and Fluid Dynamics, Chalmers University of Technology*, 1999.

12. J. Bredberg
"TCP4, Turbine Blade Internal Cooling"
In *Proceedings of GTC annual meeting*, 1999.

13. J. Bredberg
"TCP4, Numerical Investigation of Internal Cooling of Turbine Blades"
In *Proceedings of GTC annual meeting*, 2000.

14. J. Bredberg
"TCP4, Turbine Blade Internal Cooling"
In *Proceedings of GTC annual meeting*, 2001.

# Acknowledgments

This work was carried out at the Department of Thermo and Fluid Dynamics, Chalmers University of Technology, Gothenburg, Sweden. The work could not have been done without the help of many persons, of whom the following are specially acknowledged.

I would like to express my greatest precautions toward my supervisor Prof. L. Davidson, for all his advice, guidance and support to this time. I hope it will continue.

This project, Turbine Blade Internal Cooling, is part of the group Turbine Cooling Performance within GTC, a national Gas Turbine Center, headed by Sven-Gunnar Sundkvist. GTC is supervised and funded by Statens Energimyndigheten and sponsored by Volvo Aero Corporation and Alstom Power. The financial and scientific support by all parts is gratefully acknowledged.

I would also like to thank Dr. S-H. Peng, at FOI, which has been a great inspiration and given valuable comments, especially regarding the work with turbulence models. The latter work would have been severely deprived without the influence from you.

Furthermore I would like to thank Dr. H. Iacovides, at UMIST, for a very fruitful visit in Manchester, UK, in 1998. You gave most important comments and suggestions for the work in Paper II. The help of Dr. T. Craft for this work and useful discussions with Dr. M. Raisee is also acknowledged. The supply of experimental data from UMIST for a number of the simulations performed are greatly appreciated.

# Contents

# Chapter 1

# Introduction

A general introduction to the gas turbine engine is given. The importance of higher gas temperatures and the means of achieving this is discussed. A schematic cooling scheme for turbine blades is shown. The physical phenomenas due to geometrical constraints and applied forces are addressed.

## 1.1 The Gas Turbine

Of the various means of producing either thrust or power, the gas-turbine engine is one of the most satisfactory. Its main advantages are: exceptional reliability, high thrust-to-weight ratio, and relative freedom of vibration. The work from a gas-turbine engine may be given either as torque in a shaft or as thrust in a jet. A gas-turbine consist of the following main parts: an inlet, a compressor, a combustor, a turbine and an exhaust, Fig. 1.1.

The inlet section may involve filters, valves and other arrangements

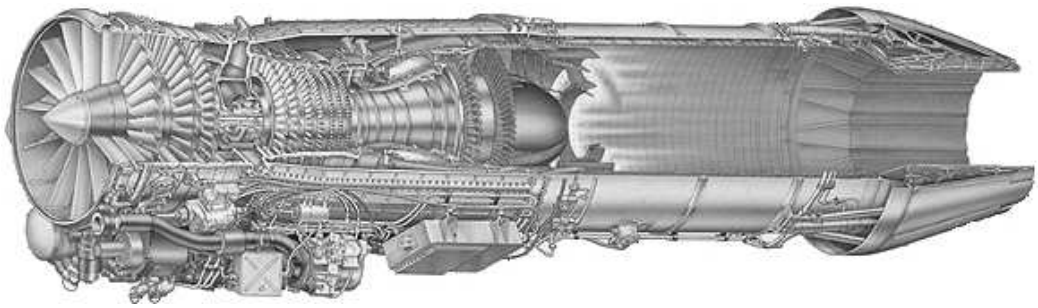

Figure 1.1: RM12, Gas Turbine

to ensure a high quality of the flow. In flying applications it is of importance to pay special consideration to the inlet as the ram-effect could boost the thrust significantly.

The pressure of the air is increased in the compressor, which is divided into several stages. There are two main types of compressors, radial – where the air enters axial but exits radially, or the more common axial compressor – where the flow is primarily axial. The rotation of the compressor increases the velocity of the air with the following diffusers converts the dynamic pressure (velocity) to static pressure. The compressor is connected to the turbine via a shaft running through the center of the engine.

The operation of a gas-turbine relies on that the power gained from the turbine exceeds the power absorbed by the compressor. This is ensured by the addition of energy in the combustor, through igniting fuel in special purposed burners. The design and operation of these burners are vital for a high efficient engine if low emissions are to be achieved.

The highly energetic gas from the combustor is expanded through a turbine, which drives the compressor in the front of the engine. After the turbine the gas still contains a significant amount of energy which can be extracted in various forms. In aircrafts the surplus energy is transformed into a high velocity jet in the nozzle which is the driving force that propels the vehicle through the air. The jet velocity and hence thrust could be further increased, through re-heating the gas in an afterburner. This is common in high performance aircraft, especially for military applications. For stationary, power generating gas-turbines, the extra energy is converted into shaft-power in a power-turbine.

## 1.2 Increasing Efficiency through Cooling

Through the increased environmental awareness and higher fuel costs, there have lately been a strong strive towards enhanced efficiencies for all automotive propulsions. For gas turbines applications, especially in aircraft, not only the specific fuel consumption (SFC) is of importance but also the specific work output. The former is equivalent to the inverse of the efficiency while the latter is a measure of the compactness of the power plant, ie. the effectiveness. The maximum theoretical

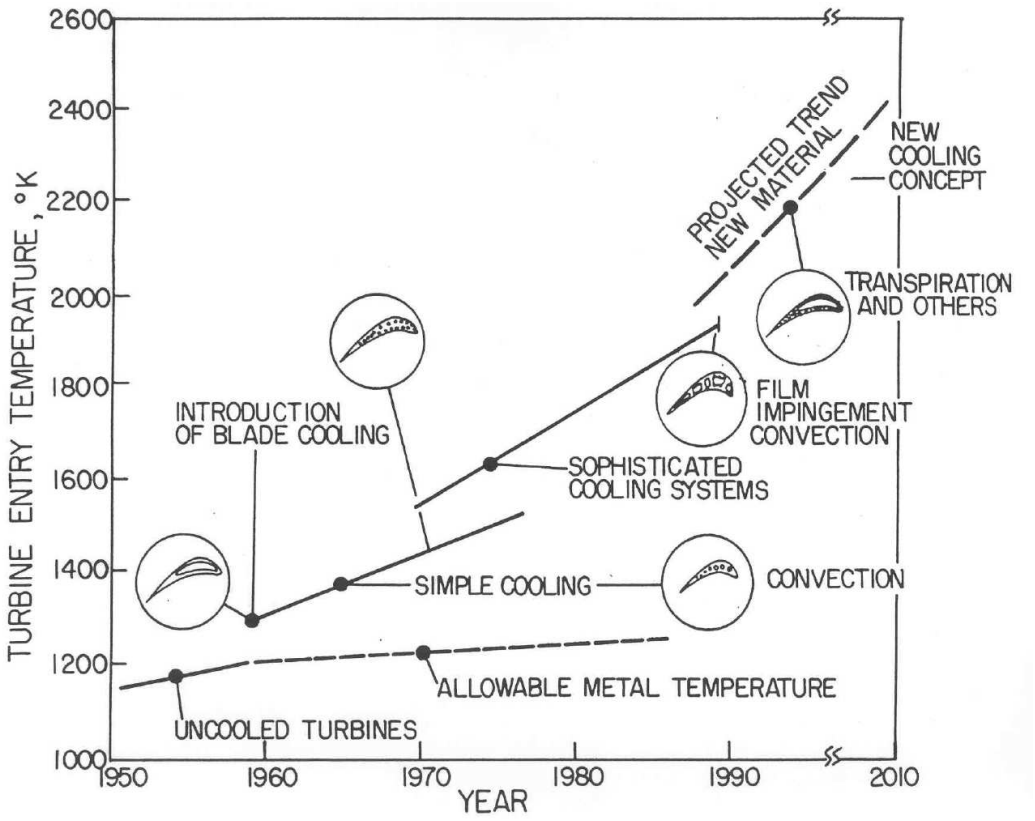


Figure 1.2: Turbine Entry Temperature (Copyright Rolls Royce plc)

efficiency of a gas turbine cycle is given by the Carnot efficiency as:

$$\eta = 1 - \frac{T_1}{T_3} \tag{1.1}$$

where $T_1$ is the inlet temperature and $T_3$ the turbine entry temperature (TET). Increasing $T_3$ yield a direct improvement in the efficiency, $\eta$. The performance of practical cycles are however lower, due to pressure and massflow losses, friction, components efficiency, non-ideal fluids etc. When these losses are taken into account, the efficiency of the simple gas turbine cycle[1] becomes dependent not only of the temperature ratio, as in the Carnot process, but also the compressor pressure ratio. Thus the gas turbine industry are trying to reach both higher turbine temperatures as well as increased pressure ratio, to improve the efficiency and effectiveness of tomorrows engines.

[1]The simple cycle consists of a compressor, a combustor and a turbine.

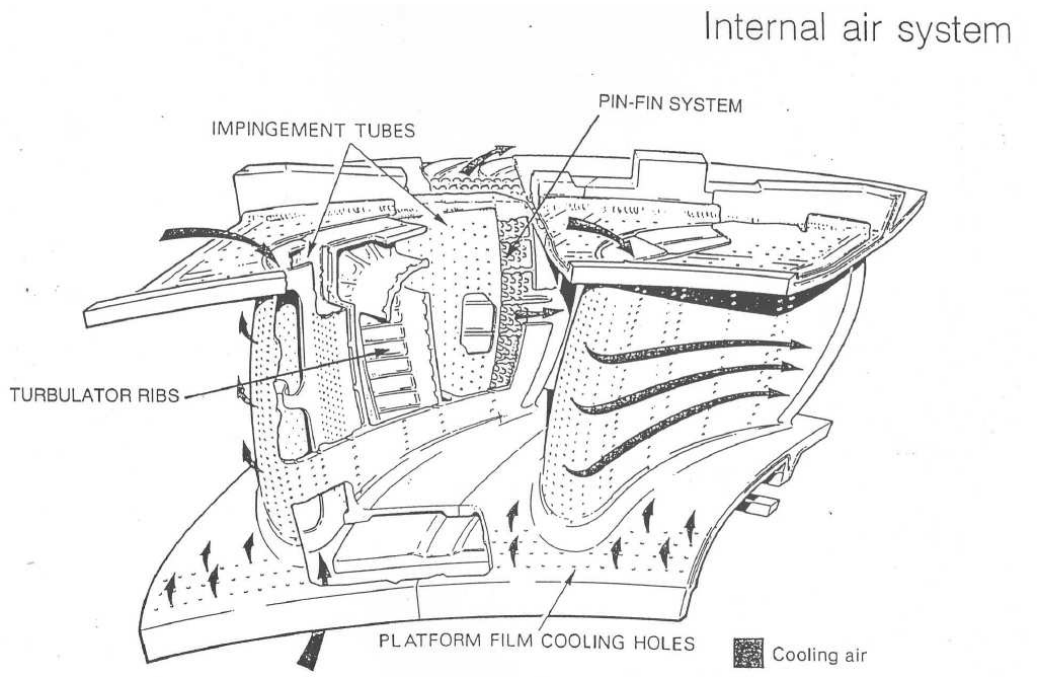


Figure 1.3: Cooling schemes, Inlet Guide Vane (Copyright Rolls-Royce plc)

Even though exotic materials are used for the most stressed environments, these have for the last decades been unable to withstand the demanded TET without yielding to the harsh environment. High-strength material such as nickel and cobalt based super alloys, (eg. Inco 738 and Rene 220) will all weaken from increased temperatures, and since the loads in a rotating turbine are extremely high, the structure fails if not counter-measures are taken. The introduction of relatively cool gas from the compressor in well selected places in the turbine extends the engine endurance, and was in practise already during the second world war. Figure 1.2 shows the increases in TET through the introduction of different cooling techniques.

The highest temperatures loads are found at the exit of the combustor, and in the first turbine stage. A comprehensive cooling system are thus needed for the inlet guide vanes (IGV). A conceptional view of such as system is shown in Fig. 1.3. These vanes employs both external cooling (film cooling), and internal cooling (convection- and impingement-cooling). The vanes are perforated by a number of small holes, through which compressed air is ejected. If correctly designed these holes will supply a cool protective air-film covering the vanes.

This technique is called film cooling. The same type of cooling is applied to the platforms, along the tip (shroud) and root (hub) of the vane. Internally the vanes are cooled using convection and impingement techniques. The compressed air is guided through ducts which cools the vane-material by means of convection/conduction from the inside. This approach is however not as effective, as the film-cooling technique, and hence a number of measures are generally made to increase the heat transfer. Ribs, positioned orthogonally to the flow, are introduced in the ducts, which makes the flow repeatedly separate and re-attach with an increase in turbulence level and a consequently enhancement of the heat transfer. These rib-roughened ducts are designed in a serpentine fashion and can completely fill out the inside of a vane. Finally the cooling air can be guided vertically towards some specifically hot regions for effective cooling. The latter is called impingement cooling.

It should be noted that the available pressure-difference between the internal cooling air and the external main gasflow, is severely limited. Hence there is a restriction to the number of turns, ribs and other pressure reducing features that can be employed within a given passage. There is also a construction limit to how complex the interior could be made, while still maintaining productivity and being cost-effective. Contemporary gas turbines may use as much 15% of the total massflow for cooling air. Even though there is significant advantage of increasing TET, the use of cooling air for achieving this has some drawbacks: 1) the addition of cool air into the main stream reduces the work output from the turbines; 2) protective films along the vanes complicates the aero-thermal design of the blades, as the momentum and blockage effect introduced by the cooling air changes gas angles dependent on engine loads; 3) cooling air does not participate in the energy enriching process in the combustor and hence the effective massflow is reduced.

## 1.3 Flow Phenomena Inside Turbine Blades

The turbine in a gas turbine engine consists of several stages, each stage having both a stationary and a rotating set of blades. The stationary row is positioned upstream the rotating row, to guide the flow from an axial to a tangential-axial direction in order to drive the turbine. To distinguish between the two rows one has chosen to denote the

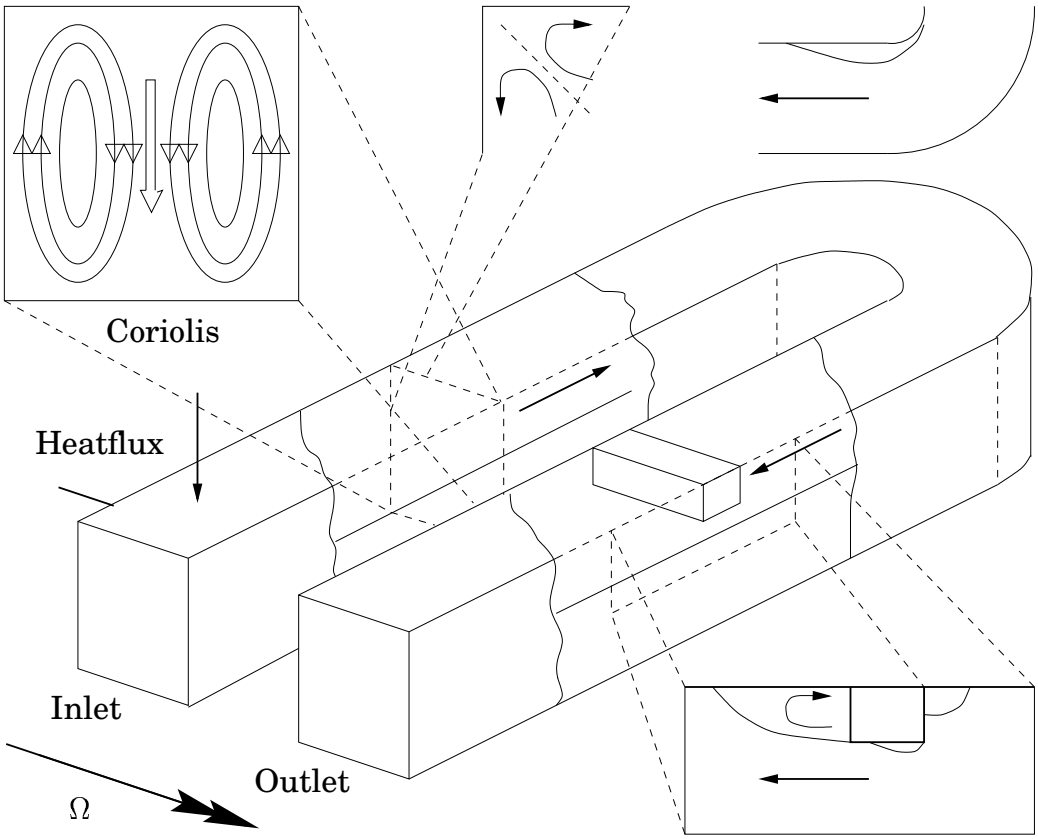


Figure 1.4: The interior of a turbine blade

stationary aerofoils as vanes and the rotating counter-parts are referred to as blades. The turbine blades, similar to turbine vanes need to be cooled using pressurized air from the compressor. The lower external gas temperature however reduces the necessary complexity of the cooling system as well as the amount of air needed, compared to the IGV discussed above, Fig. 1.3. The blades are however stressed by the rotational forces, (ie. the Coriolis- and the centrifugal-forces), in addition to the temperature loads. These rotational induced forces complicates the flow structure within the ducts, making the design and construction of turbine blades one of the most challenging and expansive industrial enterprise today. Figure 1.4 shows a schematic view of a U-bend section, located in the center of the turbine blades. In the figure several of the flow-field modifications as a result of imposed conditions, both geometrical and force related are presented. The matrix below connects

the resulting flow phenomena due to the enforced physical conditions.

| | Shearing | Sec. flow | Separation | Acc-Dec | Stabilizing | Buoyancy |
|---|---|---|---|---|---|---|
| Bends | X | X | X | X | | |
| Corners | | X | | | | |
| Heating | | | | | X | X |
| Ribs | X | X | X | X | | |
| Rotation | | X | | | X | X |
| Walls | X | | | | | |

Note that only the main and direct effects are listed. Heating eg. may under certain condition result in such destabilizing condition that the flow separates. In the table it is inferred that stabilizing also refers to the opposite destabilizing condition. The consequence and the difficulties the listed effects impose on numerical simulations are discussed in Chapter 3.

# Chapter 2

# Fluid Motion and Heat Transfer

The equations governing fluid motion, the Navier-Stokes equations are displayed. An overview of turbulence and heat transfer models with literature references are given. Special references to modification due to rotational induced turbulence are made.

## 2.1 Governing Equations

The equations that govern fluid motion and heat transfer are the continuity, momentum and energy equations. These equations, were independently constructed by Navier (1827) and Stokes (1845) and are referred to as the Navier-Stokes equations. These can be formulated in either a conservative form, or in the non-conservative form. For a nearly incompressible fluid, the density is constant, and consequently many text-books gives the Navier-Stokes equations on a density normalized formulation.

### 2.1.1 Continuity

The continuity equation states the conservation of mass, which for all but nuclear-reaction environments is valid. The conservative form is:

$$\frac{\partial \rho}{\partial t} + \frac{\partial \rho U_i}{\partial x_i} = 0 \tag{2.1}$$

### 2.1.2 Momentum

The momentum equation describes a force-balance, which – from the Newtons second law – states that the mass times the acceleration is equal to imposed forces. The forces are divided into body force $F_i$, eg. the gravitational force, and surface forces, $T_{ij}$. The surfaces forces are normally written as a combination of pressure (normal stress) and viscous stresses (shear) as:

$$T_{ij} = -p\delta_{ij} + \tau_{ij} \tag{2.2}$$

Assuming a Newtonian incompressible fluid the momentum equations becomes:

$$\frac{\partial \rho U_i}{\partial t} + \frac{\partial \rho U_i U_j}{\partial x_j} = \rho g_i + F_i - \frac{\partial P}{\partial x_i} + \frac{\partial}{\partial x_j}\left(2\mu S_{ij}\right) \tag{2.3}$$

where $F_i$ is any additional body-forces that can effect the fluid motion such as rotation, a magnetic- or electric-field etc.

### 2.1.3 Energy

The first law of thermodynamics states that the exchange of energy for a system is the result of applied work and heat transfer through that region. In its most complete formulation the energy equations is given as [154]:

$$\frac{\partial \rho E_0}{\partial t} + \frac{\partial \rho U_i E_0}{\partial x_i} = \rho U_i F_i - \frac{\partial q_i}{\partial x_i} + \frac{\partial}{\partial x_j}\left(U_i T_{ij}\right) \tag{2.4}$$

where $T_{ij}$ is the surface forces similar to the viscous and pressure terms in the momentum equations. $E_0$ is the total internal energy, including the kinetic energy. The energy equation as displayed above is however seldom used and instead the simplified temperature equation is applied:

$$\frac{\partial \rho C_p T}{\partial t} + \frac{\partial \rho C_p U_i T}{\partial x_i} = \frac{\partial}{\partial x_i}\left(\frac{\mu C_p}{Pr}\frac{\partial T}{\partial x_i}\right) \tag{2.5}$$

### 2.1.4 Rotational Modifications

The Navier-Stokes equations are derived and valid for a Newtonian inertial coordinate system, ie. system without any forced acceleration. A

coordinate system fixed in a rotating structure however involves both Coriolis and centripetal accelerations and hence the commonly applied equations are invalid. It is however straight forward to derive rotational modified NS-equations, see [19].

Assuming that the coordinate system has a fixed[1] location of origin and that the rotation velocity is constant, ie. neglecting any additional acceleration terms due to angular acceleration, the extra terms (on the LHS) in the momentum equation are:

$$a_i^{ce} = \epsilon_{ijk}\epsilon_{klm}\Omega_j\Omega_l x_m \tag{2.6}$$

$$a_i^{co} = 2\epsilon_{ijk}\Omega_j U_k \tag{2.7}$$

These terms are often considered as a body-force modification to the Navier-Stokes equation and hence included, with a change in sign, on the RHS. There is no rotational modification to either the continuity or temperature/energy equation.

## 2.2 Flow Models

The Navier-Stokes equations are composed of non-linear partial differential equations with an intricate complex dependency within the equation system. Partial differential equations are apart from some specific cases, not solvable using known mathematical tools hence the NS-equations impose a severe obstacle to the physical world. There are only a very small number of flows that entitle one to simplify the governing equations in such a way that it is possible to achieve an analytical solution. Consequently for most cases, one is referred to numerically solve the Navier-Stokes equations. The highest level of fidelity is given by Direct Numerical Simulations (DNS's) and Large Eddy Simulations (LES's). Numerical simulations performed using Reynolds Averaged Navier Stokes (RANS) solvers are apart from numerical approximations also affected by physical approximations – in the models for the turbulence field.

### 2.2.1 DNS/LES

Direct Numerical Simulations (DNS's) and Large Eddy Simulations (LES's) both solve the equations in the four-dimensional room, time

[1]The coordinate could also translate at a constant velocity, akin to Newtons second law of motion

and space. The additional modelling in LES as compared to DNS is the introduction a sub-grid scale (SGS) model [184], which legitimacy is based on the assumption of isotropocy of the smallest scales. For a given cut-off wave-length, normally related to the grid-size, LES don't resolve the smallest length-scales but rather approximate them using the SGS-model. DNS's are very appreciated as they are considered equally, or even more accurate than experiments. The numerical model enable unphysical although theoretical interesting flows to be simulated, with a degree of control unachievable in a laboratory. The numerical accuracy in DNS's are usually much higher than the uncertainty in any measuring tool. A major drawback is however that the simulations are computational expansive and can only be performed for a limited number of flows, all with relatively low Reynolds numbers.

### 2.2.2 RANS

Nearly all numerical simulations are performed using various RANS-models, as a consequence of the excessive computational resources needed for a DNS. Reynolds [173] proposed that the quantities in the NS-equation could be divided into a mean and a fluctuating part:

$$\phi = \overline{\phi} + \phi' \tag{2.8}$$

where the mean part is the time-average of a parameter over a certain time. The averaging time needs to be longer than the small turbulent fluctuation, however shorter than any mean flow oscillating period, such as pumping frequencies, or rotation-frequency induced fluctuations. If Reynolds decomposition is applied to the Navier-Stokes equation the result is an equivalent set of equations, the Reynolds Averaged Navier-Stokes equations[2]. The difference between these and the original are that the RANS equations only involves time-averaged quantities. The time averaging procedure however produces an additional term, the Reynolds stresses:

$$\tau_{ij} = \overline{u_i' u_j'} \tag{2.9}$$

which are unknown and need to be modelled using a turbulence model. This is referred to as the closure problem with Reynolds averaging.

There are two distinct approaches to model the Reynolds stresses, either the eddy-viscosity models (EVM), or the Reynolds stress models

[2]See the comprehensive analysis and alternative approaches (eg. Favre-averaging) in Hinze [75].

(RSM). In the latter the actual stresses are solved, while in the former the Boussinesq [17] hypothesis is employed to estimate $\tau_{ij}$, see Eq. 2.18. In its simplest form, the eddy-viscosity, $\nu_t$ is computed based on some geometrical/flow conditions. In the commonly employed two-equation turbulence models, the eddy-viscosity is computed using two turbulent quantities, the turbulent kinetic energy, $k = 0.5(\overline{u_i' u_i'})$ and a length-scale determining quantity. In a strive to enhance the performance of the two-equation EVMs researchers have proposed non-linear EVMs, which include, apart from the Boussinesq hypothesis, additional terms to determine the eddy-viscosity.

The ASM and EARSM (or EASM) are a different case, they compute the Reynolds stresses using algebraic equations. In ASM the convective and diffusion terms in the Reynolds stress transport equations are approximated using anisotropized versions (through multiplication with $\overline{u_i' u_j'}/k$) of the same terms in the turbulent kinetic energy. The ASM thus only need to solve two transport equations, that for $k$ and an additional secondary turbulence quantity. The Reynolds stresses could then be estimated using the constructed algebraic relations. This modelling approach is however prone to numerical instable solution and are seldom used.

It is possible, through the use of the Cayley-Hamilton theorem to derive the complete tensorial relation for the Reynolds stresses, expression in the strain-rate tensor, $S_{ij}$ and the rotation tensor, $\Omega_{ij}$. The complete set involves ten terms with their respectively coefficients [164]. Using these expressions the Reynolds stresses can, in a second moment closure sense, be exactly computed. EARSMs are thus theoretically more correct than non-linear EVMs, although the final expressions are often confusingly similar. They differ in the approach used for the coefficients in the tensor groups, which in EARSMs, at least for 2D-flows, can be based on derived analytic expressions [203].

### 2.2.3 Other flow models

The above discussed RANS-models are all single-point correlations closures, ie. the turbulence quantities are evaluated at a single point in space and time. The consequence of this is that these models cannot realize the multitude of length-scales occurring in a turbulent flow, contrary to DNS and LES. Furthermore RANS models are unable to distinguish the physical processes governing the far-field turbulent interactions to those associated with the nearly isotropic local turbulence. It is well known that these processes are distinctly different and it is

important to faithfully capture both. Mathematical models which only contains a single length-scale (or time-scale) can neither incorporate these different physical process nor model the important energy transfer from low to high wave-number. Single-point turbulence model can thus never be a general method to predict turbulent flowfields [56].

Models which incorporate several length-scales, either properly from the two-point correlation, $R_{ij}$, or from simplified assumptions, should be able to improve predictions in complex flows. Hanjalić *et al.* [72] devised a two-scale model based on the $k-\varepsilon$ concept which involves four transport equations instead of two. Guo and Rhode refined the model and proposed a two-scale [108] and a three-scale [61] $k-\varepsilon$ model both yielding a substantial improvements compared to the standard $k-\varepsilon$ model[3].

A special reference is here made to the structured based models by Reynolds *et al.* [174] and the TSDIA (Two-Scale Direction Interaction Analysis) based model by Yoshizawaw [213], which both are able to include rotational induced turbulence in a natural way.

## 2.3 Turbulence Models with Special Reference to Rotation

### 2.3.1 Reynolds stress models

Reynolds Stress Models (RSM) ([69],[118], [185]), solves the Reynolds stresses, $\tau_{ij} = \overline{u_i' u_j'}$, using individual transport equations. RSM based RANS-codes thus include, apart from three momentum equation, six stress equation, and an additionally length-scale determining equation. The transport equations for the Reynolds stresses are, with modification made for rotational induced production:

$$\frac{D\tau_{ij}}{Dt} = P_{ij} + G_{ij} + \Pi_{ij} - \varepsilon_{ij} + \frac{\partial D_{ij}^T}{\partial x_k} + \frac{\partial D_{ij}^\nu}{\partial x_k} \tag{2.10}$$

where $P_{ij}$ is the shear production term, $G_{ij}$ the rotational production term, $\Pi_{ij}$ the pressure-strain term, $\varepsilon_{ij}$ the dissipation term, $D_{ij}^T$ turbulent transport (diffusion) term, and $D_{ij}^\nu$ the viscous diffusion term.

[3]The three-scale model however gives only a marginal improvement compared to the two-scale model.

These are, see [19]:

$$
\begin{aligned}
P_{ij} &= -\left(\overline{u_i' u_k'}\frac{\partial U_j}{\partial x_k} + \overline{u_j' u_k'}\frac{\partial U_i}{\partial x_k}\right) \\
G_{ij} &= -2\Omega_k\left(\epsilon_{jkl}\overline{u_i' u_l'} + \epsilon_{ikl}\overline{u_j' u_l'}\right) \\
\Pi_{ij} &= \overline{\frac{p'}{\rho}\left(\frac{\partial u_i'}{\partial x_j} + \frac{\partial u_j'}{\partial x_i}\right)} \\
\varepsilon_{ij} &= 2\nu\overline{\frac{\partial u_i'}{\partial x_k}\frac{\partial u_j'}{\partial x_k}} \\
D_{ij}^T &= -\left(\overline{\frac{u_i' p'}{\rho}}\delta_{jk} + \overline{\frac{u_j' p'}{\rho}}\delta_{ik} + \overline{u_k' u_i' u_j'}\right) \\
D_{ij}^\nu &= -\nu\frac{\partial\overline{u_i' u_j'}}{\partial x_k}
\end{aligned}
$$

The production terms, and the viscous diffusion term are exact, while the other terms need to be modelled.

The exact formulation of the **production** terms is a fundamentally advantage of the RSMs compared to the EVMs. For a 2D dimensional shear-flow (streamwise in $x$-direction) undergoing orthogonally rotation with $\Omega = \Omega_z$ the non-zero production terms are:

| | i=1,j=1 | i=2,j=2 | i=1,j=2 |
|---|---|---|---|
| $P_{ij}$ | $-2\overline{u'v'}dU/dy$ | 0 | $-\overline{v'^2}dU/dy$ |
| $G_{ij}$ | $4\Omega\overline{u'v'}$ | $-4\Omega\overline{u'v'}$ | $-2\Omega(\overline{u'^2} - \overline{v'^2})$ |

The $k$-equation ($k = 0.5(\overline{u_i' u_i'})$) in two-equation EVM is unaffected by rotation as $G_{11} + G_{22} = 0$. In addition the shear-stress, $\overline{u'v'}$, is inaccurately estimated through the neglection of the rotational production ($G_{12}$) via the isotropic estimation of the normal stresses, ie. $\overline{u'^2} = \overline{v'^2}$:

$$
P_{12} = -\overline{v'^2}\frac{dU}{dy} - 2\Omega\left(\overline{u'^2} - \overline{v'^2}\right) \tag{2.11}
$$

This state of affairs necessitates that two-equation EVMs need to include *ad hoc* modifications in order to predict rotational induced turbulence. Although RSMs predict the correct level of production, the modelling of the other terms in the Reynolds stress equations normally exclude any influence by rotation, even though it is well known that such dependency exists, see [19].

Following Kolmogorov the **dissipation rate** is assumed to be isotropic: $\varepsilon_{ij} = 2/3\varepsilon\delta_{ij}$ and modelled using its own scalar transport equation [70]:

$$\frac{D\varepsilon}{Dt} = -C_{\varepsilon 1}\overline{u_i' u_k'}\frac{\varepsilon}{k}\frac{\partial U_i}{\partial x_k} - C_{\varepsilon 2}\frac{\varepsilon^2}{k} + \frac{\partial}{\partial x_k}\left(C_\varepsilon \frac{k}{\varepsilon}\overline{u_k' u_l'}\frac{\partial \varepsilon}{\partial x_l}\right) \tag{2.12}$$

where $C_{\varepsilon 1}, C_{\varepsilon 2}$ and $C_\varepsilon$ are tunable constants. This model becomes identical to the $\varepsilon$-equation used in the $k-\varepsilon$ model by Jones and Launder [101], when the Reynolds stresses ($\overline{u_i' u_k'}$ and $\overline{u_k' u_l'}$) are approximated using the Boussinesq hypothesis. Hanjalić and Launder [71] formulated a low-Reynolds number modification of Eq. 2.12 for use in RSMs, which includes modelling for anisotropic levels of the dissipation rate. It can be shown [19], that the dissipation rate is effected by the rotation, however these terms involve gradients of the velocity fluctuations and cannot be implemented exactly. A well established rotational-modification to the $\varepsilon$-equation is to let the destruction term coefficient, $C_{\varepsilon 2}$, vary depending on the rotational 'Richardson number', see Bradshaw [18] (2D[4]):

$$Ri = -2\Omega\left(\frac{dU}{dy} - 2\Omega\right) / \left(\frac{dU}{dy}\right)^2 \approx -\frac{2\Omega}{dU/dy} \tag{2.13}$$

Launder *et al.* [119] proposed to replace $dU/dy$ with the turbulent time-scale $\tau = k/\varepsilon$, however in the context of the similar curvature effect. Models for length-scale correction have been proposed by eg. Bardina *et al.* [10], Hellsten [74], Howard *et al.* [77] and Shimomura see [214]. These models are either incorporated in the destruction term, $\Phi$, or added as an extra source term, $E$, in the $\varepsilon$ or $\omega$-equation:

| | |
|---|---|
| $\Phi_\varepsilon = -C_{\varepsilon 2}(1 - C_c Ri)\dfrac{\varepsilon^2}{k}$ | Howard *et al.* |
| $E_\varepsilon = -C_c \varepsilon \Omega$ | Bardina *et al.* |
| $E_\varepsilon = -C_c k \epsilon_{ijk}\Omega_i \dfrac{dU_k}{dx_i}$ | Shimomura |
| $\Phi_\omega = \dfrac{1}{1 + C_c Ri}\beta\omega^2$ | Hellsten |

The **pressure-strain** term is divided into two parts, the slow part $\Pi_{ij,1}$, and the rapid part $\Pi_{ij,2}$. The slow part in most RSMs is modelled

[4]A generalized 3D formulation of the Richardson number is given in [106].

based on Rotta [179]:

$$\Pi_{ij,1} = -C_1 \frac{\varepsilon}{k} \left( \overline{u_i' u_j'} - \frac{2}{3} \delta_{ij} k \right) \tag{2.14}$$

The standard model for the rapid part is the one by Launder-Reece-Rodi (LRR) [120]:

$$\Pi_{ij,2} = -\frac{C_2 + 8}{11} \left( P_{ij} - \frac{2}{3} P \delta_{ij} \right) - \frac{30 C_2 - 2}{55} 2 k S_{ij} - \frac{8 C_2 - 2}{11} \left( P_{ij}^* - \frac{2}{3} P \delta_{ij} \right) \tag{2.15}$$

A simplified variant is the 'isotropization-of-production', IP-model [143]. Gibson and Launder [58] extended the pressure-strain model to incorporate wall-reflection and buoyancy effected terms. Launder *et al.* [123] noted that Reynolds stress equation is not invariant under coordinate system rotation, and proposed a modified pressure-strain model, through including a rotation term to correct this. Speziale, Sarkar and Gatski [193] concluded that the LRR-model and other linear[5] pressure-strain models are unable to predict the growth of turbulent kinetic energy for high rotation rates, for which their quadratic SSG-model showed improved accuracy. Further additions to the modelling of the pressure-strain terms could be found in eg. [37] and [97].

In the **turbulent transport** term, $D_{ij}^T$, the pressure-velocity terms are commonly neglected and the triple correlation is modelled using the gradient diffusion hypothesis (GDH) by Daly and Harlow [40]:

$$D_{ij} = -\overline{u_i' u_j' u_k'} = C_s' \frac{k}{\varepsilon} \left( \overline{u_k' u_l'} \frac{\partial \overline{u_i' u_j'}}{\partial x_l} \right) \tag{2.16}$$

An alternative is the expended version by Hanjalić and Launder [70].

### 2.3.2 Eddy-viscosity models

The eddy-viscosity concept is based on similarity reasoning that turbulence is a physical concept connected to the viscosity. It can be argued that similarly to viscosity, turbulence affects the dissipation, diffusion and mixing processes. Thus it is reasonable to model the Reynolds

[5] Linear in the mean velocity gradients, with terms only dependent on either $S_{ij}$ or $\Omega_{ij}$.

stresses in a fashion closely related to the viscous term. The Reynolds stress term produced by the Reynolds-averaging is:

$$D_R = \frac{\partial \tau_{ij}}{\partial x_j} = \frac{\partial}{\partial x_j}\left(\overline{u_i' u_j'}\right) \tag{2.17}$$

A turbulent flow will, compared to a laminar flow, enhance the above properties, and thus a model for the Reynolds stress could be, as proposed by [17]:

$$-\overline{u_i' u_j'} = \nu_t \left(\frac{\partial U_i}{\partial x_j} + \frac{\partial U_j}{\partial x_i}\right) \tag{2.18}$$

where $\nu_t$ is the eddy-viscosity, or the turbulent viscosity. It is computed using some turbulent quantities, such as the turbulent kinetic energy and the turbulent length scale:

$$\nu_t \sim \sqrt{k} l \tag{2.19}$$

In the commonly employed two-equation EVMs the turbulent kinetic energy is solved using a transport equation, while the turbulent length scale is computed using $k$ and a secondary (a length-scale determining) turbulent quantity. There exists EVMs based on the dissipation rate of turbulent kinetic energy, $\varepsilon$, the turbulent time-scale, $\tau$ or the specific dissipation, $\omega$. These quantities are solved using a transport equation, similar in construction to that shown in Eq. 2.12.

A comprehensive study of two-equation EVMs are included as Paper V [21]. Here only a comment on the possible rotational modification made to these turbulence models is given. As noted above the turbulent kinetic energy is unable to incorporate any effects of system rotation due to its isotropic representation of the normal stresses. The standard practice to improve prediction for rotation flows are that, similar to RMSs, to introduce a length-scale correction in the $\varepsilon$- or $\omega$-equation, see page 16. Wilcox and Chambers [210] however proposed a correction to the $k$-equation:

$$E_k = 9\Omega\nu_t \frac{dU}{dy} \tag{2.20}$$

by relating the turbulent kinetic energy to the wall-normal component of the Reynolds stresses, $\overline{v'^2}$.

### 2.3.3 EARSM and non-linear EVMs

A significant advantage of employing higher order (non-linear) schemes for the eddy-viscosity is the natural way in which rotation is introduced into the formulation. For models that are based on the rotation tensor, $\Omega_{ij}$, it possible to include the solid body rotation, $\Omega_k^S$, via a modified vorticity tensor:

$$\Omega_{ij}^* = \Omega_{ij} - \epsilon_{ijk}\Omega_k^S \tag{2.21}$$

It can be shown (Pope [164]) that the lowest level of independent non-linearity that could be introduced in an eddy-viscosity model is to add a term composed of the strain rate, $S_{ij}$ and the vorticity (rotational modified) $\Omega_{ij}^*$ tensor:

$$a_{ij} = -\underbrace{2\nu_t S_{ij}}_{Bouss.} + \underbrace{C\left(S_{ik}\Omega_{kj}^* + \Omega_{ik}^* S_{kj}\right)}_{non-linear\ term} + \text{HOT} \tag{2.22}$$

where $a_{ij}$ is the anisotropy tensor $\overline{u_i' u_j'}/k - 2/3\delta_{ij}$ and HOT is short for Higher Order Terms. Whether the model is derived based on the ten tensorially independent groups (only three in the 2D-limit) from the Cayley-Hamilton theorem as in the EARSM formulations [54], [113], [183] and [203] or from an expansion of linear EVMs [38], [39], [147], [156], and [192] is of less importance. It should be noted that the significant difference between a non-linear EVM and an EARSM is the determination of the coefficients, which in a EARSM formulation are flow dependent and in the 2D-limit can be explicitly solved, as shown by Wallin and Johansson [203]. These EARSMs are hence likely to predict rotational induced turbulence in a more natural way.

## 2.4 Turbulent Heat Transfer Models

Compared to the large amount of turbulence models for the flow field there exists only a relatively few heat transfer models. This may be a consequence of that the heat transfer model plays a inferior role compared to the turbulence model in predicting heat transfer data [170]. The coupled nature of the temperature and flow field, and thus the difficulties of accurately measure the heat transfer is however more to blame for the sparse work which has been done on heat transfer models. The appearance of DNS (eg. [103]) have however made it possible to construct new and more elaborated models, with improved predictability.

The simplest model is the SGDH (Simple Gradient Diffusion Hypothesis) which is based on similarities to the molecular heat transfer:

$$-\overline{u_i' t'} = \frac{\nu_t}{Pr_t}\frac{\partial T}{\partial x_i} \tag{2.23}$$

with $Pr_t$ is the turbulent Prandtl number with a value of $Pr_t = 0.9$ for air. Kays [104] made a comprehensive review of alternatives to the constant $Pr_t$ model, including the $Pr_t(\nu_t)$ [105]. For Paper VI [28] the author evaluated the latter model with only insignificant difference as compared to standard constant Prandtl number model.

A heat transfer model suitable when a RSM is employed for the flow field is the GGDH (Generalized Gradient Diffusion Hypothesis) which is an adaptation of the Daly-Harlow diffusion model. The model can incorporate un-alignment effects in the relations for the heat flux vector and the temperature gradient:

$$-\overline{u_i' t'} = C_\theta \overline{u_i' u_j'}\frac{k}{\varepsilon}\frac{\partial T}{\partial x_j} \tag{2.24}$$

The model however relays on similarities (an extended Reynolds analogy) to the flowfield for any transport effects in the heat flux vector as the GGDH is still a local model.

Launder *et al.* [57] and [114] derived a scalar-flux transport equation similar to the RSM, which in a matured form can be found in [118]. Noting the complexity for this level of models, and also the number of *ad hoc* and tuned constants needed, these models are seldom used with the exceptions of So *et al.* [112] and Hanjalić *et al.* [44] groups.

Similar to a two-equation EVM it is possible to derive a $k_t - \varepsilon_t$-model from the scalar-flux transport equation. Models based on this theory are eg. [82], [142], [190], [205] and [215].

Another route to construct a heat transfer model is to derive an algebraic relation for the heat flux vector, similarly to what is made in EARSMs, see Launder [117]. Models within this category are eg. [73], [187] and [206].

So and Sommer incorporated both near-wall modelling [186] and buoyancy [189], however there is no thorough study of how to incorporate rotational induced turbulence for the heat transfer. Following Bradshaw [18], it is however possible to treat rotational induced turbulence in analogy to buoyancy induced turbulence, see further in Launder [114] and [116].

# Chapter 3

# Flow phenomena in turbine blades

The combination of a complex geometry and the multitude of imposed forces develop a complicated flow structure within the serpentine ducts inside the turbine blades. The physical understanding, and eventually the modelling, of these flows are inherently demanding through the superposition of the imposed conditions. Even the individual effects of walls, corners, bends, ribs, rotation etc. are not fully understood. Below these mechanism and their influence in the flowfield are discussed. The consequences for numerical simulations and modelling implications are also addressed within this chapter.

## 3.1 Walls

Most flows of engineering interest are affected by the presence of a wall. An impermeable wall exerts a number of effects on the flow and turbulence, where the most dominant are:

- The no-slip constraint, which through viscous effects, enforce zero velocities at the wall.
- Increase of turbulent production through the shearing mechanism in the flow.
- The blocking effect which suppress the velocity fluctuations in the wall normal direction, making the turbulence anisotropic.

- The wall reflection process, which reduce the redistribution among the stress components.

The wall damping effect on turbulence was early recognized by Prandtl [167], which proposed a reduction of the turbulent length-scale as a function of the wall distance. The model was enhanced using an exponential damping function, attributed to van Driest [198]. Viscous damping, via a turbulent Reynolds number was introduced by Jonas and Launder [101] to produce a low-Reynolds number (LRN) modified $k - \varepsilon$ turbulence model. Hanjalić and Launder [71] applied the same approach to develop an LRN RSM. A model for the wall reflection redistribution effect was proposed by Gibson and Launder [58] via additional terms in the pressure-strain model. Durbin [48] modelled both the viscous damping and the wall redistribution effects by elliptic relaxation equations which ensures that the turbulent anisotropy close to walls could be faithfully reproduced.

The appearance of Direct Numerical Simulations (DNS) eg. [107], and [140] have given valuable databases which are used to enhance understanding flow behaviour and turbulence near walls. In light of this research a variety of damping functions and wall influenced terms are employed to improve the treatment of walls in low-Reynolds number modelling, see Paper V [21].

An alternative to LRN modelling is the wall-function approach [160]. High-Reynolds number (HRN) turbulence models bridge the near-wall region using wall-functions that are traditionally based upon the logarithmic law-of-the-wall. The universality of these wall functions is limited however, as they are derived from abridged governing equations. Their use has also frequently been questioned [115]. Hence an number of improvements have been proposed by eg. Launder *et al.* [33], [91], [99], [122], Amano *et al.* [7], [8] and Ciofalo and Collins [35], see Paper IV [20].

In spite of the significant increase in computational power, commercial CFD software still relay on wall function based turbulence models, and hence research has continued on improving the near-wall treatment. Recent additions to this are eg. [24], [27], [60] and [172] see further discussion in Paper VIII [24].

## 3.2 Ribs – blockage

The purpose of introducing repeated ribs in a duct is to enhance the heat transfer rate. Ribs are man-made protrusions which are placed

in a controlled way along specific walls, contrary to sand-grain roughened walls, where the surface topology is stochastically distributed throughout the duct. Ribs are normally of larger size than sand-grains, although some researcher still prefer to denote the rib-height in an equivalent sand-grain height, $h_s^+$. Roughened walls, will displace the velocity profile through a shift downwards in the standard logarithmic plot ($U^+$ vs $y^+$) [137]. This as an effect of the near-wall separated flow, which also increases friction in the duct. The enhancement of the heat transfer has thus an drawback in the increased pressure drop, which can be several times higher than for a smooth channel.

The pressure drop, and also the heat transfer is strongly connected to the size of the rib, $e$, which is measured as a fraction of the channel height as $e/H$. Equivalently to the rib-height one may chose to refer to the blockage ratio, which in contemporary turbine blades are around $10 - 20\%$.

Ribs have traditionally been arranged orthogonally to the flow, ie. that the extension of the rib is located $90^\circ$ to the streamwise direction. They have commonly be made of a square cross-sectional area. Investigations [1], [63], [65], [64], [67], [66] have however shown that both other shapes and non-normal arranged ribs may be more beneficial to maximize the heat transfer rate. The distance between two successive ribs, the pitch $P$, have also been shown to be of importance, [204]. Thus there are a number of different parameters which could be altered in order to optimize the internal cooling of a gas turbine blade. In addition it should be noted that the available pressure difference is severely limited and hence the design of rib-roughened channels is a meticulous work, which naturally benefits from a long tradition of constructing operational gas turbine engines.

The flow around a rib is characterized by several re-circulating zones which involves shear, mixing, and impinging flow which increases the turbulence level and hence the heat transfer to $2 - 4$ times that experienced in a smooth wall. The main effect is the large re-circulating zone downstream the rib. The physics within this region is similar to that behind a backward-facing-step (BFS), which has been investigated thoroughly both experimentally and numerically. Even more valuable, especially when evaluating turbulence models, are the recent DNS-data by Le *et al.* [124]

A Backward Facing Step (BFS) case with a 1.2-expansion configuration (the expansion ratio is defined as $R = (H + h)/H$) has been studied by DNS [124]. Figure 3.1 shows the velocity field behind the step using the AKN $k - \varepsilon$ turbulence model [2] for this case. In this configuration

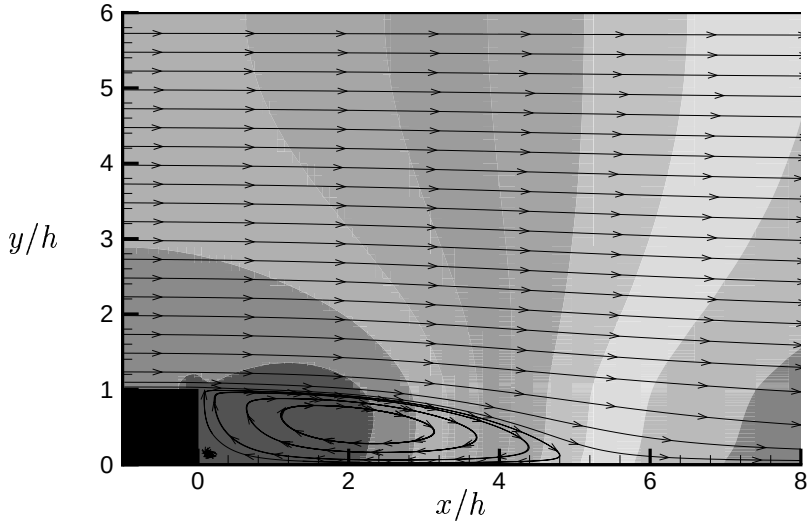


Figure 3.1: Re-circulating bubble in a backward-facing step flow. Streamlines and static pressure contours.

the main re-attachment point is located at $x_r/h = 6.3$ (DNS-data), with a reverse flow from $2.5 < x/h < 5$. Inside the main re-circulating region, there is a secondary bubble close to the step which yields a forward motion along the bottom wall up to $x/h \approx 1$. Even though there are differences between a BFS-case and a repeated rib-roughened channel, the characteristics of the main separation region is similar.

Vogel and Eaton [200] made a careful examination of both the flow- and thermal-field in a 1.25-expansion channel. A significant finding from their measurements was that the peak in Nusselt number were located slightly upstream of the re-attachment point at roughly $0.9x_r$. This coincides with the peak in turbulent intensity. A comparative result for the DNS-case is given in Fig. 3.2 where the predicted skin-friction and the Nusselt number using the AKN-model is shown. Even though the heat transfer was not included in the DNS-data and that the model under predicts the re-attachment point, located at $C_f = 0$, the predicted upstream shift of the maximum heat transfer compared with the re-attachment point is notable.

Through varying the Reynolds number Vogel and Eaton [200] derived a relation between the Nusselt number and Reynolds number as: $Nu \sim Re^{0.6}$, similar to the ratio previously found for separated flows, Richardson [176] and Sogin [188]. Furthermore it was concluded that

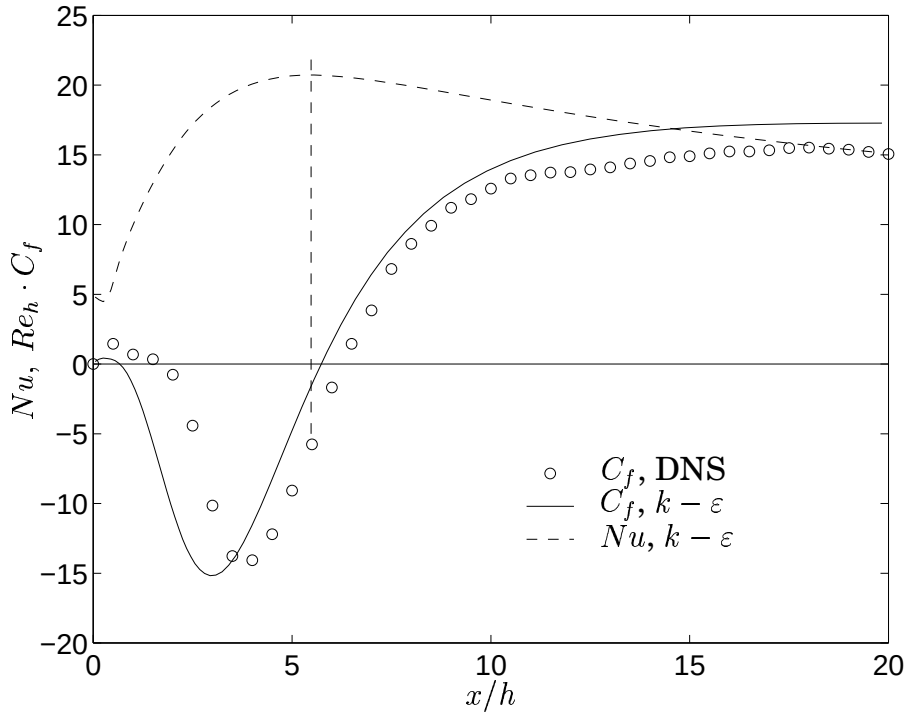


Figure 3.2: Skin friction and Nusselt number.

the Reynolds analogy, ie. the connection between skin friction and heat transfer, completely fails in separated regions, which is also observable in Fig. 3.2.

Investigations on single mounted, ie. non-repeated, ribs shows the appearance of additional re-circulating zones around the rib (experimentally: [9], [130], and experimentally/numerically: [4], [6]). There is a relatively large, $x/h \approx 1$, secondary bubble immediately upstream the rib. Dependent on the geometry condition of the rib, there may also be a re-circulation zone on the top of the rib. Investigations shows that the additional bubble on the rib-top appears only when the rib-width is more than four times the rib-height, [9], [130]. There is however an upstream influence on the formation of this bubble as noted in [30]. In repeatedly rib-roughened channels, for which the turbulence level is significantly larger than in a smooth channel, the rib-top separation bubble may thus appear for smaller rib-aspect ratios as indicated in Fig. 3.3. The author is however unaware of any such experimental evidences.

Apparent from the above discussion is that the flow pattern around the rib, varies dependent on the shape and size of the rib. In addi-

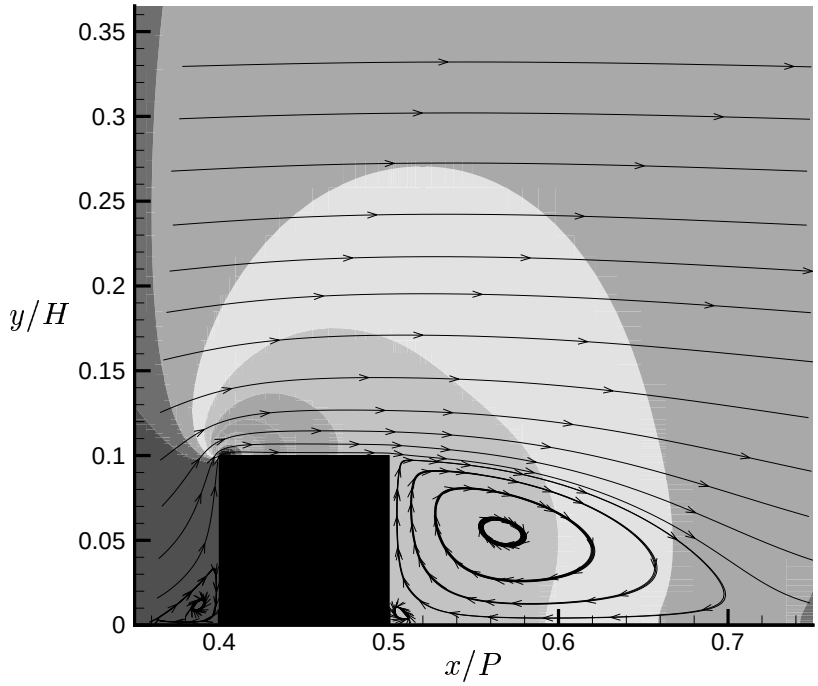


Figure 3.3: Re-circulating bubbles around a rib. Predictions using AKN $k-\varepsilon$ turbulence model [2], Paper VI [28].

tion the distance between two consecutive ribs, the pitch $P$ is also of importance. In experiments on rib-roughened channels, the two most significant parameters, apart from the Reynolds number, $Re$, are the dimensionless geometry defining ratios: the rib-height to channel-height, $e/H$ and the rib-pitch to rib-height, $P/e$. The rib-width, although important for the flow structure is less influently on the heat transfer. It should also be pointed out that most rib-roughened channel have ribs of fairly squared cross-section.

Webb *et al.* [204] compiled a number of experimental investigations to characterize the flow pattern within the interval of two success ribs for repeatedly rib-roughened channels, see Fig. 3.4. It was concluded that when the ribs are positioned far enough from each other, $P/e > 15$, the flow behaves as for a single mounted obstacle (similarly to a BFS flow), with a large re-circulating zone behind the rib, stretching roughly 6 to 8 rib-heights downstream the rib. If the pitch is smaller, the two re-

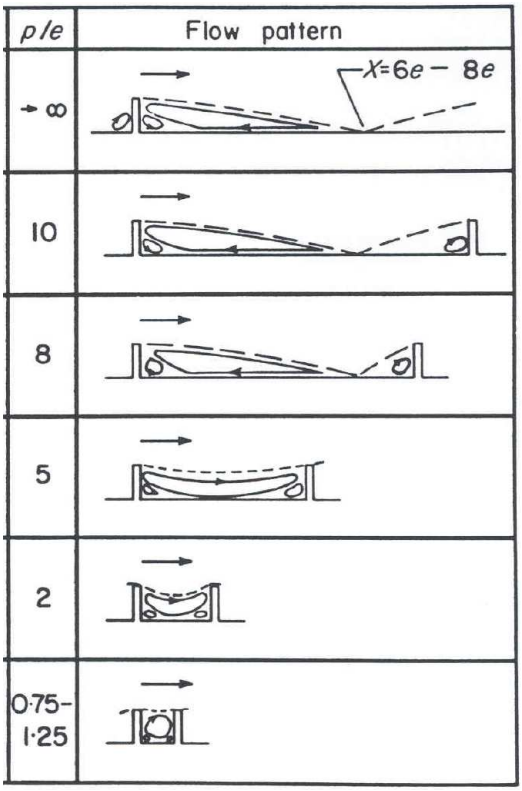


Figure 3.4: Flow patterns as a function of $P/e$, from [204]

circulating zones (upstream and downstream the rib) start to interact. Until $P/e \approx 8$ there is still two reverse flow regions in the rib-interval, however for $P/e < 8$ the flow does not re-attaches on the channel floor between the ribs and instead a single large re-circulating bubble is created. For even smaller rib-pitches the flow forms driven cavities, with a significant different heat transfer behaviour. It has been shown that the most advantageous flow behaviour, for heat transfer purposes, is when the flow re-attaches in-between the ribs, without re-developing before separating due to the blockage effect of the next rib. The influence the Reynolds number, the shape and rib arrangement have on the flow structure, should however be recognized.

Liou and Hwang [128] found for the rib-roughened flow that the Nusselt number and the turbulent kinetic energy are well correlated in the separated region behind a rib. The peak of Nusselt number was for this configuration, similarly to the BFS flow [200], located around one rib-height upstream of the re-attachment point. Corresponding results were obtained in Paper II [26]. The usage of several turbulence mo-

dels in the paper showed that the even though similar levels of $k$ were predicted the Nusselt number differed by nearly a factor of two. It is argued, that the representation of the length-scale is vital for the correct assessment of heat transfer in separated flows using two-equation models. This is also the argument behind the length-scale correction of Yap [212]. A detailed study and extensive discussion on the turbulent mechanism around ribs using an octant analysis, is given by Panigrahi and Acharya [153].

Scherer and Wittig [181] found that the discretization scheme may be a source of error in the location of maximum heat transfer behind a BFS. They erroneously predicted heat transfer maxima in the center of the re-circulating bubble, and blamed this on the used numerical scheme. This conclusion may however be questionable as they inaccurately predicted the re-attachment point, due to the use of wall functions. The found discrepancies may thus be more attributed to the choice of turbulence models than the used discretization schemes. The application of LRN turbulence models to rib-roughened channels in Paper II [26] also showed that, similarly to experiments, there is a slight upstream shift in the peak heat transfer as compared with the re-attachment point.

Investigations on angled ribs, eg. [63], have showed that there is a substantial benefit of positioning the ribs with an angle of $45^\circ$ to the streamwise direction as such an arrangement could achieve a $25\%$ increase in heat transfer as compared to normal ribs using the same pressure drop (friction factor). This effect may be attributed to the change in flow structure, as skewed ribs produce a secondary motion that flows transversally along the rib due to the induced cross-stream pressure gradient. A similar pattern is not found for orthogonally arranged ribs. A much weaker secondary flow with downward motion (towards the rib) along the centerline and upward along the side-wall in a circulating fashion is however present, although the latter is hardly discernible in Fig. 3.5. This motion is a result of both a difference in the static pressure, and turbulent generating processes as recognized in [171] and [131], respectively. The latter give rise to secondary flow of the second kind as denoted by Prandtl [168] and is described in the next section. Two-equation eddy-viscosity models, such as the $k-\varepsilon$ turbulence model, are unable to reproduce turbulence generated secondary flows (due to their isotropic representation of the Reynolds stresses) they still capture the vortical motion via the pressure difference as obvious from Fig. 3.5.

The more three-dimensional the flow becomes, as a result of incre-

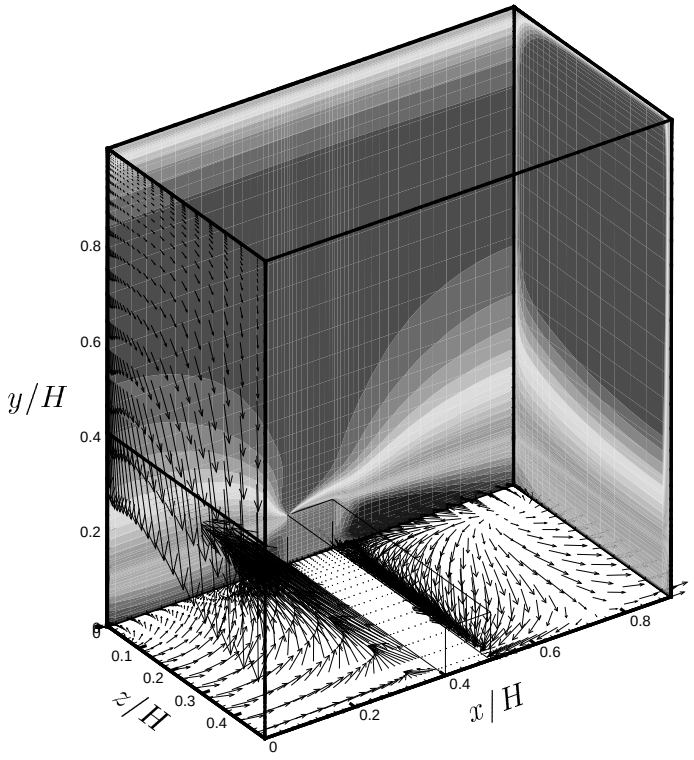


Figure 3.5: Vectors for secondary flow and contours of streamwise velocity. Levels not to scale. Prediction using AKN $k-\varepsilon$ turbulence model [2], Paper VI [28].

ased rib-height, angled ribs, reduced pitch etc., the more difficult it becomes to construct correlations that are valid for a wide range of configurations. In design situations when correlations are not valid, or when it is necessary to perform an extensive optimization process, it is most valuable to do numerical simulations. In order to evaluate CFD-codes, and also to improve understanding of the physics, it is beneficial to have detailed local velocity and heat transfer data. Drain and Martin [46] performed a laser Doppler velocimetry (LDV) on several rib-configurations.

Baughn and Yan [12] made a detailed study of the distribution of the local Nusselt number, including the rib-top. They found that the position of the maximum heat transfer varies with the Reynolds number, and was positioned further downstream for higher values. Their data are well correlated with the Dittus-Boelter equation, Eq. 3.1, for

the two higher Reynolds numbers ($Re = 80\,000, Re = 50\,000$) however the lower ($Re = 15\,000$) case follows the Reynolds number raised to $0.6$. In Paper II [26] this Reynolds number effect for rib-roughened channel was studied using three different types of turbulence model. The experimental data [144] coincide with the behaviour given by Richardson [176] and Sogin [188] behind bluff-bodies, ie. $Nu \sim Re^{2/3}$. The numerical simulations however, for all turbulence models, erroneously follow the smooth duct correlation by Dittus-Boelter [43],[135]:

$$Nu = 0.023 Re^{0.8} Pr^{0.4} \tag{3.1}$$

In Paper I [23] it was shown that turbulence models that agree well with a low Reynolds numbered case, over predicted the heat transfer for a high Reynolds numbered case. A similar behaviour can be deduced from the data presented in [94].

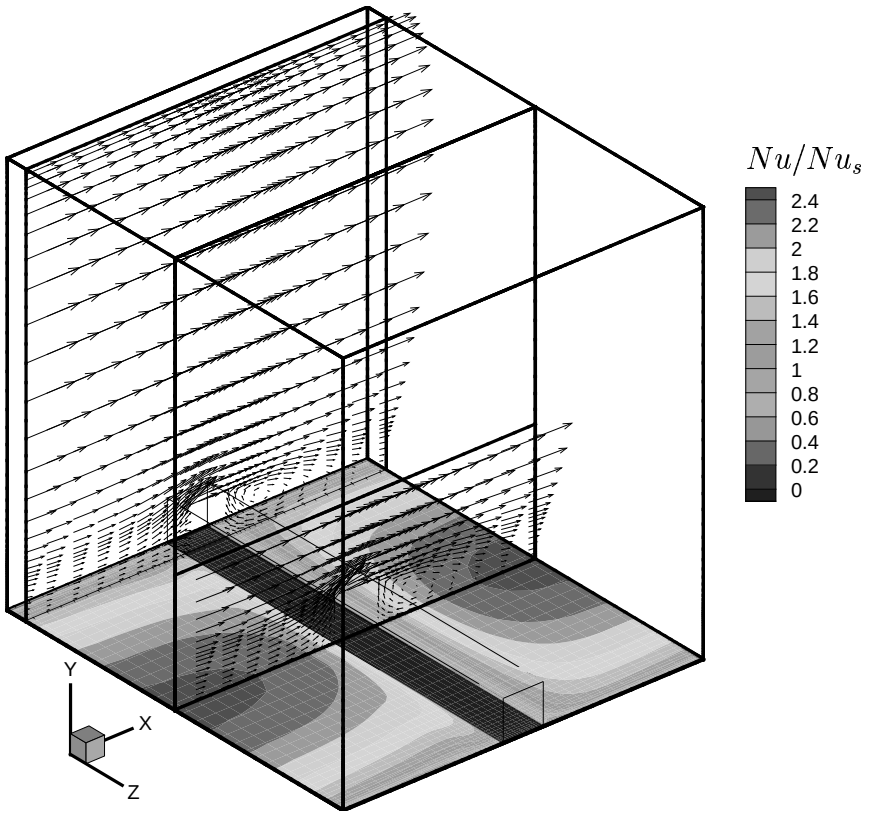


Figure 3.6: Normalized nusselt number, rib-roughened wall. Prediction using the AKN $k - \varepsilon$ turbulence model [2], Paper VI [28].

Kukreja *et al.* [110] investigated the effect of the spanwise distribution on the Sherwood number due to differently angled ribs, and

found that the vortical cells produced by the angled ribs produce a very complex pattern in the local mass transfer (or equivalent heat transfer) which is impossible to correlate to any empirical function. Even for orthogonal ribs, a substantial variation of the heat transfer in the spanwise direction is evident, see Fig. 3.6. The results from these and similar experiments show the necessity to perform three-dimensional computations. In Paper VI [28] it was however concluded that for orthogonally ribs the centerline Nusselt number could still be reasonably approximated using a 2D simulation, see further discussion in Section 4.5.

Assessment of turbulence and heat transfer models are laborious by the fact that most experiments only measure heat transfer data, and hence it is impossible to separate the performance of the heat transfer model from that of the turbulence model. The detailed study by Rau *et al.* [171] includes both flow field and heat transfer measurements, which makes this experiment exceptionally valuable for turbulence model evaluation. The case have consequently been used as comparative data for several numerical simulations: [149],[180], and by the author in Paper VIII [24] and VI [28], see Fig. 3.6.

## 3.3 Secondary flows

In most flows it is possible to identify a pre-dominant flow direction – the streamwise. Flow structures, which are not arranged in that direction are normally referred to as secondary flows. These can originate as a result of either geometrical constraints, eg. ribs, or due to imposed forces. Prandtl [168] classified secondary flows into two distinct groups:

1. Generated by inviscid effects.
2. Generated by Reynolds stresses.

The first process, denoted *secondary flow of the first kind*, is generated by turning a shear-layer perpendicular to its main vorticity direction. Flow in a channel with a large aspect ratio (wide) can for the centerline be simplified to a two-dimensional flow, with (say) the streamwise direction along the $x$-axis and the wall-normal direction along the $y$-axis. Vorticity, defined as

$$\omega_i = \varepsilon_{ijk}\frac{\partial U_k}{\partial x_j} \tag{3.2}$$

thus exists only in the spanwise direction: $\omega_z = \partial V/\partial x - \partial U/\partial y$. In order to produce secondary flow of the first kind for this flow there needs to be a process which generates either a $x$- or a $y$-component of the vorticity vector. The main re-circulating bubble in a ribbed channel flow is thus not *per se* a secondary flow, as the ribs only generate spanwise vorticity, through an increased shearing.

*Secondary flow of the second kind* develops in corners of a duct, where the cross-stream gradients of the Reynolds stresses generate weak streamwise vorticity, see the predicted cross-section velocity vectors in Fig. 3.7. DNS's ($Re_\tau = 300$ [55], and $Re_\tau = 600$ [80]) and LES's [152] (included as Fig. 3.7(c)) clearly show this type of turbulence induced secondary motion. The flow in the cross-stream plane is characterized by two contra rotating vortices in each corner. Because these structures are driven by gradients of Reynolds stresses they cannot be captured using an isotropic eddy-viscosity models, as notable in Fig. 3.7(d). The two additional figures in Fig. 3.7 (Fig. 3.7(a) and 3.7(b)) show the predicted secondary flows using an EARSM [54] with two different pressure-strain models (SSG [193] and LRR [120]).

Demuren and Rodi [42] made a thorough review of the, at that time (1984), modelling achievements with comparisons to experiments. The present available DNS-data however make it possible for a more fundamental analysis. Based on their DNS-data [81] Huser *et al.* concluded that although the basic secondary motion can be captured using non-linear models, no turbulence model can accurately predict the turbulence characteristic of Prandtls secondary flow of the second kind. A recent computation by Petterson and Andersson [163] using an RSM with an elliptic relaxation [48] and the non-linear SSG pressure-strain model confirms the problems of accurately predicting these secondary flows even with the most complex and advanced second-moment closures. Noting the weakness of these structures ($2 - 3\%$ of the bulk velocity) the influence of the Reynolds stress induced secondary flow is less important in complex and disturbed flows. In the result section it is shown that for rotating rib-roughened channels, where the flow is characterized by large-scale separation and rotational induced secondary flows, there is only a minor modification by adding non-linear terms (EARSM) to the eddy-viscosity turbulence model. The performance in a squared duct should thus not be used as an argument for using Reynolds stress based turbulence models in ducts with ribs.

Contrary to Prandtls secondary flow of the second kind, the secondary flows governed by inviscid processes are significantly simpler to predict and also more influential on the flow structure. There are two

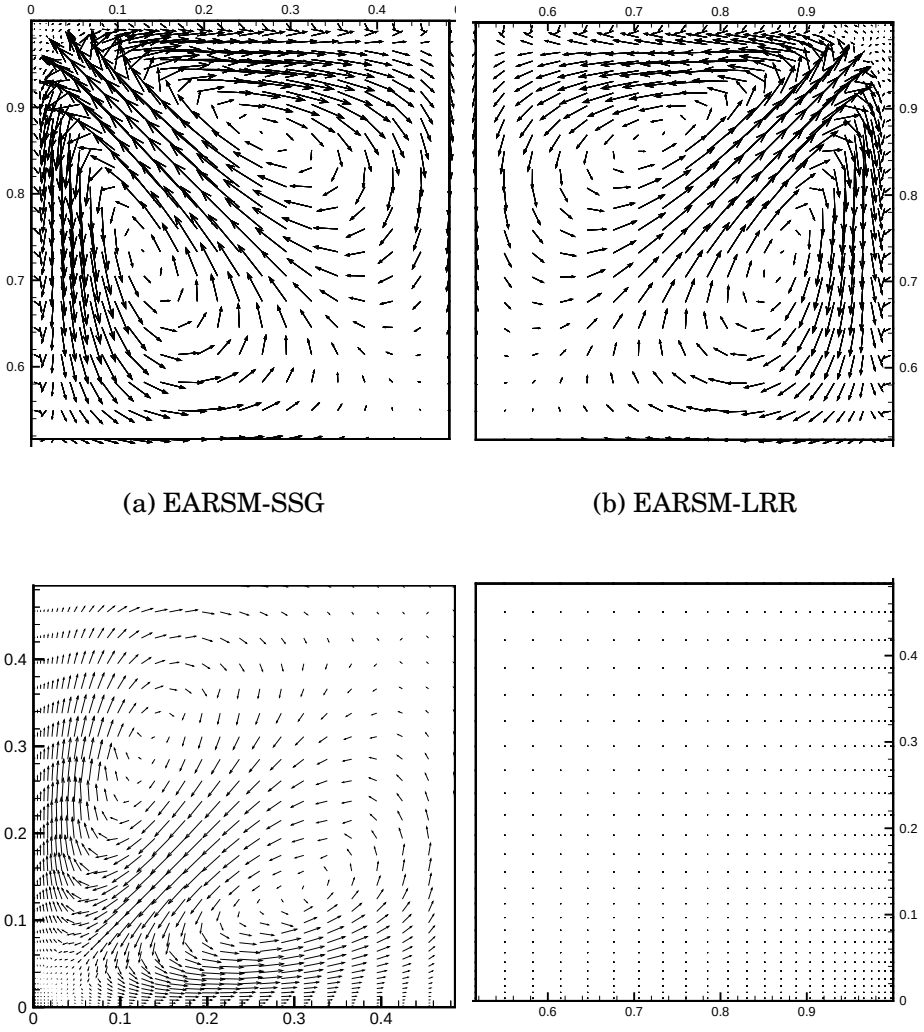

(a) EARSM-SSG

(b) EARSM-LRR

(c) LES

(d) EVM

Figure 3.7: Predicted secondary flow in a square duct. Each sub-figure represents one-fourth of the duct. EARSMs are able to capture the general flow structure with eight turbulence induced vortices, while linear EVMs are unaffected by the corners. EARSM by Gatski and Speziale [54] using either SSG [193] or LRR [120] pressure-strain model. The EVM is the $k-\omega$ model by Abid *et al.* [3]. LES results supplied by Pallares [151]

mechanism that drives the generation of secondary flows of the first kind, either: 1) a pressure gradient or 2) an imposed body-force in the cross-stream plane. The latter could be the Coriolis force due to rotation, or buoyancy as a result of uneven heating. The former, ie. pressure gradient induced secondary flows, is generated by geometrical conditions, eg. ribs as discussed above.

In rib-roughened channels, the void behind the rib generates a downward motion within the re-circulating region. This motion, accompanied by the no-slip condition along the side-walls, will generate a circular motion with two opposite rotating cells [76]. The downward flow in the center of the duct is seen in Fig. 3.5. In the same figure a transversal motion along the bottom wall is also noted. This is the result of the spanwise difference in pressure due to the ribs, which for angled ribs is further amplified. When the ribs are arranged in a V-configuration, the highest pressure is found in the center of the duct, at any given streamwise location. Kukreja *et al.* [110] found that such an arrangement further enhances the strength of these cells, with a significant re-distribution of the heat transfer pattern as a consequence.

## 3.4 Bends – curvature

The internal cooling systems of gas turbine blades are commonly arranged in a serpentine manner, with a number of rib-roughened ducts connected using sharp $180^\circ$ bends. Motion within a bend will generate a centripetal acceleration which is balanced by an opposing pressure gradient. To a first order approximation the following condition is applicable:

$$\frac{\partial p}{\partial r} = \rho \frac{U^2}{R} \tag{3.3}$$

where $U$ is the streamwise velocity. In bends with a low curvature[1], the pressure gradient will vary linearly from the inner- to the outer-radii. High momentum fluid in the center tends to drift outwards in accordance with the above relation. Continuity requires that the outward motion in the center of the duct, is balance by a reverse flow along the walls, where the streamwise velocity is lower and hence the centrifugal force is less. A circular motion in the cross-stream plane is therefore generated. The flow out from a bend is characterized by two opposing

[1]The curvature is the inverse of radius

rotating cell, with vorticity in the streamwise direction. A parameter that measure the curvature effect, relatively to the viscous effect is the Dean number. The curvature induced cells are consequently also referred to as Dean cells.

The stability of the flow in a bend can be studied through a perturbation analysis. If a fluid lump along the inner radius (convex) is slightly displaced outward into a high-velocity region, the lump with a now unbalanced low momentum will return, due to the imposed pressure gradient, to its original position. Such a flow is denoted a stable flow. The opposite condition is true for the outer (concave) side, and hence this side is unstable. A measure of the degree of stability is given by the Dean number. Exceeding a critical Dean number results in the development of instabilities in the flow, as given by Rayleighs criteria, see [154]. An analog is found in boundary layer flows over concave walls, for which Görtler vortices is produced if the centrifugal instability is large enough.

Flows in curved ducts and the associated stability problems have been studied by numerous peoples including the great turbulence researchers Prandtl, van Karman, Taylor. A recent investigation [29] using LES clearly shows the complex multiple cells in the cross-stream plane within the bend. Although fundamentally the secondary flows in curved ducts are govern by the inviscid centrifugal force, the stability of the system is based on the viscosity and hence the level of turbulent viscosity for turbulence modelling is of most importance. The first to propose a model to account for turbulence modifications due to curvature was Prandtl [169]. He proposed to add a correction to the mixing length, based on a local dimensionless curvature parameter:

$$\frac{U/R}{dU/dy} \tag{3.4}$$

Bradshaw [18] used the similarly defined Richardson number, see Eq. 2.13, to modify the turbulent length scale. In standard two-equation models ($k-\varepsilon$, $k-\omega$), the turbulent length scale is not given explicitly and hence such a modification is not applicable. Launder *et al.* [119] instead introduced a Richardson number modification in the $\varepsilon$-equation. Wilcox and Chambers [210] argued that the modification should be applied to the turbulent kinetic energy, since streamline curvature makes a redistribution among the Reynolds stresses. Under de-stabilizing conditions the wall-normal component is amplified accompanied by a reduction of the streamwise component. The opposite is valid for a stable, convex side. It is thus not surprising that isotropic EVMs have

limited capability to correctly assess the complex secondary flows in a bend as shown in [118]. Although the Wilcox-Chambers model may sound plausible, the level of turbulence energy is markedly different on the concave and convex side of a bend, and hence their strategy for achieving improved predictions, through only re-distribution among the stress components is questionable. In the result section (and also [19]) more realistic profiles for the turbulent kinetic energy is given using a Richardson number modified $\varepsilon$-equation than with the Wilcox and Chambers $k$-equation modification, albeit for rotating flows. More recent attempts to improve predictions in curved duct have all focused on the $\varepsilon$-equation [74], [182]. Numerical simulations using RSM [133] have shown that even these models benefits from a modification to the length scale for highly curved ducts.

## 3.5 Rotation

In the study by Bradshaw [18] it was shown that the effect of an imposed rotation can be treated in analog to streamline curvature. The extension to include buoyancy effect due to heating was also assessed, however such an analog can only be a rough approximation, as the driving mechanism differs. The connection between rotation and curvature can easily be demonstrated, and in cases when the rotation axis is parallel to the curvature-axis these two process will generated similar secondary motions. Neglecting buoyancy and wall-effects the only remaining rotational induced force, will be the Coriolis-force ($2\Omega U$), which corresponds to the centripetal force ($U^2/R$) for a curved surface. In a bend the streamwise velocity could be approximated by a linear variation from the inner to the outer wall with a slope of $U/R$. In a duct exposed to system rotation a similar behaviour is present, although the skewness of the velocity profile is given by the magnitude of $2\Omega$ (referred to as the background vorticity in [100]) instead of the curvature parameter, $U/R$. In inviscid regions, where wall effects are negligible, the DNS by Kristoffersen and Andersson [109] confirms the validity of this relation. In experiments, the inevitably introduction of spanwise walls disturb the clean results achievable in a DNS. In a recent high fidelity LES (DNS-like) by Pallares and Davidson [152] the interaction of Prandtls secondary flow of the second kind (stress-induced) with those of the first kind (rotational-induced) is studied. It is apparent that for increasing rotational numbers, the corner vortices are suppressed and that the cross-stream secondary motion is mainly

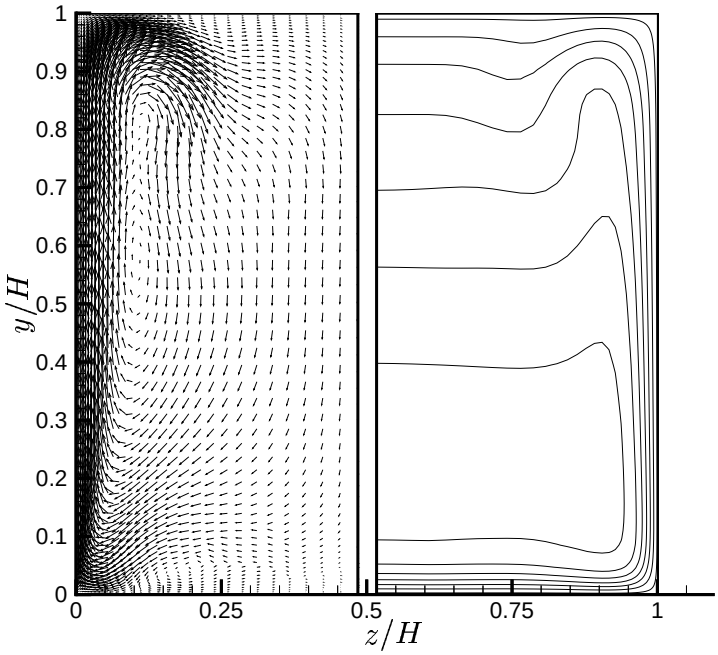


Figure 3.8: Cross-section velocity vectors (left) and contours of streamwise velocity (right). Rotation around $z$-axis: $Ro_z = 0.2$. LES [152].

govern by the Coriolis force, see Fig. 3.8 and compare with Fig. 3.7 (stationary).

The equations governing fluid motion are, as discussed in Chapter 2, the Navier-Stokes equations. The additional terms, due to rotation, are the centrifugal and Coriolis accelerations, which translates into the following body-forces:

$$f_i^{ce} = -\rho\epsilon_{ijk}\epsilon_{klm}\Omega_j\Omega_l x_m \tag{3.5}$$

$$f_i^{co} = -2\rho\epsilon_{ijk}\Omega_j U_k \tag{3.6}$$

These terms are generally found on the RHS of the NS-equation. For incompressible flow, or a flow with negligible buoyancy, the centripetal force is conservative and can be assimilated into a reduce pressure gradient [59]. The contribution of the Coriolis force is, as obvious from the definition, perpendicular to the rotation axis and placed in the cross-stream plane ($\Omega \times U$). In a rotating square duct, the cross-stream flow will be aligned with the Coriolis force in the core of the duct, for which

the streamwise velocity, and hence the Coriolis force is strongest. Along the side-walls a reverse flow is found, as dictated by continuity, see Fig. 3.8.

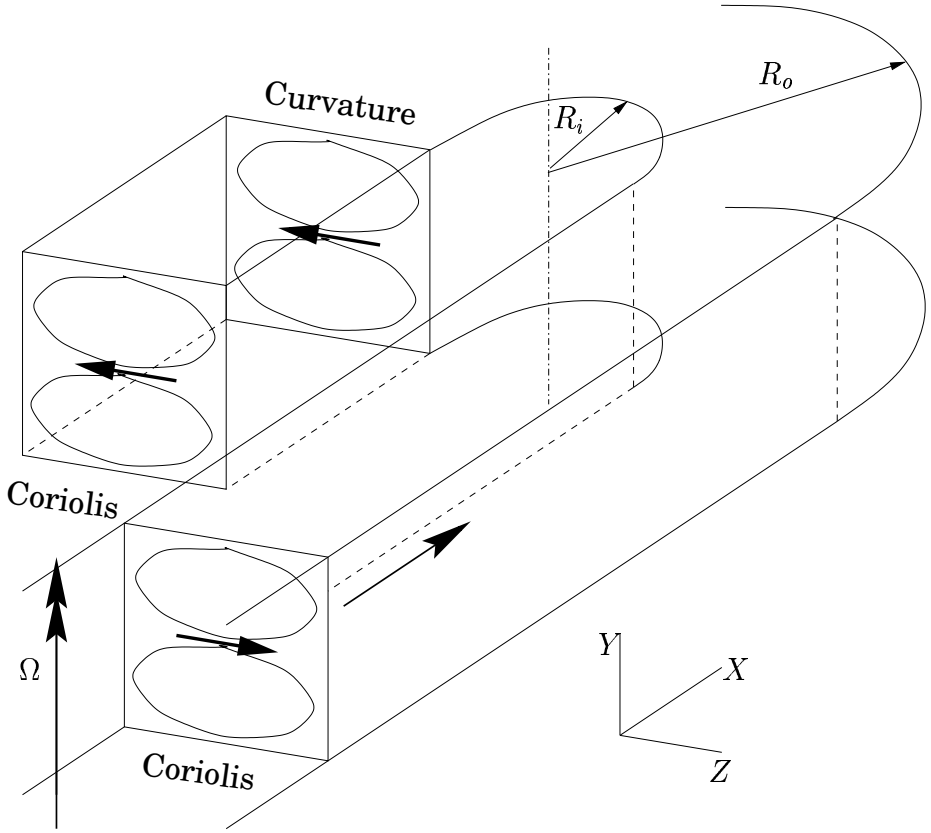


Figure 3.9: Rotational and curvature induced secondary flows.

A connection between the rotation and curvature induced secondary flows can be visualized in a rotating U-bend, Fig. 3.9. With $x$ as the streamwise component $U_i \approx |U|(1,0,0)$ and a rotation around the $y$-axis $\Omega_j = |\Omega|(0,1,0)$, the Coriolis force $f^{co} = \pm 2|\Omega||U|$ is parallel to the $z$-axis, and generates a secondary flow in the cross-stream plane, $y-z$. The curvature effect, as discussed in the previous section, produce a similar secondary motion within the bend and in the downstream leg, as shown in Fig. 3.9.

The analog between streamline curvature and rotation can be extended to stability analysis. When the main Coriolis component is perpendicular to the surface a perturbated fluid particle will either be forced back, or driven away from the surface, dependent on the direction of the Coriolis force. If the rotational induced acceleration (opposite to

the force) is directed into the surface the flow is stabilized. As pointed out previously a stabilized boundary layer suppress turbulence, and can under strong rotation even laminarize. The reverse is true for the de-stabilizing surface (impinging secondary flow), for which the turbulence is enhanced. In a square duct the stress-induced corner-vortices are significantly reduced for increasing rotational number on the stable side, see Fig. 3.8. The formation of Taylor-Görtler vortices, similar to those for a convex surface on the unstable side of the duct, was shown in [152]. An accurate numerical simulation of rotating flows thus necessities a higher-order turbulence model, although the main vortices, governed by the inviscid Coriolis force, is captured using even the simplest flow model.

## 3.6 Review, experiments and numerical simulations with reference to turbine blade internal cooling.

The importance of improving the cooling of gas turbine blades have seen an increasing demand of, initially experimental evidences, and now well validated numerical methods for use as optimization tools. The effect of variating rib-sizes, Reynolds number etc. have been documented in both numerical simulations and experimentally.

Although the many merits of experimental evidence, there is a problem that should be recognize when performing experiments: it is very difficult to achieve conditions which enable measured data to be dependent on only a single parameter. In many investigations the data is obscured by slight perturbations in Reynolds number, different heating, rotation number etc. These unknowns add up to a level of uncertainty in the measured data, which should be considered when making comparisons to the predicted result. In numerical simulations on the other hand it is very easy to ensure an exact Reynolds number or that the flow is incompressible, or that the temperature behave as a passive scalar etc., all conditions which can only be an approximation of the real world. It is thus important that both measurements and predictions are made under as identical conditions as possible, to enable an accurate evaluation of turbulence and heat transfer models. The appearance of Direct Numerical Simulations have had a great impact on turbulence modelling as these numerical 'experiments' could be completely controlled, with known boundary conditions. These simulations

also provide a wealth of information. DNS are however very computational costly, and only some fundamental flows can be studied with this approach. In other cases, such as the internal cooling systems of a gas turbine blade, one needs to rely on data from experiments.

### 3.6.1 Experiments:

Many of the early investigations were made to evaluate the concept of rib-roughened ducts for enhancing cooling performance. Initially the size of the ribs could be maintained relatively small, $e/D \approx 0.05$, as the cooling needs was much less than today. Because of this it was possible to compare rib-roughness with an equivalent sand-grain roughness, $h_s^+$. The latter has been studied extensively by Nikuradse [146] and is well documented. The experiments were thus aimed at constructing correlations between rib-size, $e/D$, Reynolds number, $Re$, and the friction factor, $f$, similarly to those given by Nikuradse. The heat transfer can then be computed for different fluids using correlations based on the Prandtl number, $Pr$, and the previously achieved friction factor, $f$, as shown in [204], [102]. An early compilation on rib-roughened circular tubes is found in [204].

It was however soon realized that an increased heat transfer performance was needed. The simplest way to achieve this is to increase the size of the ribs. This however also increases the pressure drop. In order to enhance the heat transfer performance[2] the effect of different rib cross-sectional shapes and skewed ribs were investigated in Han *et al.* [63], [65], [67]. It was shown that the effect of ribs on the opposite wall also modifies the results when the rib-to-channel-height is large. In other studies, [62], [64], the aspect ratio of the channel was varied. Constructing correlations which incorporate all these parameters have now become a rather delicate business. In subsequently studies [66], [67] it was also concluded that it is impossible to curve-fit such a wealth of data. A recent and comprehensive compilation of the effect on heat transfer from a variety of rib-configuration could be found in the van Karman Lecture series given by Taslim [196], or alternatively, but less complete [197].

Although the importance of understand rib-roughened channels, there are other flow phenomenas that appear in internal cooling ducts of turbine blades, such as rotation, curvature and buoyancy. In the above discussion on rotation, the effect of buoyancy was neglected, to simp-

[2]Heat transfer performance also consider the friction coefficient/pressure drop.

lify the treatment of the already severely complicate flow structure. Experiments made with a bearing to the gas turbine industry, will naturally focus on heat transfer rate, and hence the buoyancy effect can only be neglected for certain special cases. In most studies of rotating ducts the measured data is thus affected by a buoyant force, as are eg. [68], [111], [16]. Generally there are however several effects present, such as rotating channels with roughened walls [139]. U-bends (ie. including curvature effect) with roughened walls are studied in [52], [88] and rotating U-bends in [31], [83], [89]. [127], [138], [201] and [202].

Experiments that simulate conditions in a turbine blade need to superimpose all these effects (rotating, rib-roughened U-bends) see eg. [157], [158] and [50]. In the latter two the effects of different model orientation was also included. Other investigations [90], [98], [216] have studied skewed ribs. Most experiments only measure heat transfer, however [87] also gives accurate flowfield data using LDV. The value of such experiments for the assessment of turbulence models, should be emphasized. Reviews on experimental investigations are given in [78] and [79].

### 3.6.2 Numerical simulations:

Apart from some rather academic case, the complexity of each of the above phenomena (rib-roughened walls, streamline curvature and rotation) necessarily means that a three-dimensional simulation must be performed. Due to the tremendous advances in computational power lately, the most interesting numerical simulations are hence fairly recent.

A review on numerical simulations is given by Prakash and Zerkle [166]. Their contribution was a computation of a rib-roughened rotating duct with cyclic streamwise boundary conditions to reduce computational costs. Furthermore the buoyancy-centrifugal effect was neglected, for simplicity. The turbulence model used was the $k - \varepsilon$ with either wall-functions or a zonal approach for the wall treatment. Prakash and Zerkle inferred that a number of refinement were necessary, however without any experimental data their conclusions could only be based on phenomenological discussions.

**Rib-roughened channels:**
An early and valuable investigation was made by Liou *et al.* [129] who performed both heat transfer measurements and numerical simula-

tions using a $k-\varepsilon$ algebraic stress turbulence model. The case studied was the one previously measured by Drain and Martin [46] using LDV. In the 7:th ERCOFTAC Workshop the result from Liou *et al.* was used to evaluate CFD-codes and turbulence models. Significantly different heat transfer results were presented at the workshop dependent on used models, see eg. the authors contribution: [22]. Two of the groups, re-visited the test-case using more advanced turbulence models. The extension using an EARSM formulation [3] of the $k-\omega$ turbulence model did however little to improve the result, see Paper I [23]. Manceau *et al.* [134] applied the $k-\varepsilon-v^2-f$ turbulence model [47] with impressive results for the floor between the ribs. The heat transfer around the rib, was however not accurately captured although different boundary conditions were used.

Another test case in the workshop was a 3D rib-roughened channel with ribs placed on two opposite walls in a staggered arrangement. However only a single group contributed with any predicted data. The result using a zonal DSM and a LRN $k-\varepsilon$ turbulence model was later published [84] and [95]. The mean quantities were accurately predicted, however heat transfer was under predicted using the zonal-EVM. The LRN $k-\varepsilon$ necessitates the inclusion of a Yap-correction [212] to yield acceptable heat transfer rates. Similar conclusions, for the same measurement data [87], [88] were drawn by the author [19], when comparing a zonal $k-\varepsilon$ with a $k-\omega$ and EARSMs. A subset of this data is included in Section 5.2. Ooi *et al.* [150] also studied this case, with the $k-\varepsilon-v^2-f$ turbulence model, and achieved good agreement.

Other interesting numerical studies on rib-roughened channels are eg. the combined measurements and simulations using both a standard and a non-linear $k-\varepsilon$ turbulence model in [5]. The predicted Nusselt number different only marginally dependent on the selected turbulence model. A comparison between wall function based turbulence models for a single rib was performed in [4]. Abdon and Sundén [1] investigated different rib-shapes similar to that of [63] and found that de-graded ribs (with rounded edges) yield superior heat transfer to friction ratio. The only LES (although rather coarse) which has simulates these configurations is the one made by Ciofalo and Collins [36]. A notable qualitatively improvement in the predicted Nusselt number was found when comparing the LES with a standard $k-\varepsilon$ turbulence model. The treatment of ribs using spectral methods however pose a severe obstacle in DNS and LES studies. A way to circumvented this could be, as done in the DNS by [141], through simulating the ribs with source and sink terms in the momentum equations.

**Curvature:**
In the case of predicting curvature there is a distinct additional modelling complexity if the flow separates as a result of the adverse pressure gradient due to the bend. In simulations with only a moderated curved bend, there have been attempts to predict the flow without any length-scale corrections, even though their inclusion is theoretically well founded as discussed in Section 3.4. In [13] and [34] it was concluded that it is essential to resolve the near-wall region in curved ducts, as the predictions using the PSL and wall-functions, respectively, were inferior to that using a refined mesh and employing the mixing-length model. Using the same case, Iacovides *et al.* [92] employed a differential stress model (DSM), with and without modification to the $\varepsilon$-equation. The results with the DSM were similar to those achieved earlier, using ASM, however with detectable improvements in certain regions.

For stronger curvature, as the case studied by Cheah *et al.* [31] ($R_c/D = 0.65$) the flow separates within the bend, and hence more stringent conditions is imposed on turbulence modelling. In separated regions the mixing-length hypothesis fails and hence it is necessary to employ more elaborated schemes in the near-wall region. In Iacovides *et al.* [93] a comparison was made between using different wall treatments in connection with an ASM. The near-wall region was resolved either using an one-equation model [211] ($\varepsilon$ determined from a prescribed length-scale) or a two-equation based turbulence model ($\varepsilon$ given from its transport equation). For all models the separated region was inaccurately predicted, with only a slight improvement using the full LRN-version of the model. In a subsequently study [145] it was concluded that for heat transfer predictions a LRN turbulence model is preferable to a zonal model in the near-wall region. The separation was however not well predicted using any of the turbulence models. The Iacovides group have continued with a number of numerical simulations using wall-functions [148]. That study shows that the core model (EVM vs RSM) is of importance for the heat transfer, even though the near-wall is rudimentary modelled.

Luo and Lakshminarayana [132] made a similar comparison for a high Reynolds number U-bend of strong curvature. To reduce computational costs the simulations were restricted to a plane 2D duct and similarly to previous computations the zonal technique was employed when resolving the near-wall region. The result using an RSM was superior to the other turbulence models ($k-\varepsilon$, non-linear $k-\varepsilon$ and ARSM)

with the linear $k-\varepsilon$ performed the worst. In a subsequent paper [133] they introduced length-scale modifications by [119] and [182] to their RSM and achieved significant improvements on the concave surface. Bauer *et al.* [11] compared a number of higher-order turbulence models (non-linear EVMs: [38], [183] and EARSM [54]) with the standard $k-\varepsilon$ [101] and the LRR RSM [120], for the same high Reynolds number case. They found similarly to Luo and Lakshminarayana that the $k-\varepsilon$ turbulence model is inadequate. They concluded that although improved results were achieved with the non-linear turbulence models, the cross-velocity coupling in the momentum equation can lead to solver divergence, and hence they used truncated versions of the models. Methods to improve numerical stability, other than simply truncating the turbulence models are discussed in [69]. In these simulations the assumption of a 2D flow and the use of an one-equation model [132], or wall functions [11] to bridge the near-wall region may however influence the result, particularly in separated regions.

Unpublished results by the author from numerical simulations in the Cheah *et al.* [31] U-bend using unmodified LRN two-equation models indicate the need for length-scale corrections, especially when predicting heat transfer within the bend region. The results presented in Paper VII [25], although for a rib-roughened U-bend, also shows severe discrepancies in this region. Another U-bend simulation using LRN turbulence model was performed by Rigby *et al.* [178]. They used the $k-\omega$ turbulence model by [208] and achieved reasonable accuracy even for heat transfer.

**Rotation:**
In the 7:th ERCOFTAC workshop a two-dimensional like (high aspect ratio) rotating flow was used to evaluate turbulence models. DNS-data for this flow was supplied by [109]. The result from the workshop showed, not surprising, that the isotropic EVMs are unable to capture the increase/decrease of turbulent kinetic energy on the unstable/stable side. Better agreement were achieved when non-linear EVMs, EARSM and RSMs were used, although discrepancies still persisted in the near-wall region, especially on the stabilizing side. Most turbulence models over-predicted the suppression of turbulence, with a too early flow laminiarisation. In Chapter 5 it is shown that notable improvements can be achieve if rotational modified length-scale corrections – in analog to those used for streamline curvature – are applied. It has been shown [150] that even the $k-\varepsilon-v^2-f$ model necessitates rotational modifi-

cation to capture the skewed velocity profile in rotating ducts.

It should be noted that even RSMs, which have an exact formulation of rotational induced stresses, benefit from these length-scale corrections as the $\varepsilon$-equation is affected by rotation. In addition the Reynolds stress equations are not frame invariant, and hence an imposed acceleration alters these equations similarly to the NS-equations. Launder *et al.* [123] proposed a correction for this effect through a modified pressure-strain model. For non-linear EVMs and EARSM the rotational induced stresses can be included through a modified rotational tensor, $\Omega^*_{ij}$ [54], [183], [203]

Howard *et al.* [77] compared predictions with and without length-scale correction for both a high- and low-aspect ratio channel. They concluded that any rotational modification to the turbulence model was less important for low-aspect channels. A similar conclusion is given by the presented results in Chapter 5, where rotational induced turbulence modification are significantly more important in the 2D channel when compared with the 3D squared channel. Although it is not possible to make a proper comparison between the two test cases, as the latter channel is also equipped with ribs, the conclusion from 3D flow is of a higher engineering interest as that is more in line of real life problems. It is thus not surprising that many numerical simulations do not bother to incorporate these corrections.

A review of theoretical and experimental achievements for rotating channels could be found in [165]. In their paper they used a $k-\varepsilon$ turbulence model to simulate a flow affected by both buoyancy and rotation and achieved acceptable agreement without any turbulence model modification. Their use of wall-functions for the near-wall treatment would anyhow have drastically reduced the likely improvements of such a modelling effort.

**Numerical simulations of combined effects:**
Judging from the above discussions on the problems of achieving a high degree of fidelity for the different flow phenomena it is not surprising that in cases when combined effects are present, less attention is given to theoretical consideration and more to practical issues. A significant restriction when computing eg. rotating U-bends is the need for a 3D simulation, and hence both computing time and resources increases tremendously. In many cases one is restricted to a single mesh and a single model to evaluate the configuration, not an ideal situation when performing numerical simulations. Furthermore, the computational

demands necessitates as many simplifications as possible, such as the application of wall function based $k-\varepsilon$ turbulence model by Dutta *et al.* [49], [51]. The same rotating (smooth) U-bend case[3] was studied by Bonhoff *et al.* [14] and Iacovides *et al.* [93] using higher-ordered turbulence models (ASM and RSM respectively). Similar to previous studies by the UMIST-group (Launder, Iacovides) the latter study employed a one-equation model in the near-wall region, while [14] used standard logarithmic wall function in a commercial code. For a lower Reynolds number case, $Re_B = 25\,000$, Stephens and Shih [195] was able to use a LRN $k-\omega$ turbulence model on a $1.1 \times 10^6$ mesh for their compressible simulation. The result was in good agreement with the measured data by [201] and [202].

Even larger meshes are needed for U-bends with rib-roughened walls. The author estimated that the required number of nodes on a well resolved mesh for the case studied in Paper VII amounted to $20 \times 10^6$. All the following computations; [15], [85], [96], [126] [177], and [194] have through a number of simplifications been able to reduce this requirement by a magnitude, including the author in Paper VII [25] where the simulations was made on $1.9 \times 10^6$ mesh.

A case investigated by several of the above authors is the one studied by [98] and [202]: $Re_B = 25\,000$, $Ro = 0.24$ with staggered ribs skewed at $45^\circ$ angle to the streamwise direction. In Bonhoff *et al.* [15] the number of nodes were reduced through employed wall-functions in their computation using $k-\varepsilon$ and Reynolds stress turbulence models. The commercial code FLUENT was able to predict the trends correctly when comparing smooth with ribbed channel, and stationary with rotating, although the magnitudes of the changes were inaccurate. In addition the overall difference between the predicted and measured heat transfer levels was greater than desired. Better agreements were achieved by Stephens *et al.* [126] and [194] for the same case through employing LRN $k-\omega$ turbulence model in [194] and the SST turbulence model in [126]. The usage of a LRN turbulence model however significantly increases the number of nodes, and even though the total number of ribs (in all 20) was reduced compared with the experiment they still needed $761 \times 65 \times 65 = 3.2 \cdot 10^6$ node points. They made however only rudimentary comparisons to measured data, and not for the important ribbed case. In Jang *et al.* [96], a reduction in the number of nodes was accomplished through restricting the computational domain to a single leg of the U-bend. Their grid-refinement study with the used LRN ver-

[3] Measurements by [31].

sion of a RSM showed a significant difference ($20\%$) in the predicted heat transfer between a mesh with $21 \times 21$ nodes and one with $41 \times 41$ nodes in the cross-section plane. Further refining the mesh to $61 \times 61$ nodes gave a difference of $4\%$. Using the $570 \times 41 \times 41 = 9.6 \cdot 10^5$ mesh they achieved a comparable good agreement with measured data. The prediction, similarly to the experiment, showed a significant change in the heat transfer levels due to the rotational induced Coriolis force, with a reduction of up to $40\%$ on the leading face, and an increase on the trailing face by up to $35\%$.

In a similar case [155], however with normal ribs, and at a lower Reynolds number ($Re_B = 7\,900$) Rigby [177] employed the LRN $k-\omega$ turbulence model [208]. A satisfactory agreement with measured data could however only be achieved through a modification to the boundary for $\omega$ as proposed in [136], in connections with the rough-wall modification by Wilcox [207]. It was found that the predicted heat transfer (or actually mass transfer) was significantly influenced by the assumed wall-roughness and varied by a factor of three between the used roughness values. With the assumption of a smooth wall the flow didn't re-attach in-between the ribs, and hence the turbulence level and consequently the mass transfer was severely under predicted. Improved results were achieved with the rough wall, however the trends in the upstream and downstream leg were not captured.

The ribbed case equivalent to the smooth case studied in [31] was investigated by Iacovides *et al.* (experimentally: [87], [88] and numerically [85]) and also by the author, Paper VII [25]. Iacovides could reduce the computational requirement[4] through adoption of zonal turbulence models ($k-\varepsilon$ and RSM) and the usage of a bounded QUICK discretization scheme. The results showed the advantage of using the RSM in regions of flow separation, however the main flow features were still captured by the $k-\varepsilon$ model. In the case of negative rotation, with the rotation and curvature induced force opposed each-other, the agreements were significantly reduced as compared to the case with positive rotation. The cause may be the inability of zonal models to accurately asses these phenomenas within the near-wall region. Heat transfer predictions were not included in the study.

The author, in Paper VII [25], made a numerical study of the same case, $Re_B = 95\,000$, $Ro = 0.2$, with normal ribs arranged staggered, using a modified LRN $k-\omega$ turbulence model. The baseline model was

[4]The total number of nodes, with symmetry in the curvature-plane, were: $147 \times 38 \times 15 = 84 \cdot 10^3$

developed in Paper VI [28] with the coarse mesh modification introduced in Paper VIII [24]. It was discovered during the simulations that the cross-diffusion terms was numerically problematic and an additional modification was necessary to limit these terms. The result was both enhanced stability of the code and improved prediction of the heat transfer. Similar to previous studies discrepancies were found within the U-bend and immediately downstream the bend, however overall both the trends and the magnitude were in good agreement with measurements.

# Chapter 4

# Numerical Considerations

The CFD-code used in this thesis is presented. The consequences of numerical approximations and computational simplification are discussed. Mesh dependency problems in regards to turbulence models and geometrical configurations are addressed.

## 4.1 Numerical Method

The solution method used in this thesis for the governing equations (Navier-Stokes equations), is the Finite Volume Method (FVM). Using this method the particular computational domain is divided into a number of control volumes. The differential equations are discretized onto the computational mesh and numerically integrated over the control volumes. The set of equations are then solved iteratively until a convergence criteria is reached.

For these computations the incompressible FVM-code CALC-BFC [41] is used. There is a selection of discretizing schemes: hybrid, central, van Leer [199] or QUICK [125]. The governing equation for a specific variable, $\phi$, are after discretization expressed as:

$$a_p \phi_p = \sum_{nb} a_{nb} \phi_{nb} + S \tag{4.1}$$

where $a_i$ are the coefficients from the convective and diffusive terms. Index $p$ represents the nodal point and $nb$ the contribution from the neighbouring nodes. Source terms in the governing equations are included in $S$. In CALC-BFC this equation system is solved iteratively using a Tri-Diagonal Matrix Algorithm (TDMA). In order to improve

the diagonal domination in the TDMA solver, the source terms in the governing equations are added to the left-hand side if they are negative and on the right-hand side otherwise.

For incompressible flows the pressure needs to be carefully treated as the equation of state, $p = \rho RT$, is not suitable to use. In CALC-BFC the SIMPLE-C[1] [45] algorithm is used to deal with the velocity-pressure coupling.

The code uses Boundary-Fitted-Coordinates (BFC), with the nodes and grid points located in a non-staggered (ie. co-located) configuration. This procedure can induce a so-called checker-board solution, due to the velocity-pressure coupling. In CALC-BFC, as in many other CFD-codes, the Rhie-Chow [175] interpolation is used to smooth non-physical oscillations, arising from this type of grid arrangement.

## 4.2 Discretizing Schemes and Mesh Dependency

To discretize the diffusion terms CALC-BFC uses the central differencing scheme. In the numerical simulation performed within this thesis the convective terms are discretized using either the hybrid, or the van Leer scheme. It should be noted that the popular QUICK scheme is unbounded, which could lead to numerically stability problems if not care is taken. The hybrid and van Leer schemes on the contrary are bounded. In this work the pre-dominant choice has been the van Leer scheme.

The hybrid [191] scheme selects, dependent on the local Peclet number ($U/\Delta x$), whether an upwind or a central differencing approach is used. The order of accuracy for the hybrid scheme is between one and two.

In the van Leer [199] scheme the following algorithm is used:

$$\begin{aligned} \phi_e &= \phi_P && \text{if} \quad |\phi_E - 2\phi_P + \phi_W| > |\phi_E - \phi_W| \\ \phi_e &= \phi_P + \frac{(\phi_E - \phi_P)\,(\phi_P - \phi_W)}{(\phi_E - \phi_W)} && \text{otherwise} \end{aligned} \tag{4.2}$$

where $W, P, E$ are the west (upstream), point and east (downstream) nodal values, and $e$ is the approximated east face value. The van Leer scheme is second-order accurate, except at local minima.

[1] SIMPLE-C is a slightly modified extension of the SIMPLE [160] algorithm.

The progress of computer power, which enables increasingly fine mesh to be employed, along with the development of highly accurate discretizing schemes, has reduced the numerical errors. The result of this have made CFD-workers believe that the results from their CFD-codes are purely an effect of the chosen flow models (turbulence models), boundary conditions etc. This is to a certain degree true, however in special cases and for sensitive quantities there is still an influence on the result from numerical approximations made in the CFD-codes and from the meshes. To visualize this, two different cases are selected: I) a backward-facing step (BFS) case and II) the heat transfer from a rib-roughened channel. The two cases were simulated using CALC-BFC with both the hybrid and the van Leer discretizing schemes and with different levels of mesh refinement.

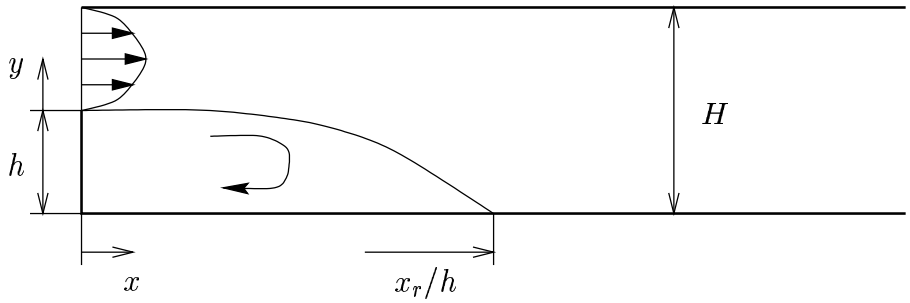


Figure 4.1: Geometry of Gartling BFS [53].

The BFS-case is the one studied by Gartling [53] who produced benchmark data. The Reynolds number is low[2] enough to enable a laminar simulation to be performed. The demands on the discretizing scheme increases as a result, as any numerical (artificial) diffusion will be much more pronounced if it is not clouded by the turbulent diffusion. The geometrical condition is shown in Fig. 4.1. The expansion rate, ie. the step-height to channel-height ratio, for this case is $h/H = 2$.

Two different meshes were used in the computations: a $100 \times 90$ mesh and a $200 \times 180$ mesh (streamwise by wall-normal), with the outflow located sufficiently far downstream ($x/h = 60$) to minimize the influence on the predicted results. The inlet was specified as a parabolic profile in $U$, as in [53]. The walls are well resolved on both meshes, with four and six nodes located within $y^+ = 1$ for the $100 \times 90$ and $200 \times 180$ mesh, respectively. In the region of interest the meshes are

[2]The Reynolds number is $Re_H = 800$ based on the channel height, $H$ and the bulk velocity

un-stretched in the streamwise direction, and only gently stretched in the wall-normal direction, with a maximum ratio, located at the walls of 4% and 1%[3], respectively.

The discretizing schemes are compared for the predicted streamwise ($U$), and the cross-stream ($V$) velocity profiles at $x/h = 7$. This station is located immediately downstream the re-attachment point, at $x_r/h = 6.1$ (benchmark data).

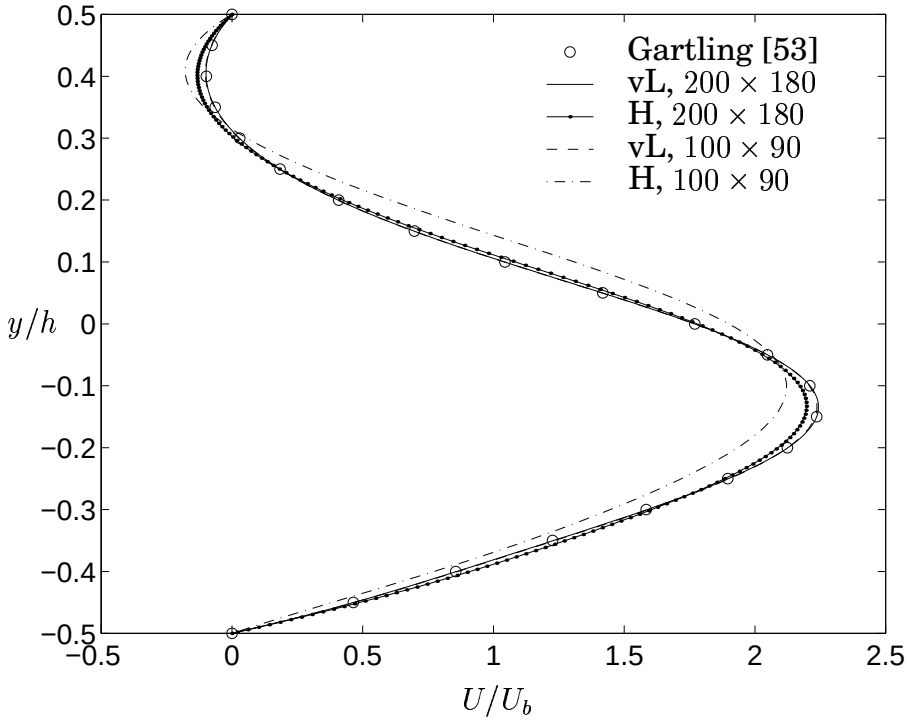


Figure 4.2: $U$-velocity at $x/h = 7$, BFS. Prediction using: Hybrid (H) and van Leer (vL) discretizing schemes.

It is shown in Fig. 4.2 that the hybrid scheme is rather sensitive to the used mesh, while the van Leer scheme predict identical profiles for both meshes. The hybrid scheme is even for the refined mesh unable to accurately estimate the streamwise velocity. The discrepancies for the $V$ profile is even more pronounced, see Fig. 4.3, with the van Leer scheme on the fine mesh is the only simulation which produced an acceptable accuracy.

The rib-roughened channel is the one studied experimentally by Rau *et al.* [171]. The Reynolds number based on the bulk velocity is $Re_B =$

[3]The stretch-rate is defined as the ratio of the cell-heights of two neighbouring cells: $\Delta y_{j+1}/\Delta y_j$

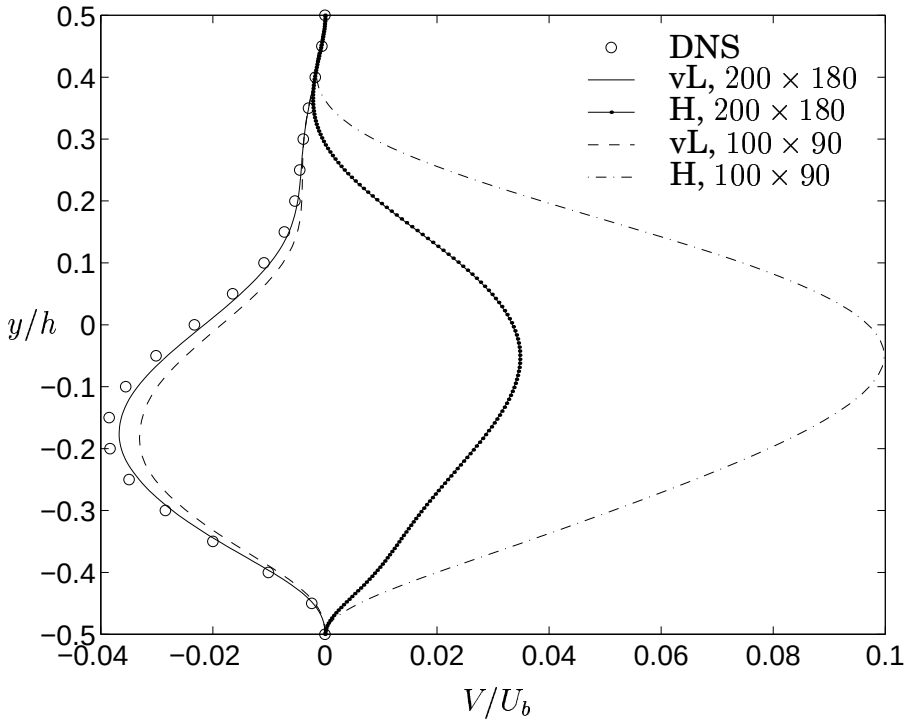


Figure 4.3: $V$-velocity at $x/h = 7$, BFS. Prediction using: Hybrid (H) and van Leer (vL) discretizing schemes.

30 000. The ribs are square with a rib-size of $e/H = 0.1$, and located along the bottom (south) wall with a pitch of $P/e = 9$, see Fig. 4.4. A constant heat flux boundary condition was applied at the bottom wall, with the rib insulated.

The measured and the predicted Nusselt numbers are normalized with the Dittus-Boelter equation [43], as introduced by McAdams [135]:

$$Nu_\infty = 0.023 \cdot Re^{0.8} \cdot \mathrm{Pr}^{0.4} \tag{4.3}$$

The computations were made using periodic boundary conditions at the streamwise boundaries.

Four different meshes were used: one with $200 \times 240$ nodes, two with $100 \times 120$ nodes and one with $50 \times 60$ nodes (streamwise $\times$ wall normal). For the coarsest mesh the first interior computational node was located beyond $y^+ = 1$, although within the viscous sub-layer.[4] It was thus of importance to use a turbulence model which is insensitive to the

[4]It would however be possible through a better node distribution to construct a $y_1^+ < 1$ mesh.

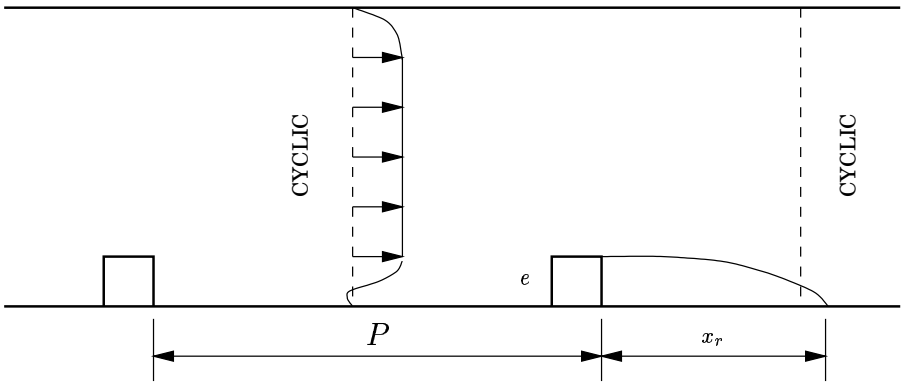


Figure 4.4: Geometry, rib-roughened channel, [171].

location of the first node. Using the conclusions from Paper VI, the AKN $k-\varepsilon$ turbulence model [2] was selected. The meshes with some predicted data are summarized in the table below:

| Mesh | $200 \times 240$ | $100 \times 120*$ | $100 \times 120$ | $50 \times 60$ |
|---|---|---|---|---|
| $y_1/H$ | $6 \cdot 10^{-5}$ | $1.2 \cdot 10^{-4}$ | $5 \cdot 10^{-4}$ | $2 \cdot 10^{-3}$ |
| $y^+_{1,s,max}$ | 0.09 | 0.2 | 0.7 | 2.8 |
| $y^+_{1,n,max}$ | 0.15 | 0.3 | 1.0 | 4.6 |
| $\Delta y_{j+1}/\Delta y_j$ | 14% | 30% | 15% | 12% |
| $Nu^h_{av}$ | – | 190 | 192 | 188 |
| $Nu^{vL}_{av}$ | 186 | 190 | 191 | 192 |

$y_1/H$, $y^+_{1,s}$ and $y^+_{1,n}$ denotes the first node location for the south (ribbed) and north wall, expressed both as normalized with the local friction velocity ($y^+$) and the channel height ($y/H$). Due to the variation of the skin-friction the $y^+$ along the south wall varies between the maximum values, given by the table, and zero at re-attachment points.

$\Delta y_{j+1}/\Delta y_j$ gives the maximum stretching for a certain mesh. A rule of thumb is that this should be less than $20\%$ to ensure that the predictions are not corrupted by negligence of higher order terms in the estimation of gradients. Even for the most stretched mesh a comparison between the predicted result using the hybrid and van Leer scheme does not indicate any influence from this numerical approximation.

Figure 4.5 gives the predicted variation of the normalized Nusselt number along the south, ribbed, wall. The insulated rib is located at $4 < x/e < 5$. To more clearly show the difference the graphs are cut for $Nu/Nu_s < 2$, which yield a visual impression that there are substantial difference between the predicted results. The maximum deviation

is however a mere $5\%$, which is less than the deviation between two turbulence models. The used discretizing scheme is irrelevant for a mesh independent solution, however on coarse meshes the results may differ by a percent or two.

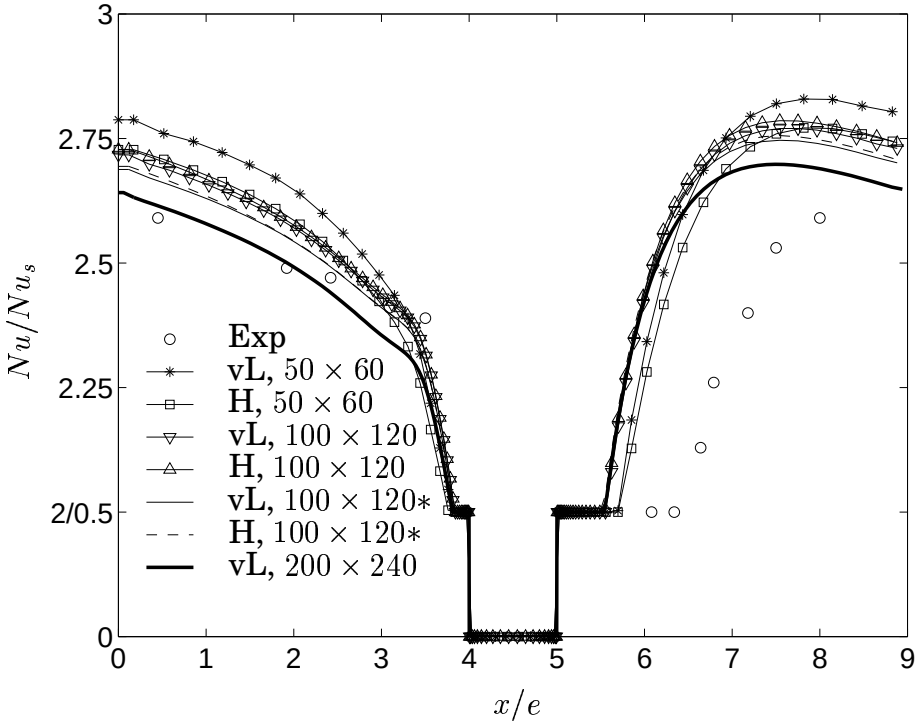


Figure 4.5: Normalized Nusselt number for rib-roughened channel [171]. Predictions using Hybrid (H) and van Leer (vL) discretizing schemes. Observe the non-uniform $y$-axis.

## 4.3 Boundary Conditions

What distinguishes how a fluid flow in a case from another case depends solely on the boundary condition. The treatment of boundary conditions are thus of paramount importance in numerical simulations. Improper boundary conditions treatment may cause significant discrepancies in predicted results. Boundary conditions may be classified into:

- Inlet/outlet conditions
- Walls

In numerical simulations there also exists periodic and symmetry conditions which can only be an approximation of the real nature. See further in the Sections 4.4 and 4.5 below.

It is uncommon that all the required data are measured to enable an exact specification of the inlet condition. Numerical simulations will thus, at least for a certain distance, be corrupted as a result of the erroneous inlet. The outlet condition on the other hand could for most experiments be fairly accurately specified. For certain flows, with periodic repeated geometries, the specification of the inlet and outlet are given by the periodic boundary condition, and hence these cases are advantageous from a numerical standpoint, see Section 4.4 below.

For impermeable, stationary walls the correct near-wall behaviour is govern by the no-slip condition which states the following conditions for the flow quantities:

$$\begin{aligned} U &= 0 \\ V &= 0 \\ W &= 0 \end{aligned} \tag{4.4}$$

The thermal boundary condition is case-dependent, however for all cases within this thesis a constant heat-flux relation is applied at the wall. The turbulent quantities adhere to the following near-wall asymptotic relations, see eg. [161]:

$$\begin{aligned} -\overline{u'v'} &\sim y^3 \\ k &\sim y^2 \\ \varepsilon &\sim y^0 \\ \omega &\sim y^{-2} \end{aligned} \tag{4.5}$$

The modelling issues due to these conditions were briefly discussed in Section 3.1 above. A lengthier discussion is found in Papers IV [20] and V [21].

## 4.4 Periodic Flows

For a constant property fluid, flowing in a duct with constant cross-section area, the velocity profile becomes independent on the streamwise coordinate at some distance from the inlet. The flow is then said to be fully developed. For numerical simulations this case is advantageous as it is sufficient to use only a one-dimensional computational domain

to compute the flow. It should be recognized that a fully developed flow could be difficult to realize in an experimental rig, as the inlet condition can influence sensitive flow parameters, such as the Nusselt number, as far as 100 diameters downstream the inlet [105]. Care must thus be taken when comparing experimental data with results from a simulation.

A case similar to the fully developed flow, is the periodic flow. There exists a number of engineering applications where the geometry is repeated at a certain interval. One example is ducts in a turbine blade, where ribs are inserted at specific intervals to augment heat transfer. The flow will, after an entry length, repeat itself in a periodic manner within each rib-interval. In a duct for which the ribs are located at repeated intervals, $L$, the velocity components exhibits a periodic behaviour, in the streamwise direction, as:

$$\begin{aligned} U(x,y,z) &= U(x+L,y,z) \\ V(x,y,z) &= V(x+L,y,z) \\ W(x,y,z) &= W(x+L,y,z) \end{aligned} \tag{4.6}$$

The pressure may be decomposed in a similar manner. If the pressure distribution is plotted for two rib-intervals, the curves will have identical shapes (sufficiently downstream the inlet) but with a shift in level. The reason for this shift is the continuous pressure drop in the streamwise direction due to the friction along the walls and the pressure loss as a result of the ribs. The distance between the curves is the total pressure drop from a rib-interval, which can be expressed as:

$$\beta = \frac{P(x,y,z) - P(x+L,y,z)}{L} \tag{4.7}$$

The pressure at any streamwise location may thus be formulated as:

$$P(x,y,z) = -\beta x + \tilde{P}(x,y,z) \tag{4.8}$$

where $\tilde{P}$ denotes the pressure variation within the rib-interval. When the independent variables can be decomposed in the above manner, the numerical solution may be restricted to only a single rib-interval, with a substantial reduction in computational resources. The only modification needed to the Navier-Stokes equation is to include the streamwise pressure drop coefficient, $\beta$.

The thermal equation may be treated in a similar fashion to the momentum equations. If a constant heat-flux wall boundary condition

is applied a particularly simple relation is found for the temperature variation:

$$T(x, y, z) = \gamma x + \tilde{T}(x, y, z) \tag{4.9}$$

where $\gamma$ is the continuous rise in the temperature in analogy to the pressure drop. $\gamma$ is deduced from the applied total heat-flux as:

$$\gamma = \frac{Q}{\dot{m} C_p L} \tag{4.10}$$

See Patankar *et al.* [159] for a discussion and examples of different thermal boundary conditions.

## 4.5 2D Approximations

A common approximation made in numerical simulation is to reduce the computational domain to 2D to save both computational resources and time. It is only recently (the last couple of years) that it has become reasonable to perform 3D simulations on a regular basis. However the affordable grid density on a 3D mesh is still not enough for accurately resolving near-wall sensitive parameters, such as the Nusselt number. Because the emphasis of the thesis is heat transfer predictions, most results presented in the papers have been based on 2D computations. Occasionally a 3D mesh dependency check have been made for a certain mesh density (obviously rather coarse) see eg. Paper VI [28]. The general anticipation when making use of 2D simulations is that they are a fair representation of the conditions along the center-plane of the configuration. The accuracy of such a simplification depends on the degree of secondary flows present in the flow. If they are weak, in eg. a smooth square duct, the conditions for a 2D and along the center-plane of a 3D simulations becomes indistinguishable. In cases when the secondary flows have an influential effect on the flow, a 2D simulation can only be rough estimation of the real conditions.

A questionable example is the rib-roughened channels, as the one examined by Rau *et al.* [171], which have been repeatedly used as a test case in this thesis. Even though there is no direct generation of secondary flow, the ribs introduce a weak spanwise redistribution, as previously discussed and visualized in Fig. 3.6. From that figure it is obvious that the Nusselt number along the centerline is different from the one predicted closer to the side-walls. The question whether the

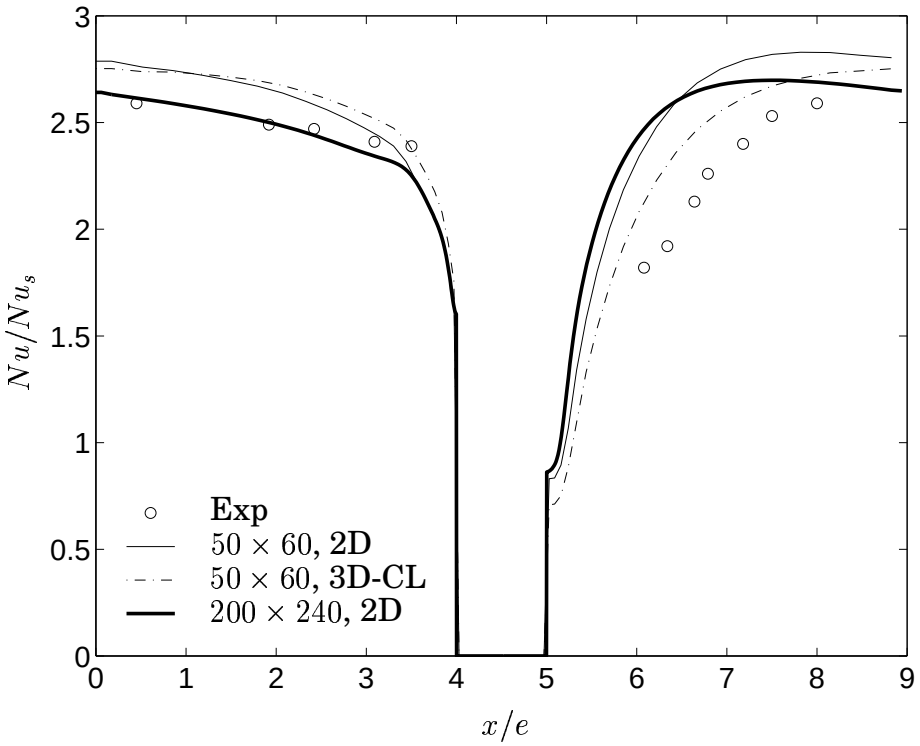


Figure 4.6: Normalized $Nu$ on centerline for a rib-roughened channel [171] using 2D and 3D computational domains. 3D-CL represent the result along the centerline for a 3D domain.

centerline Nusselt number in a 3D domain is in accordance with that predicted using a 2D approximation is partly resolved by Fig. 4.6. Comparing the 2D and 3D simulations using the $50 \times 60$ mesh (streamwise by wall-normal), it is apparent that the overall heat transfer level in the center of the 3D duct is similar to that in the 2D duct. The main difference is found in the region downstream the rib, $5 < x/e < 8$ in the figure. The 3D secondary flows delays the increase in Nusselt number in the re-circulating zone, however the discrepancies are less than $10\%$. The inclusion of a refined 2D mesh in the figure also show that the results on the $50 \times 60$ meshes are not asymptotically valid, and hence the conclusion drawn from this comparison may be altered. Ooi *et al.* [150] made a 2D and 3D comparison on a similar rib-roughened configuration [87] and found that the predicted Nusselt number were almost the same but the streamwise velocity differed by 10%.

# Chapter 5

# Results and Discussion

It was the desire to leave the presentation of result and discussion to the individual papers. However as significant results and conclusions were only included in the thesis for the degree of licentiate of engineering [19], some of those results are republished below. That refer especially to the effect that rotation has on turbulence, and the way models can account for this effect. It will become obvious, as discussed in Chapter 3, that although turbulence induced by rotation is of importance for simple flows it is less so for more complex flows, such as a rib-roughened 3D-channels.

## 5.1 2D Rotating Channel

In a rotating 2D case with infinite width, the otherwise dominant Coriolis force is not present, and instead the cross-stream flow is governed by second-order effects. As previously discussed the standard two-equation eddy viscosity model cannot capture turbulence induced secondary flows and as a consequence the predicted velocity profiles are fully symmetric irrespectively of the rotational numbers. To mimic the features shown in DNS-data and experiments, a number of modifications are possible for the standard EVM; these include adding non-linear terms, as in EARSM, or modifying either the $k$- or $\varepsilon/\omega$-equation.

The models and modifications that have been used by the author in simulations for the 2D rotating duct are listed in Table 5.1. A number of the listed models, marked, are only included in the thesis of Licentiate of Engineering [19]. The reader is thus also referred to [19] for a more extensive discussion and analysis of the present case.

| # | Baseline model | Non-linear terms | Modification | Notes |
|---|---|---|---|---|
| 1 | ARG $k-\omega$ | - | - | In [19] |
| 2 | ARG $k-\omega$ | - | $k$-equation | In [19] |
| 3 | ARG $k-\omega$ | - | $\omega$-equation | In [19] |
| 4 | WLR $k-\omega$ | - | - | |
| 5 | WLR $k-\omega$ | - | $k$-equation | |
| 6 | WLR $k-\omega$ | - | $\omega$-equation | |
| 7 | ARG $k-\varepsilon$ | - | - | In [19] |
| 8 | ARG $k-\varepsilon$ | - | $k$-equation | In [19] |
| 9 | ARG $k-\varepsilon$ | - | $\varepsilon$-equation | In [19] |
| 10 | ARG $k-\omega$ | LRR-EARSM-GS | - | |
| 11 | ARG $k-\omega$ | LRR-EARSM-GS | $\omega$-equation | |
| 12 | ARG $k-\omega$ | SSG-EARSM-GS | - | In [19] |
| 13 | ARG $k-\omega$ | SSG-EARSM-GS | $\omega$-equation | In [19] |
| 14 | ARG $k-\varepsilon$ | SSG-EARSM-GS | - | In [19] |
| 15 | WLR $k-\omega$ | LRR-EARSM-WJ | - | |
| 16 | ARG $k-\varepsilon$ | LRR-EARSM-WJ | - | In [19] |

Table 5.1: Turbulence models, 2D rotating duct. ARG is the Abid, Rumsey and Gatski $k-\varepsilon$ and $k-\omega$ models [3]. WLR is the low-Reynolds number modified Wilcox $k-\omega$ model [208]. EARSM-GS is the EARSM by Gatski and Speziale [54]. EARSM-WJ is the EARSM by Wallin and Johansson [203]. LRR [120] and SSG [193] denotes the pressure-strain model. Modifications to $k, \varepsilon$ and $\omega$ equation according to Wilcox and Chambers [210] and Hellsten [74], respectively.

The rotating 2D case studied by Kristoffersen and Andersson [109] using DNS is the one used here to evaluate the capability of turbulence models to capture rotational induced turbulence. The Reynolds number based on the channel half-height is $Re = U_m h/\nu = 2900$, which is equivalent to a wall-shear Reynolds number of $Re_\tau = u_\tau h/\nu = 194$. The present computation was made on mesh measuring $30 \times 100$, with 100 nodes in the wall normal direction, giving enough nodes to achieve a $y^+$ value of less than one for the first node. 30 nodes were used in the streamwise direction, even though the flow is fully developed and essentially a 1D prediction could have been done. The extra nodes in the streamwise direction were used to smooth out any iteration fluctuations in the massflow rate. The DNS database has a number of different rotational numbers, only the $Ro_H = 2\Omega h/U_m = 0.2$ has been

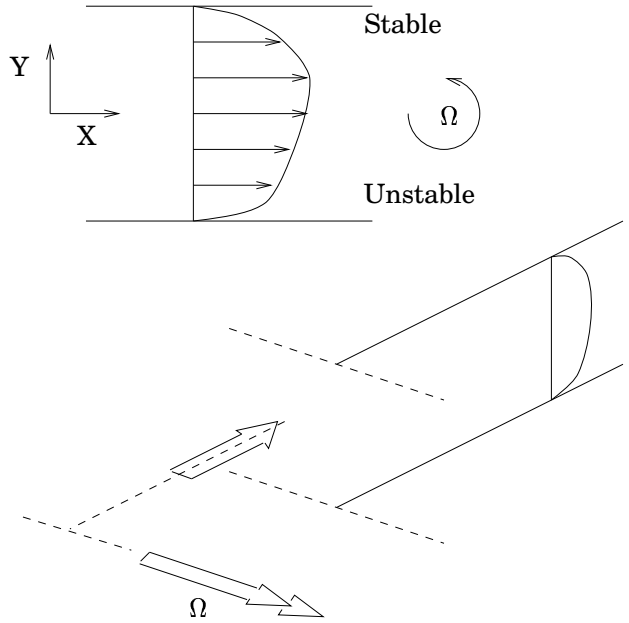


Figure 5.1: Geometry of 2D rotating channel

used for comparison here. This rotational number was chosen because it is in the range found in turbine blades in gas turbines and it is high enough to clearly indicate the problems the different turbulence models have in predicting the flowfield. The most striking difference between a rotational and a stationary 2D duct prediction is the amplification of the turbulent kinetic energy on the unstable side, and the reduction of the same on the stable side for the rotating case. This changed level of turbulent kinetic energy affects the mean velocity profile as well through a stabilization process on the stable side and a more sharp gradient on the unstable side – as can be seen on the schematic figure, Fig. 5.1.

One of the fundamentally important parameters closely connected to this process is the friction velocity, $u_\tau$, at the two walls. Table 5.2 compares the predicted friction velocity from the different turbulence models and from the DNS data. A high $U_m/u_\tau$, and thus a low $u_\tau$, indicates a low value of the turbulent kinetic energy. Apart from the standard EVM (eg. the $k-\omega$ model), all models predict higher levels of $u_\tau$ on the unstable side than on the stable side. Two-equation EVMs predict equal friction velocities on both sides, clearly a large discrepancy for non-modified EVMs. However none of the models yield accurate agreement with near-wall DNS data, although reasonable mean properties

| # | Model | $U_m/u_\tau$ | $U_m/u_{\tau s}$ | $U_m/u_{\tau u}$ |
|---|---|---|---|---|
| - | DNS | 15.23 | 18.54 | 10.76 |
| 4 | $k-\omega$ | 13.77 | 13.77 | 13.77 |
| 5 | $k-\omega$ mod $k$ | 12.79 | 15.79 | 11.03 |
| 6 | $k-\omega$ mod $\omega$ | 15.09 | 20.12 | 12.59 |
| 10 | EARSM-GS-$k-\omega$ | 16.00 | 17.17 | 15.04 |
| 11 | EARSM-GS-$k-\omega$ mod $\omega$ | 12.54 | 15.67 | 10.75 |
| 15 | EARSM-WJ-$k-\omega$ | 18.46 | 20.16 | 17.13 |

Table 5.2: Predicted wall friction (friction velocity) with models used here. Numbers as given in Table 5.1. $u_{\tau s}$ stable side (laminar), $u_{\tau u}$ unstable side (turbulent), $u_\tau = \sqrt{0.5(u_{\tau s}^2 + u_{\tau u}^2)}$.

could still be predicted as noted in the figures below.

The velocity profiles normalized with the bulk velocity, $U(y)/U_B$, are depicted in Fig. 5.2. Note that DNS data in [109] is given as $U^+(y)$ and hence the data presented here is re-normalized. The 2D duct is rotating (positively) around the $z$-axis, and thus the stable (laminar) side is found at $y = +1$ and the unstable (turbulent) side at $y = -1$.

In the case of the standard two-equation turbulence model without any modifications, a fully symmetric velocity profile is predicted, as expected from the discussion in Chapter 3. Adding the modification to the $k$-equation according to [210] (mod $k$) gives quite a large shift in turbulent kinetic energy, see Fig. 5.3(a), although the asymmetry of the velocity profile is under predicted. If instead the length-scale equation is modified according to [74] (mod $\omega$), the velocity profile agrees with the DNS data more closely, but still the slope of the velocity profile in the center of the channel is somewhat off. The slope of the velocity profile is connected to the stability criteria and is thus an important parameter. Neutral stability is given by $Ri = 0$, see Johnston *et al.* [100], which is equivalent to $2\Omega - du/dy = 0$ from the Richardson number definition.

The EARSMs predict the slopes rather well, see Fig. 5.2(b), although they predict too a strong laminarization process on the stable side. The near-wall behavior ($u_{\tau s}$) is however rather close to the DNS data in most cases, see Table 5.2. Using the Wallin and Johansson EARSM instead of the Gatski and Speziales EARSM alters the velocity profile so that the agreement with the DNS data improves. However, the only way to predict very good agreement is to add a Richardson number modification to the length-scale equation as can be seen in Fig. 5.2(b).

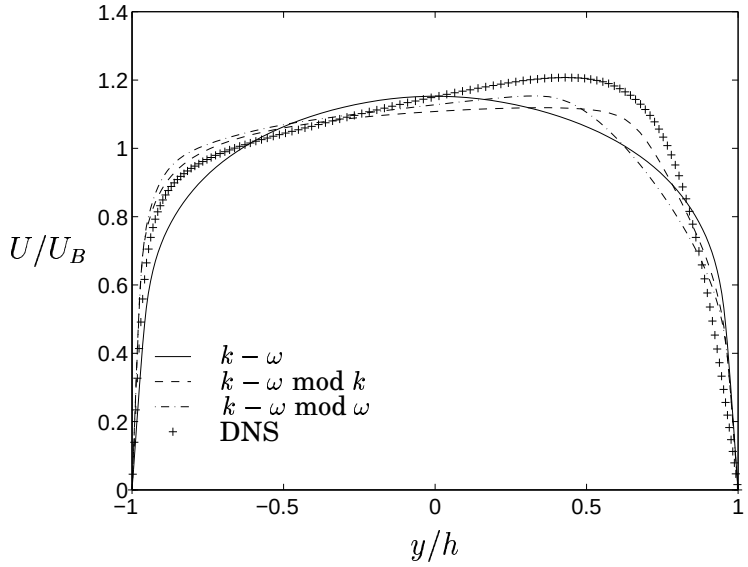


(a) $k-\omega$ models.

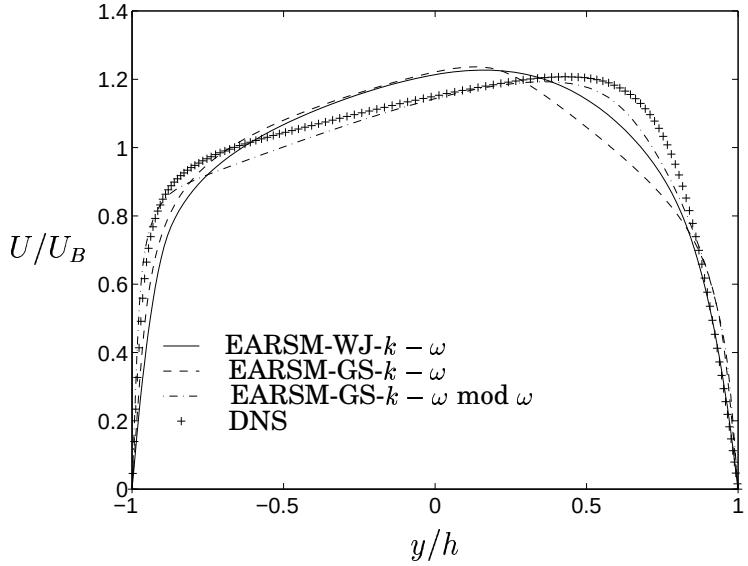


(b) EARSM models.

Figure 5.2: Velocity profiles, rotating 2D-duct

The velocity profile is the most important parameter in any engineering flow and is of great value when discussing the turbulence models. Still in order to quantify turbulence models, a turbulent quantity is

necessary. In this case, the turbulent kinetic energy was chosen. The turbulent kinetic energy profiles, normalized with the bulk velocity, $k(y)/U_B^2$, are shown in Fig. 5.3.

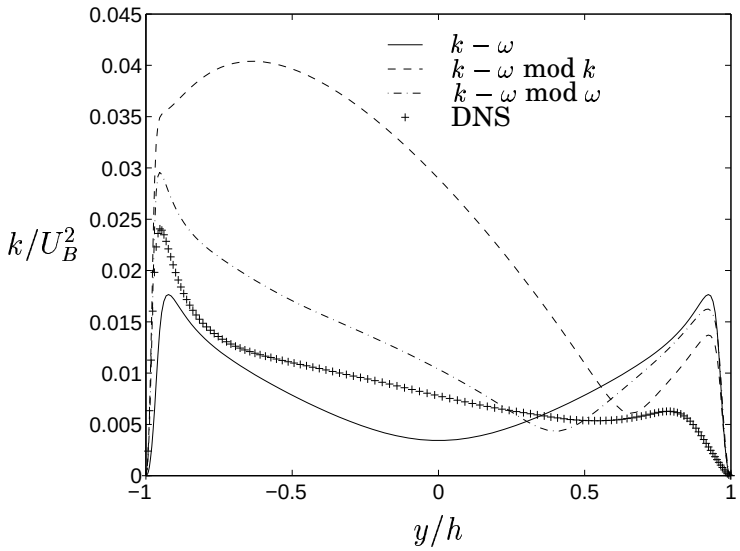


(a) $k - \omega$ models.

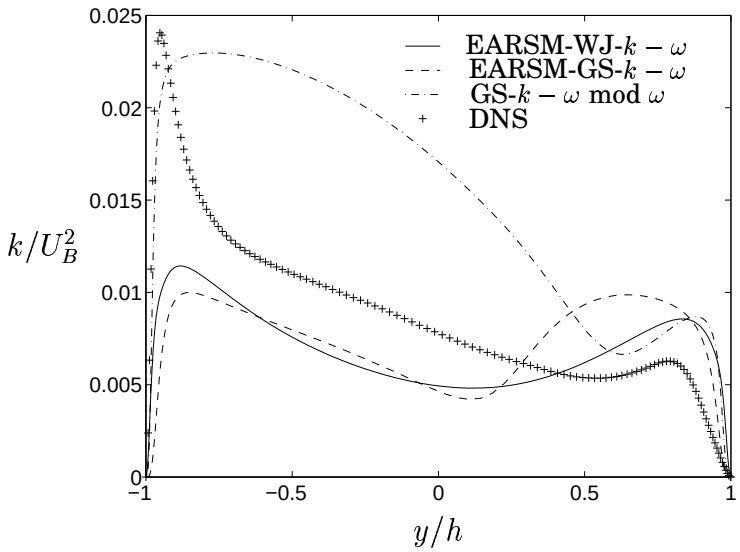


(b) EARSM models.

Figure 5.3: Turbulent kinetic energy, rotating 2D-duct

The first striking discrepancy is the terrible prediction of $k$ using

the modified $k$-equation in Fig. 5.3(a). Almost equally bad is the $k$-profile using the non-modified EVM, which, as for the velocity profile, is fully symmetric around the centerline of the duct. By adding the simple Richardson number modification, the $k$-profile improves quite a bit. The peaks in the turbulent kinetic energy close to the walls is fairly well captured, as is the asymmetric profile. The overall agreement may however leave a bit more to desire.

In the case of the EARSMs, Fig. 5.3(b), the EARSM-GS do not greatly change the symmetric profile of the standard EVM which can be explained by the rather small anisotropy values captured by this model. Since the model is constructed in such a way, that only small anisotropy values are allowed, it is expected that only a slightly asymmetrical profile of the turbulent kinetic energy is predicted. A comparison of the EARSM-GS and the EARSM-WJ, shows some differences. The EARSM-WJ is able to capture more of the re-laminarization process on the stable side, and the peak on the unstable side is a bit higher, although the differences are quite small. Similar to the two-equation model it is necessary to add the Richardson number modification to the EARSMs to achieve satisfactory agreement with DNS data. From Fig 5.3, it is completely clear that the most important change is the Richardson number modification. Notable is also the small difference between the EARSM-GS-$k-\omega$ mod $\omega$ and $k-\omega$ mod $\omega$.

## 5.2 3D rib-roughened channel with periodic boundary conditions

The previous test case, the rotating smooth 2D duct, showed a significant impact of the chosen turbulence model on the predicted flowfield. It was concluded that the commonly used two-equation EVM did a poor job for that case. Below it will be shown that the inclusion of ribs and a finite spanwise length reduces the importance of accurately capturing the rotational effects on the turbulence field. Secondary flows generated by geometry and system rotation are govern by pressure and Coriolis effects (in the momentum equations) – both which are exactly captured even by the simplest turbulence model. Through comparing an EARSM and an EVM it will be shown that the turbulence induced secondary flows (corner effects) and the rotational induced turbulence are of significant lower magnitude and affect the result only marginally.

The geometric conditions for the present cases (pitch-to-height ratio of $P/e = 10$ and a height-to-height ratio of $e/H = 0.1$) are shown in Fig. 5.4. As indicated in that figure, there are ribs on both walls, which are staggered in relation to each other. For a staggered configuration, the calculation domain is increased, as compared to a inline arrangement, because the symmetry condition on the centerline cannot be applied and hence both the upper and lower walls with the ribs must be included in the computation. For the current case there exists however a symmetry plane in the $z$-direction, at $z/H = 0.5$, which enables the calculation domain to be reduced to half. For these two cases (the stationary and rotating), three different computation meshes have been used: the coarse mesh which measured $60 \times 60 \times 25$, the medium mesh of $96 \times 96 \times 40$, and the fine mesh of $100 \times 115 \times 50$.

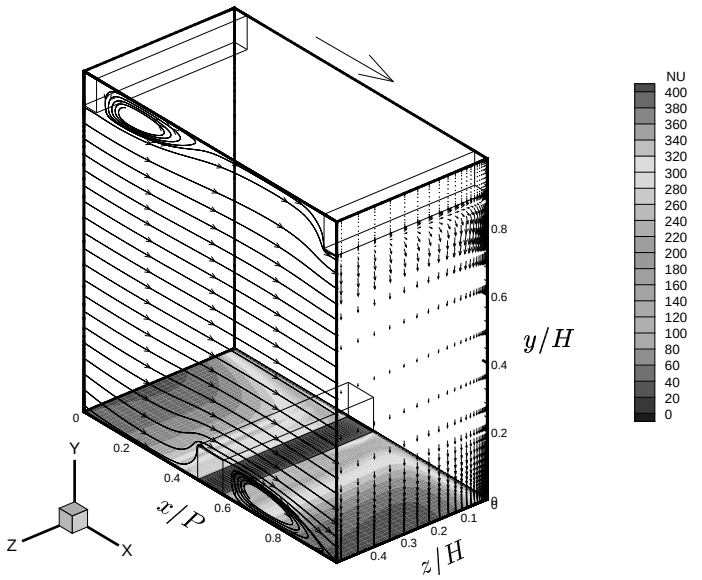


Figure 5.4: Streamlines and Nusselt number Abid *et al.* $k - \omega$ model [3], stationary ribbed channel. Symmetry plane at $z/H = 0.5$. Every second node is plotted.

In the licentiate thesis [19] an grid-independence check was included. On the basis of the compared velocity profiles it was found sufficient to use only the coarse and medium meshes. For the present analysis computations made on the fine mesh was also included as it is apparent that near-wall sensitive quantities, such as the Nusselt num-

ber shown in Fig. 5.5(a) is not grid-independent.

The measured data of Iacovides *et al.* [86], [87] include: the streamwise velocity, $U$, the cross-stream velocity, $V$, the shear stress $\overline{u'v'}$, the normal stresses, $\overline{u'u'}$ and $\overline{v'v'}$, and the Nusselt number along the lower wall[1]. The Reynolds number based on the channel height for both test cases is $Re_H = 100\,000$[2], and the rotating number based on the channel height for the rotating case is $Ro_H = 0.2$. In the case of the velocity field the data are taken from four selected points, at the top of the ribs and in between the ribs. These four points are defined by $x/P = 0$ (at the inlet, centered on the first rib on the upper wall), $x/P = 0.25$ (in the middle between the first upper rib and the lower rib), $x/P = 0.5$ (at the top of the rib on the lower wall) and, finally, at $x/P = 0.75$ (in the middle between the rib on the lower wall and the second rib on the upper wall). The Nusselt number was measured along the lower wall excluding the rib. The heat-flux is transmitted through an electrical heater fixed at both the upper and lower walls. This enables a constant heat-flux at the walls to be achieved, which is also the boundary condition used in the computations.

The turbulence models used here are the Abid *et al.* $k-\omega$ model and the Gatski and Speziale EARSM [54] based on the Abid *et al.* $k-\omega$ with the LRR pressure-strain model [120]. In the licentiate thesis [19] results using the SSG pressure-strain model in connection with the Gatski and Speziale EARSM and the Chen and Patel zonal $k-\varepsilon$ model [32] were also used.

The stationary and rotating cases are presented separately below, starting with the stationary case.

### 5.2.1 Stationary:

The experimental and predicted Nusselt numbers with the two turbulence models for the stationary case are depicted in Fig. 5.5(b). The predicted Nusselt numbers are generally reasonable. The two turbulence models return similar profiles from $x/P = 0$ to the rib, although with different levels. On the downstream side of the rib the models deviate somewhat, with the $k-\omega$ predicting a larger plateau, indicating a larger secondary re-circulating zone downstream the rib. In [19] it was shown that the SSG-EARSM recovered slower than the two models presented here, more in agreement with the measurements.

[1]Heat transfer data was not measured for the rotating case.

[2]The heat transfer data in [87] was however measured at $Re_H = 95\,000$

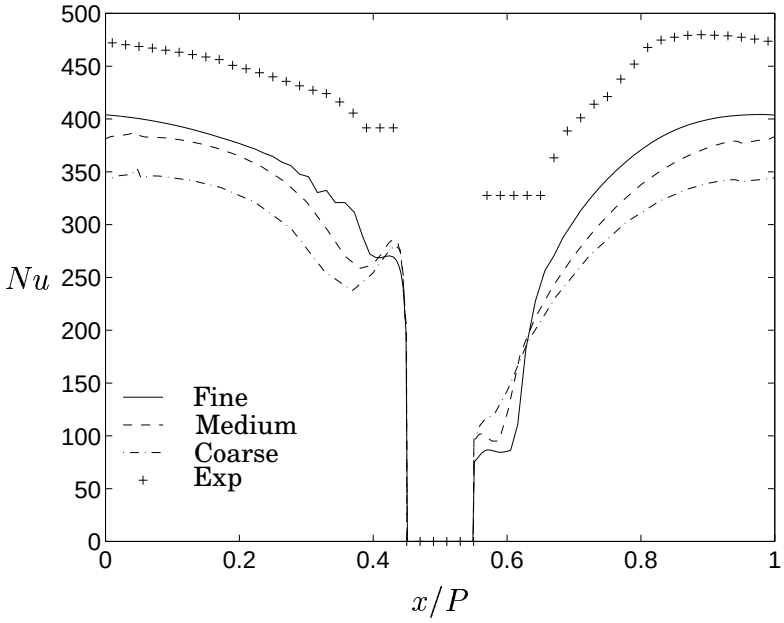


(a) Different meshes. $k-\omega$ model.

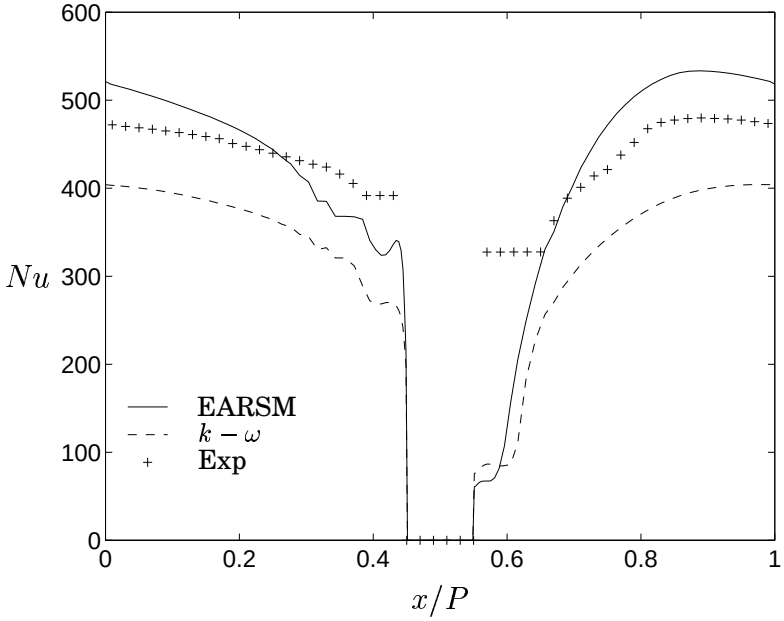


(b) Turbulence models.

Figure 5.5: Nusselt number. Stationary ribbed channel.

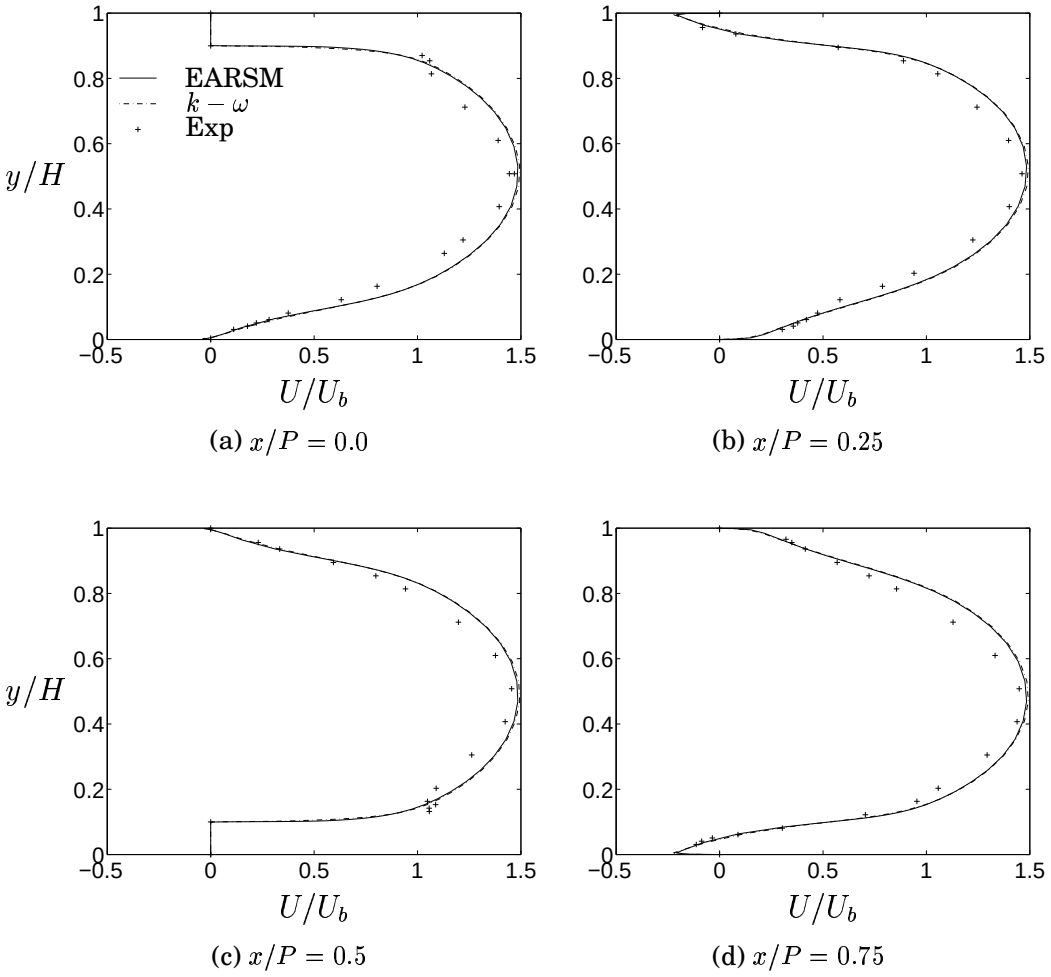


Figure 5.6: U-velocity profiles. Stationary ribbed channel.

The peak was predicted at the same point however, which is roughly in the middle between the ribs. The increased performance on the downstream side of the rib of the SSG-EARSM was however counterbalanced by a rather large predicted bump in front of the rib, see [19].

Moving on to the velocity field comparisons, there is great amount of data, and here only some of the more interesting profiles are included. In [19] there are in total 20 figures with five different velocity variables, at four different locations along the channel. For a general view of the velocity field for this test case, see the streamline plot in Fig. 5.4. The flow is characterized by a large re-circulation behind each rib, with a smaller bubble in front of each rib, as discussed in Section 3.2. The

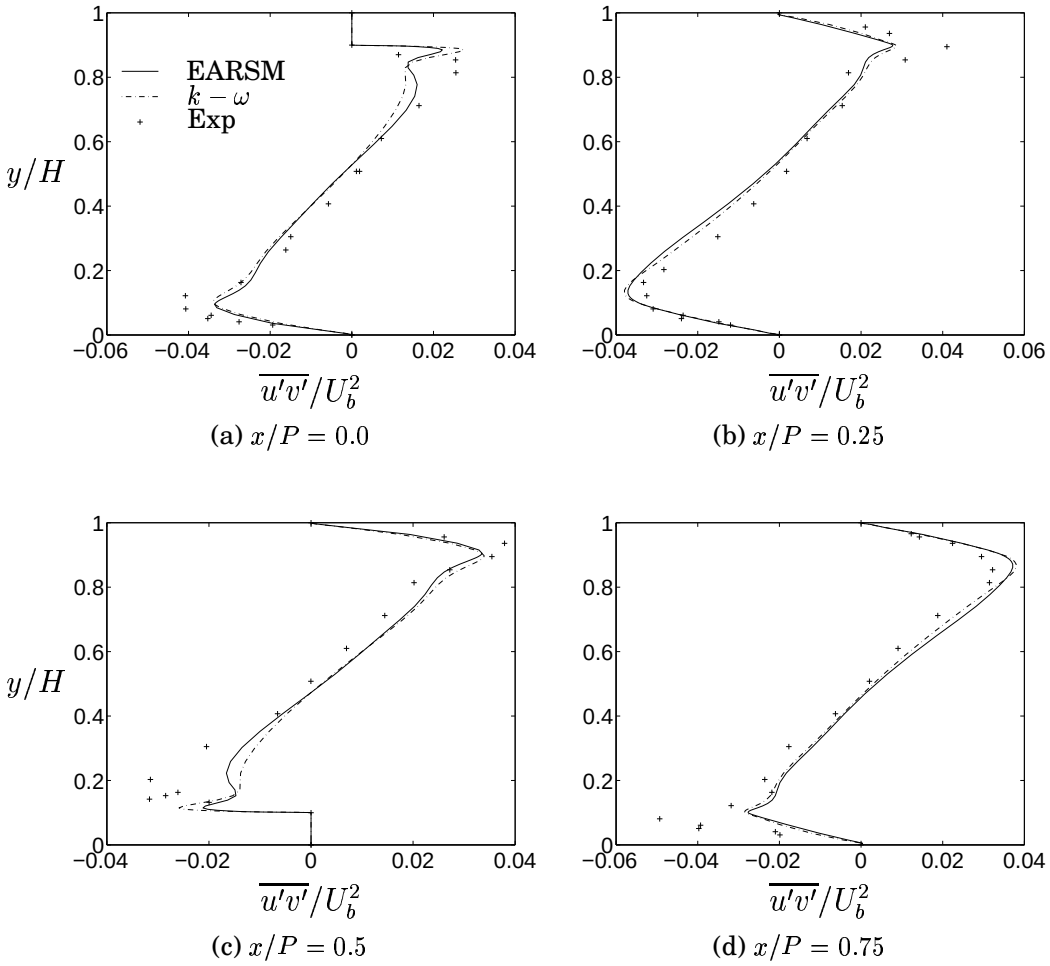


(a) $x/P = 0.0$ (b) $x/P = 0.25$

(c) $x/P = 0.5$ (d) $x/P = 0.75$

Figure 5.7: $\overline{u'v'}$-shear stress. Stationary ribbed channel.

streamwise velocity profiles are plotted in Fig. 5.6, with an almost indistinguishable difference between the models, both being in fairly close agreement with the experiment data.

The shear stresses, $\overline{u'v'}$, are depicted in Fig. 5.7. Both models return a rather good result for the important shear stress, which is the main influential Reynolds stress on the mean flow.

Fig. 5.8 shows the streamwise normal stress. As can be seen in these figures, the EARSM achieve slightly better agreement with the experimental data than the $k-\omega$ model, which is not surprising since EVMs cannot predict any anisotropy level for normal stresses.

The cross-stream normal stress, $\overline{v'v'}$, included in [19] showed a rat-

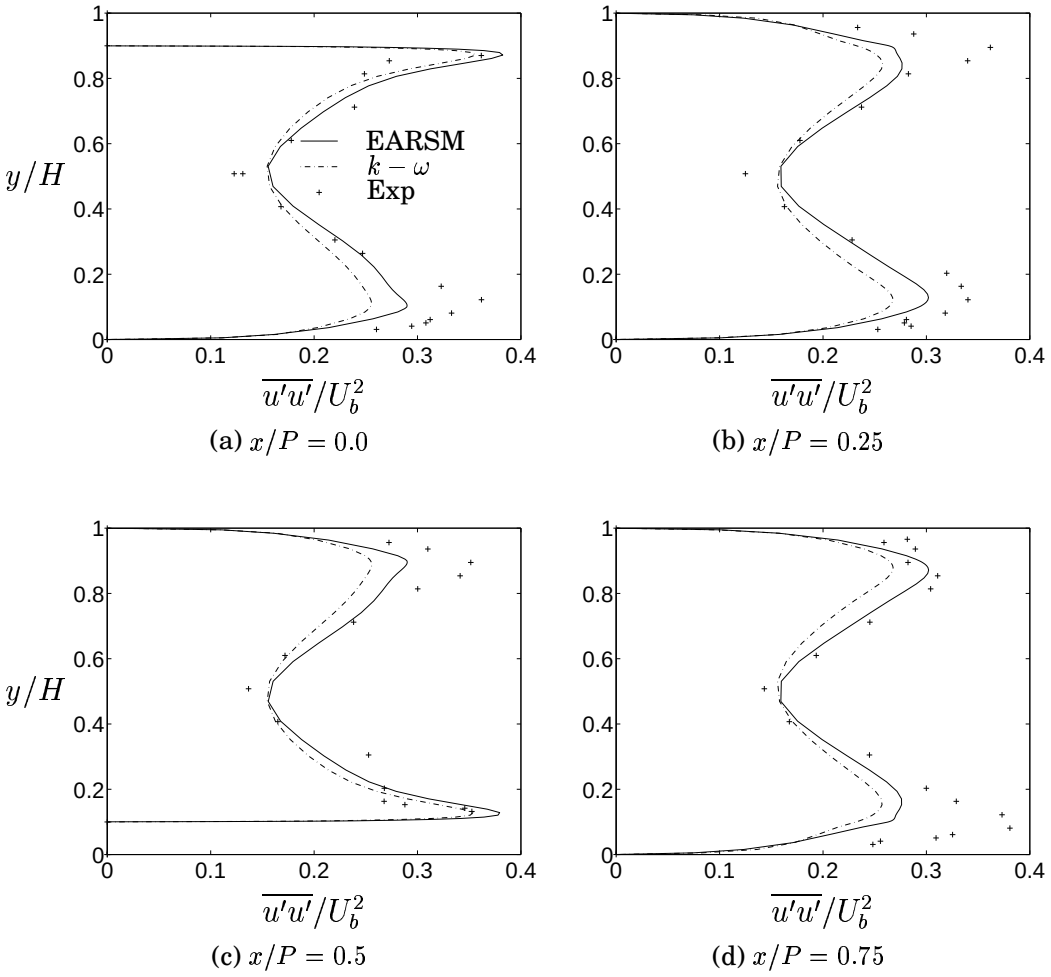


Figure 5.8: $\overline{u'u'}$-normal stress. Stationary ribbed channel.

her poor presentation of the SSG-EARSM, where the $\overline{v'v'}$ fluctuates violently behind the ribs, resulting in slow convergence rates. The conclusion was that the reason for this behavior was most likely mesh-dependent. The SSG-EARSM was not included here because of this, although the current mesh ($100 \times 115 \times 50$) is most probably better than the one used in [19].

### 5.2.2 Rotating:

For the rotating case, there are two sets of measurement data: velocity data for either a positive rotation at $Ro_H = 0.2$ or a negative rotation

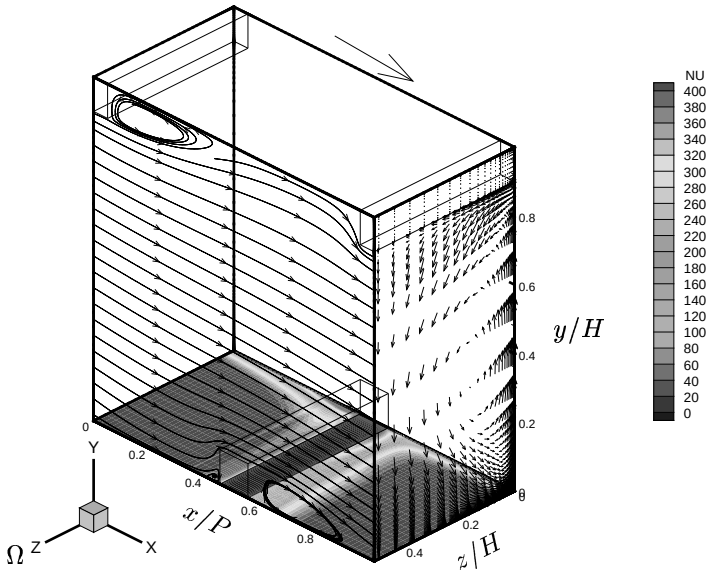


Figure 5.9: Streamlines and Nusselt number Abid *et al.* $k-\omega$ model [3], rotating ribbed channel. Symmetry plane at $z/H = 0.5$, rotation around $z$-axis: $Ro_z = 0.2$. Every second node is plotted.

of $Ro_H = -0.2$. In [19] predictions using both the clock-wise and the counter-clock-wise directions of the channel, ie. rotation around both the positive and negative $z$-axes, were compared. The rotationally induced forces shift the flowfield either to the upper wall (negative rotation) or the lower wall (positive rotation). It was concluded that, when mirrored, the predicted velocity profiles from the two rotational directions were identical for both models. However, depending on the rotational direction, the measurements deviate. This is not a surprising result as all experiments include some errors and, for any two sets of measured data, there will always be some deviation. The differences of up to $20\%$ can thus be seen as an error estimation for the experimental data.

Although there are several measured velocity profiles available, there are unfortunately no measured Nusselt numbers. The Nusselt number was nevertheless predicted as shown in Fig. 5.10. Figure 5.10(a) compares the difference between the upper wall – which in the case of positive rotation is the stable side – and the lower wall – the unstable side for the predicted Nusselt number. The inclusion of the stationary

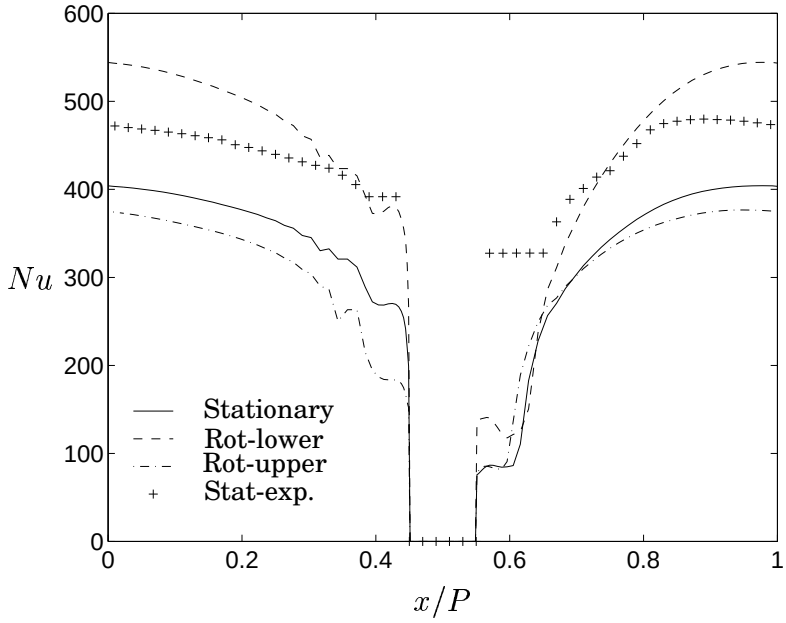


(a) Stationary vs rotating. $k-\omega$ model.

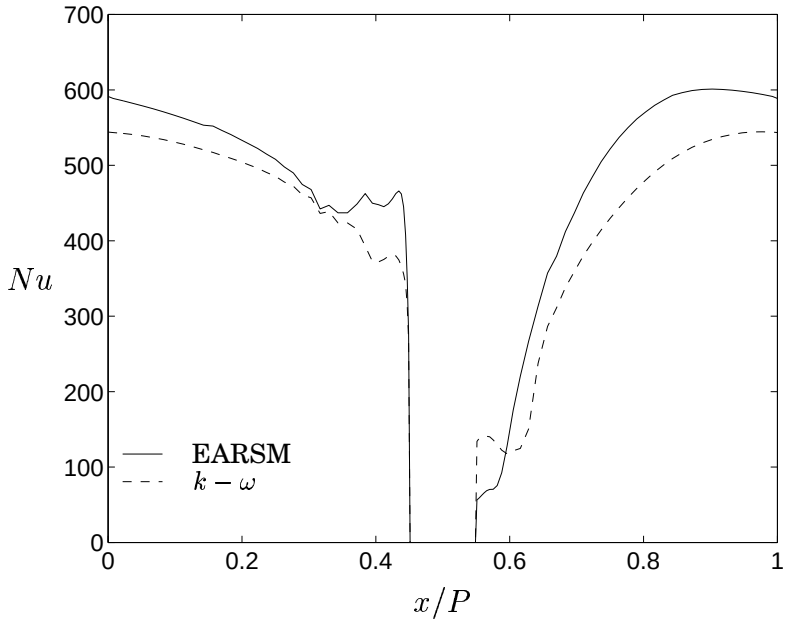


(b) Turbulence models.

Figure 5.10: Nusselt number. Rotating ribbed channel.

data gives a visual impression of the effect of rotation.

The main difference between the predicted Nusselt number for the rotating case as compared with the stationary case is the shift of the Nusselt number on the lower wall (increased) and upper wall (decreased), as can be seen in Fig. 5.10(a). The decrease on the upper wall is very slight, less than 10%. On the lower wall the increase is however much more dominant and amounts to roughly 30%, which is surely a desired affect. From this it can be concluded that the rotation increases the general level of heat transfer in ribbed channels. The relative change of the heat transfer is of course associated with the increase in turbulent kinetic energy on the unstable side (lower) and a similar decrease in the turbulent kinetic energy on the stable side (upper). Through the heat transfer model used in this report, equation Eq. 2.23, the eddy viscosity is directly related to the heat transfer, and thus an increase in turbulent kinetic energy would yield a higher Nusselt number and vice versa.

Apart from the change in the magnitude of the Nusselt number, the profiles are essentially the same, and the same conclusion as was made for the stationary case can be drawn regarding the performance in front of the rib and behind the rib. It can thus be concluded that there is no significant advantage of using an EARSM compared to an EVM for a rib-roughened 3D duct, stationary or rotating. A correct level of Nusselt number was also predicted for this case in Paper VII [25] using a $k-\omega$ turbulence model.

Moving on to the velocity field, the streamlines for the Abid *et al.* turbulence model are shown in Fig. 5.9. Comparing the rotating case, Fig. 5.9, with the stationary case, Fig. 5.4, reveal a change in flow structure. The latter, stationary case, has a symmetric behavior, where the flowfields on the upper wall and the lower wall are essential the same, although shifted half a pitch. The rotating case, on the other hand, do not posses this symmetry, as the Coriolis force ($2\Omega_z U$) shifts the velocity field downwards. Consequently the re-circulation region behind the upper first rib is much larger than that behind the lower mid-rib, see Fig. 5.11. As in the stationary case, there is a re-circulation bubble in front of the ribs as well, although this is very much suppressed on the lower wall, while it is amplified on the upper wall.

The streamwise velocity profiles are depicted in Fig. 5.11. The described differences in the re-attachment point behind the upper and lower rib is shown in this figure, although it is perhaps graphically more clear in the streamline plot of Fig. 5.9. In Fig. 5.11(b) and 5.11(c) it can be seen that the flow is still moving backwards along

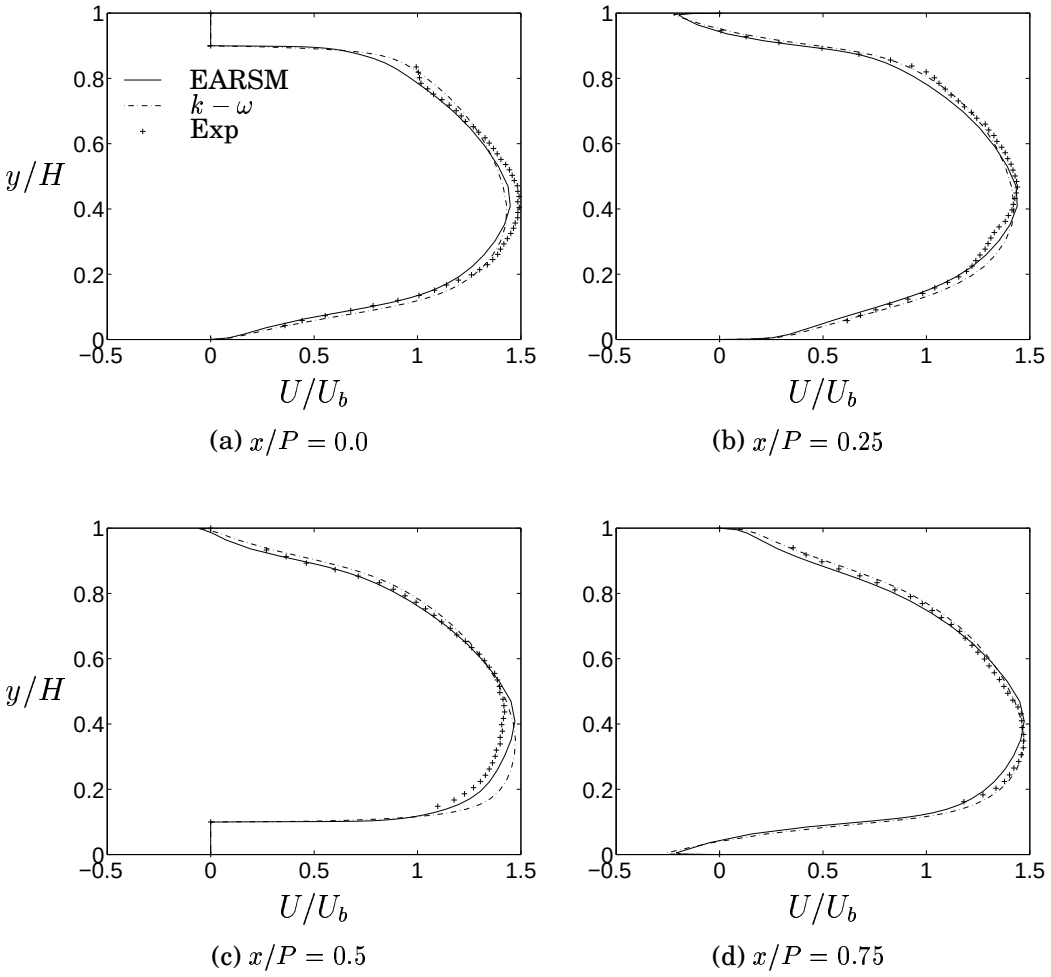


Figure 5.11: U-velocity profiles. Rotating ribbed channel.

the upper wall five step heights downstream of the upper rib (Fig. 5.11(c)). Along the lower wall, however, the flow is attached five step heights downstream of the rib (Fig. 5.11(a)). In Fig. 5.11(d), it can be seen that, despite the downward shift of the flowfield, the flow still re-attaches along the upper wall and thus the pitch in this ribbed channel is sufficiently large to enable increased heat transfer – through higher turbulence levels – even in the rotating case. The downward shift of the flow also affect the smaller re-circulation bubbles upstream the ribs. Comparing the velocity profiles upstream the upper and lower ribs, Figs 5.11(b) and 5.11(d), it is evident that the near-wall velocity is much higher 2.5 step heights upstream of the lower rib than at the

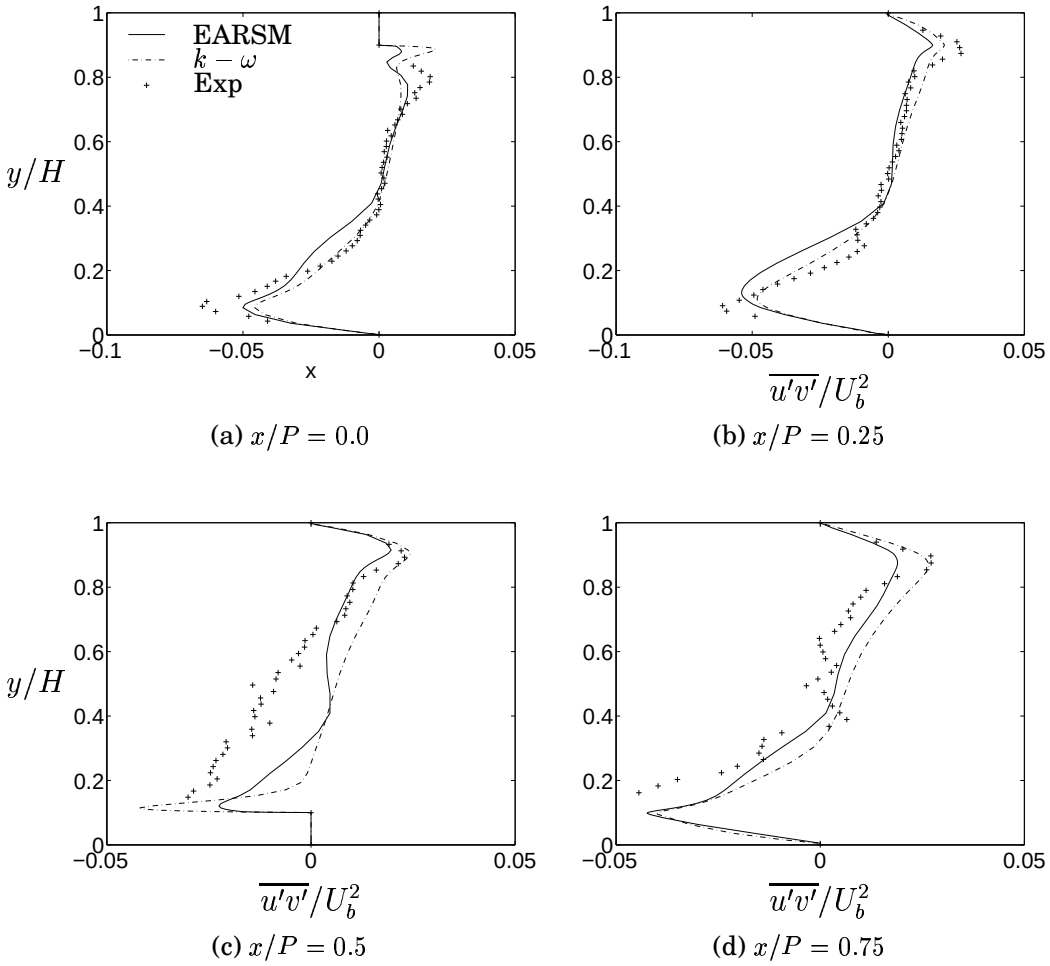


(a) $x/P = 0.0$ (b) $x/P = 0.25$

(c) $x/P = 0.5$ (d) $x/P = 0.75$

Figure 5.12: $\overline{u'v'}$-shear stress. Rotating ribbed channel

same distance upstream of the upper rib, indicating a much stronger upstream re-circulating bubble on the upper wall. An effect which is difficult to discern from the predicted Nusselt numbers in Fig. 5.10(a).

Both models predict the downward shift of the velocity field, due to rotation, accurately, with a maximum velocity around $y/H = 0.4$, slightly changing from one part of the channel to another owing to the alternating blockage effect of the ribs. The overall behavior of the two models is satisfying, with only a marginal effect of the additional terms in the EARSM formulation.

The shear stress, $\overline{u'v'}$, is shown in Fig. 5.12. The agreement between the predictions and the measurements have deteriorated as compared

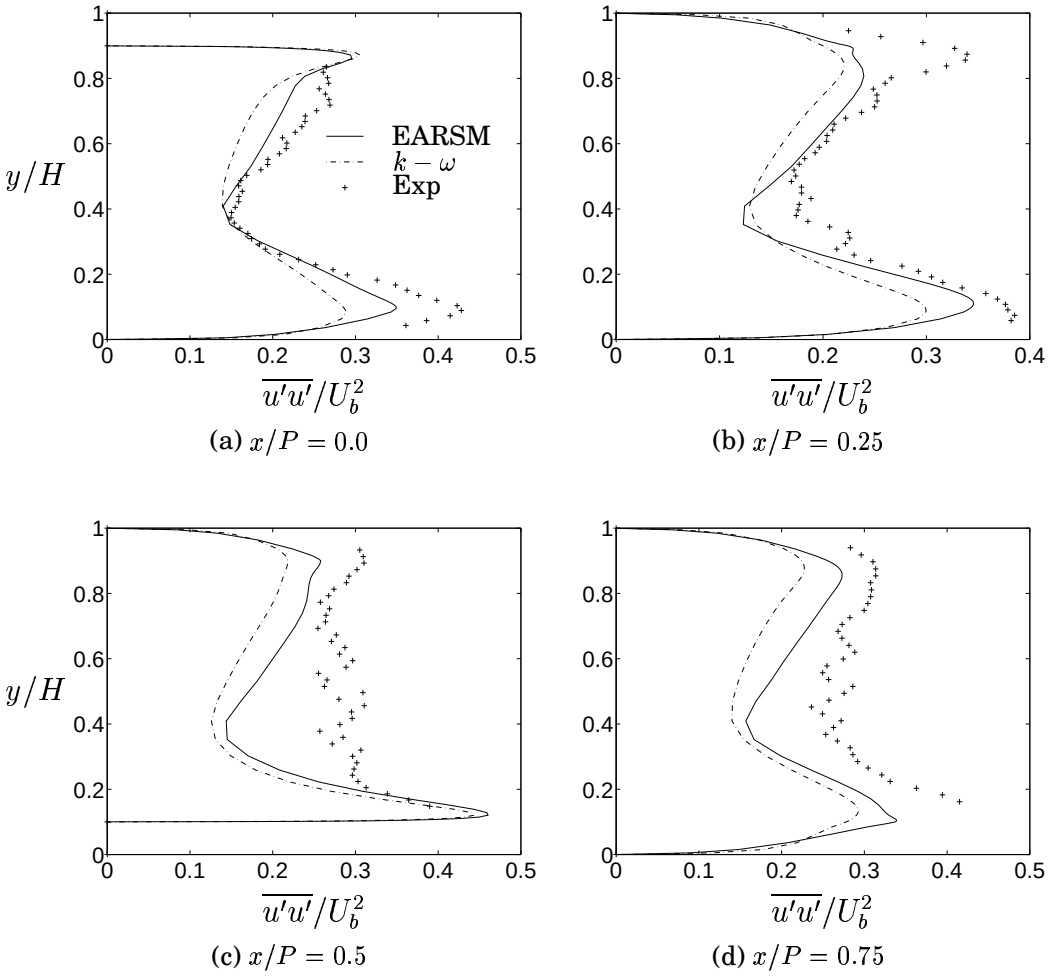


Figure 5.13: $\overline{u'u'}$-normal stress. Rotating ribbed channel.

with the stationary case, see Fig. 5.7, and there is also a larger difference between the two turbulence models. The most notable problematic area is at the top of the lower rib, in Fig. 5.12(c), where none of the models capture neither the correct profile nor the correct level. Moving further up in the channel at this position, the experiment shows almost a linear relation of the shear stress between the lower and upper wall, which none of the models capture. The deviation is larger for the EVM, although the profiles of the EARSM act rather strangely – in the center part of the channel, the EARSM predicts zero shear stress, which is not found in the measurements.

Figure 5.13 shows the normal stress. As for the stationary case, the

EARSM return slightly better agreement, which reflects the increased physics involved in these models, enabling the models to deviate from the isotropic relation of the Boussinesq hypothesis.

# Chapter 6

# Summary of Papers

Below are some comments on the papers included in this thesis. They are here to place the papers in a broader frame of reference and also to connect them more closely with the main objectives of the present research. The summaries are intentionally different from the abstracts included in the papers, and are made to emphasize useful insights not fully recognized at the time. Furthermore, in contrast to the abstracts, these summaries are not deprived of healthy criticism which have been valuable for the progress of this work.

## 6.1 Paper I

J. Bredberg and L. Davidson
"Prediction of flow and heat transfer in a stationary two-dimensional rib roughened passage using low-Re turbulent models"
In *Proceedings of 3:rd European Conference on Turbomachinery: Fluid Dynamics and Thermodynamics*, pages 963-972, IMechE 1999.

The paper presents a comparison between four different turbulence models on a 2D rib-roughened channel. Complementary to the evaluation of the turbulence models, the paper validates numerical procedures implemented in CALC-BFC, namely the periodic boundary conditions and the blockage routines. As a result of this, a disproptionally large part of the paper is devoted to numerics. Being the first proper paper, excluding the contribution to the ERCOFTAC workshop [22], the structure and presentation of the results is slightly different to forthcoming papers. Nevertheless the conclusions from this paper

constitutes the foundation for later work. Apart from the thesis for the degree of licentiate [19] written at the same time as this paper, the EARSM type of turbulence models were not to be used anymore, as a result of the findings in this paper. The grid dependency analysis showed that the criteria of Wilcox [209] for the $\omega$ boundary condition is too strong. In subsequently simulations $\omega_w$ was to be specified only for the two first interior grid-nodes. The paper concluded that none of the evaluated turbulence models were adequate for heat transfer prediction. Models which performed reasonable in the $Re = 122\,000$ case, did poorly in the $Re = 12\,600$ case and vice versa. This erroneous Reynolds number dependency for heat transfer using eddy-viscosity models was to be further discussed in the next paper. This paper also visualize the difficulties in specifying the correct boundary condition, as some of the large discrepancies in the predicted Nusselt number around the rib for the $Re = 12\,600$ case can be attributed to the simplistic treatment of wall heat flux at the rib-faces. Although the code was later modified to enable conjugate heat transfer problems to be solved effectively, discrepancies still persisted in this area.

## 6.2 Paper II

J. Bredberg, L. Davidson and H. Iacovides
"Comparison of Near-wall Behavior and its Effect on Heat Transfer for $k-\omega$ and $k-\varepsilon$ Turbulence Models in Rib-roughened 2D Channels"
In *Proceedings of 3:rd Int. Symposium on Turbulence, Heat and Mass Transfer*, pages 381-388, eds. Y. Nagano and K. Hanjalić and T. Tsuji, Aichi Shuppan 2000.

The paper is the result of questions raised in the previous paper and a fruitful visit to Prof. Launders group at UMIST, Manchester. The co-author Dr. Iacovides is part of that group which has a long tradition on numerical simulations on configurations of interest for this thesis, as the one in question for this paper. The measured data for the simulations was also the result of a diploma work at UMIST [144]. Dr. Iacovides greatfully supplied the data and gave valuable discussions and suggested important alterations to the paper. The main emphasis of the paper was to discuss and try to explain the believed erroneous Reynolds number dependencies of eddy-viscosity models for heat transfer predictions in separated flows. The results from the previous paper could only suspect such an idea, as the two studied cases different both

in Reynolds number as well as in geometry. The advantage of using the UMIST-data, which only varied in Reynolds number, for such an analysis is obvious. In addition to the zonal $k-\varepsilon$ and the $k-\omega$ model, studied previously, the Launder-Sharma $k-\varepsilon$ [121] was also included in this paper. In retrospective the used $k-\omega$ model [3] should have been substituted with the more commonly employed model by Wilcox [207], to make the results in the paper attractive to a broader audience. The conclusions are however general, and confirms the suspicion raised: two-equation turbulence models gives a too strong Reynolds dependency for heat transfer in separated flows. The importance of correctly estimating the near-wall turbulence level when employing a constant Prandtl number heat transfer model for an accurate prediction of Nusselt number was shown. Although the lack of turbulence measured data, the noted strong connection between heat transfer and turbulence has later been verified repeatedly. Extending the analysis to the solved turbulent quantities in the latter part of the paper was less conclusive. The importance of a correctly estimated length-scale in separated regions was however addressed. The result for the turbulent kinetic energy ($k$) showed a distinct difference between the $k-\varepsilon$ model and the other two models, which confirms the futility of trying to relate heat transfer to only one of the solved turbulent quantities. The inaccuracy of the zonal model, for which the length-scale is only vaguely effected by the flow, is a testimony of this. The paper could however not give any conclusive solution to the erroneous Reynolds number dependency, and it is unfortunate that the effect of the Yap correction for the $k-\varepsilon$ model was not included, as that could have given valuable information for further research. The Yap-correction thread was again given attention in Paper VI, however without any decisive conclusion. Paper II also included the predicted friction coefficient along the lower, rib-roughened, wall for both Reynolds number. The comparison of $C_f$ and $Nu$ re-confirms the erroneous behaviour of employing Reynolds analogy when estimating heat transfer in separated flows. The $C_f$-plots also resulted in the final abolishment of zonal models, as this type of models was found to be inadequate for estimating even the flowfield in separated flows.

## 6.3 Paper III

J. Bredberg, S.-H. Peng and L. Davidson
"On the Wall Boundary Condition for Computing Turbulent Heat Trans-

fer with $k - \omega$ Models"
In *Proceedings of the ASME Heat Transfer Division - 2000*, HTD-Vol. 366-5, pages 243-250, ed. J.H. Kim, ASME 2000.

In accordance with the obligations made to GTC, Paper III represents the first attempt to develop a method to estimate heat transfer rates sufficiently accurate using only modest computation requirements. The final goal of the project is to simulate the flow and heat transfer inside a turbine blade. Previous achievements in the literature with numerical simulations indicates the necessity of fully resolving the geometry of the serpentine ducts, including the ribs. A rough estimation of the amount of computational nodes for a typical 3D geometry however showed the impossibility of making a LRN simulation. Thus it would be necessary to employ wall function based turbulence models. On the basis of results from computations performed on 3D rib-roughened channels the prospect of achieving a high degree of fidelity using such an approach is however small. Time was spent to find a model and/or method with a higher ratio of accuracy to computational efforts. The literature survey gave however only a few alternatives to the standard wall function model. The study, which later resulted in Paper IV, showed the improvement through solving, rather than setting, the turbulent kinetic energy equation, as is done in the Launder-Spalding (LS) model. The Chieng-Launder (CL) model, which sub-divides the first cell into layers, each with its own individual treatment was also studied. Although the latter model only yields meager improvements compared to the LS model, the idea of splitting the first cell into a viscous and a turbulent region with its respectively modelling approach was adopted in the present paper. The stability problems encountered by the author using the CL model however necessitated a change in methodology. It was early decided to base the new model on a $k - \omega$ model rather than a $k - \varepsilon$ as in the Chieng-Launder model, mainly due to the previous good experience – within the group – when using the Wilcox models. Furthermore an additional coefficient was introduced to enhance numerical stability through blending the two layers, rather than adding them together. The latter approach also substantially facilitated the treatment within both the LRN and HRN zones, and enabled an almost straight-forward adoption of well established methods for the respective zones. The resulting model however became sensitive to the blending function which can be noted in the peculiar profiles for the Nusselt number on intermediate refined meshes. Improved results could only be achieved using a non-standard

heat transfer model, which is seen as a drawback of the model. Although the model give results similar in accuracy to those using the Wilcox $k-\omega$ model on refined meshes and to those using the LS-model on coarser meshes, a general high degree of accuracy was not achieved. However as most experiences in life, new ideas need to mature before they can be employed successfully. The knowledge gained with this model later resulted in the model with a substantially improved heat transfer performance as shown in Paper VII and VIII.

## 6.4 Paper IV

J. Bredberg
"On the Wall Boundary Condition for Turbulence Models"
*Report 00/4, Department of Thermo and Fluid Dynamics, Chalmers University of Technology*, 2000

This paper is the result of the study on wall functions along the development of the hybrid model in Paper III. The paper is mainly devoted to the HRN type of turbulence models and special treatments needed to take care of the large variation in the buffer layer. Paper V is entirely focused on the LRN turbulence model and the aspect of accurately modelling the viscous sub-layer. The present paper concerns, with a few exceptions, on $k-\omega$ models and should be seen as an extension to Paper III, rather than a general overview on wall treatments. The thorough derivations and explanations to modelling approaches made for Paper III may also be useful as an introduction to constructing new wall functions. In addition the paper give complementary information for the description of the Launder-Spalding and Chieng-Launder models. The presentation of alternatives to the standard wall function for the temperature equation may also be valuable.

## 6.5 Paper V

J. Bredberg
"On Two-equation Eddy-Viscosity Models"
*Report 01/8, Department of Thermo and Fluid Dynamics, Chalmers University of Technology*, 2001.

Paper V constitutes a comprehensive work on theory and modelling

approaches made for two-equation turbulence models. Similar to Paper IV, this internal report is a also the product of research made in connection with another published paper. For the development of the $k-\omega$ model in Paper VI it was necessary to thoroughly examine the concepts and relations of the secondary quantity, ie. $\varepsilon$, $\omega$ and $\tau$ in two-equation EVMs. Most of the latter part of the report, excluding the appendices, also focus on similarities and differences between a $k-\varepsilon$ and a $k-\omega$ model. The report tries to explain, especially in Chapter 6 and 7, the ideas behind modelling approaches made for turbulence models. The attempt however falls short of the target, mainly due to the, in many cases, lacking theoretical foundations for terms and functions introduced in turbulence models. The report is divided into several separated sections, for which the introduction part is treated in Chapter 1 and 2. Chapter 3 deals with 'exact' relations, from derived equations and DNS-data. The modelling approaches made for EVMs are treated either in Chapter 4 or 5. The partition is made dependent on whether the models are based on what is referred to as the classic theory, ie. mainly on experimental data, or based on data from numerical simulations (DNSs). As stated above the latter part of the report (Chapter 6 and 7) compares and summarizes modelling approaches for the different types of two-equation models. A particular important addition is appendices A and B which give a complete list of eleven turbulence model with comments (A) together with their usefulness in three different generalized test-cases (B). Other useful information is given in eg. Section 4.1.2 where different types of wall distance relation are given. From a modelling point of view Sections 6.3, 6.4, 7.3 and 7.4 along with Appendix C are of interest as these sections attempts to explain the rationale behind the introduced cross-diffusion terms in the new $k-\omega$ model. These parts could be treated as an addition to Paper VI.

## 6.6 Paper VI

J. Bredberg, S.-H. Peng and L. Davidson
"An improved $k-\omega$ turbulence model applied to recirculating flows"
Accepted for publication in *Int. J. Heat and Fluid Flow*, 2002.

The initiation to this paper is a combination of several factors. The strive to improve upon the previous revealed inadequacy of many EVMs is the dominant factor. Paper I and II showed the erroneous Reynolds number dependency for heat transfer predictions that two-equation

turbulence model experience. It should however be admitted that the model presented in Paper VI does not improve upon this deficiency. Another important contribution is the previously developed a cross-diffusion modified $k-\omega$ turbulence model [162], which has showed to have some advantages feature compared to the standard $k-\omega$ model. That model was unfortunately optimized using incorrect DNS-data, resulting in insufficient accuracy for fully developed channel flow. A remedy to this, with maintained accuracy for other flows, is given by the new model. Although the predictability on coarse mesh is only treated in Paper VIII, the present model was developed with grid-robustness in mind. It is considered that much of the grid sensitivity experienced using LRN turbulence model arise from too stiff damping functions. As a result, the degree of empiricism added to the new model was maintained at a minimum. It was possible through the introduction of a viscous cross-diffusion term in the $\omega$-equation to reduce the number of damping functions to only one. An additional advantage with this term is that the wall boundary condition for $\omega$ could be made theoretically consistent with DNS-data. Furthermore the cross-diffusion terms reduces the sensitivity to the specification of $\omega_\infty$ for free shear flows, as compared with other $k-\omega$ models. The inclusion of free shear flows was the result of a reviewer comments (which is greatfully acknowledged), and not considered in the designing of the model. It should be recognized that there is always a certain degree of freedom in the specifications of coefficients and terms in the transport equations. For the present model these numerical optimizations were made in as close accordance as possible with well accepted rules and values. Thus many of the coefficients in this model are equivalent to those used in the standard $k-\varepsilon$ model, eg. $C_\mu = 0.09,\ \sigma_k = 1,\ C_{\varepsilon 1} \approx 1.5,\ C_{\varepsilon 2} \approx 1.9$. A number of different values were tried for $\sigma_\omega$, the one used (=1.8) is slightly unconventional, but it offered the best compromise. As a defense one may note that Wilcox $k-\omega$ models use the even more extreme value $\sigma_\omega = 2$. It was also noted that a change in the cross-diffusion term coefficient ($C_\omega$) would enable a more common value, however at the expense of a change in the boundary condition for $\omega$ from its theoretically exact value. The discussion in Paper V, Section 7.3, should also be considered: "there is little theoretical foundation for any particular value on $\sigma_\omega$ as the Schmidt numbers should generally vary as a function of the wall distance".

## 6.7 Paper VII

J. Bredberg and L. Davidson
"Prediction of turbulent heat transfer in stationary and rotating U-ducts with rib roughened walls"
Accepted to the *5:th International Symposium on Engineering Turbulence Modelling and Measurements*, 2002.

Paper VII and Paper VIII were written simultaneously with this introduction part of the thesis and hence the comments made here could as well have been included in the papers. The papers may be considered inconsequently numbered, as this paper (VII) presents the results, while the next (VIII) discusses the model. The papers were however written in this order. There is a small addition to the turbulence model in Paper VII as compared to Paper VIII. This is the limiters which are included in Eq. 6. These are the result of stability problems encountered when using too a coarse mesh to approximate the gradients in the cross-diffusion terms. Their inclusion is however not controversial, as they are in accordance with physics. The limitation of the viscous term ensures that it is only affecting the flow in the near-wall region where the gradients of $k$ and $\omega$ are of opposite sign. The limit for the turbulent term is also theoretically well posed. The only ambiguity is the damping function in the turbulent term, as the heat transfer prediction is sensitive to the exact formulation of this function. The term could however not be removed as this would change the predicted result even for simple channel flow. Although these comments, the results presented in the paper represent a good combination of accuracy and computational efficiency. There is only a small flaw with the used mesh which results in unphysical variation of the Nusselt immediate upstream the ribs, mostly notable in Fig. 5 and 6.

## 6.8 Paper VIII

J. Bredberg and L. Davidson
"Low-Reynolds Number Turbulence Models: An Approach for Reducing Mesh Sensitivity"
*Submitted for journal publication.*

When initiating, in Paper III, the development of a turbulence model that would be capable of accurate near-wall prediction on coarser

meshes, the author was only familiar with the work made by Grotjans and Menter [60]. Later, as noted by the introduction, there have been an increased interest in such models, especially at UMIST. It should be noted that even though academia have used LRN turbulence models as a basis when performing numerical simulation for a long time now [101], [121], industry have strongly relied on wall function based methods, and only recently started to experimenting with models requiring more refined meshes. The contribution of Paper VIII, is thus similarly to Paper III, aimed at constructing reliable engineering models rather than achieving unmatched accuracy. Mating the previously developed $k-\omega$ model (Paper VI) with some simple correction derived from experience gained with the hybrid model (Paper III) resulted in a very trustworthy model, applicable for meshes with the first near-wall node at $y^+ \approx 5$. The decrease in mesh demands may be consider marginal, however as notable in eg. Fig. 9 and Table 3 the accuracy could be maintained using only one-tenth of the number of nodes (for a 3D application). Comparing also the minor modification necessary to the baseline model, with the additional performance gain, it is considered as a well invested work. Contrary to the hybrid model (Paper III) modifications are not needed for any other wall boundary conditions, apart from the one used in the turbulence model. The increased stability via the extension presented in Paper VII, is recommended for complex geometries. It would be desirable to continue this work to further extend the applicability of the model to include computation made on meshes for which the first node is located within the buffer layer, $5 < y^+ < 30$. Such a model may however necessitate modifications to both the momentum and temperature equations in addition to the turbulence equations.

# Chapter 7

# Conclusions

- Two-equation models have an erroneous Reynolds dependency for the Nusselt number in separated regions. The predictions show a closer agreement to the that of the smooth ducts correlation by Dittus-Boelter, $Nu \sim Re^{0.8}$, rather than the experimental evidence of $Re^{0.6-0.7}$.
- The un-alignment of the re-attachment point and the maximum heat transfer in separated flows necessary the use of transport models for turbulence. The turbulence intensity and Nusselt number are well correlated, however the present study shows the importance of also correctly estimate the turbulence length-scale.
- For flows in ribbed ducts, the advantage of higher-order turbulence scheme, such as EARSM, is marginal.
- One of the reasons for the mesh dependency of LRN turbulence model for FVM-codes is the result of inaccurately estimating the volume integral of near-wall variations. The discrepancies could however be reduced through adding analytical derived corrections for the first interior node, when placed in the viscous sub-layer.
- The large variation of the turbulence quantities in the buffer layer, $5 < y^+ < 30$, makes it extremely difficult to construct a turbulence model with a high degree of accuracy on both refined and coarse meshes.

# Bibliography


[1] A. Abdon and B. Sunden. A numerical study on the influence of rib shape on the thermodynamic performance of a cooling duct. In *Proceedings of the ASME IMECE 2001*. The American Society of Mechanical Engineers, 2001.

[2] K. Abe, T. Kondoh, and Y. Nagano. A new turbulence model for predicting fluid flow and heat transfer in separating and reattaching flows - I. flow field calculations. *Int. J. Heat and Mass Transfer*, 37:139–151, 1994.

[3] R. Abid, C. Rumsey, and T. Gatski. Prediction of nonequilibrium turbulent flows with explicit algebraic stress models. *AIAA Journal*, 33:2026–2031, 1995.

[4] S. Acharya, S. Dutta, and T.A. Myrum. Heat transfer in turbulent flow past a surface-mounted two-dimensional rib. *J. Heat Transfer*, 120:724–734, 1998.

[5] S. Acharya, S. Dutta, T.A. Myrum, and R.S. Baker. Periodically developed flow and heat transfer in a ribbed duct. *Int. J. Heat and Mass Transfer*, 36:2069–2082, 1993.

[6] S. Acharya, S. Dutta, T.A. Myrum, and R.S. Baker. Turbulent flow past a surface mounted two-dimensional rib. *J. Fluids Engineering*, 116:238–246, 1994.

[7] R.S. Amano. Development of a turbulence near-wall model and its application to separated and reattached flows. *Numerical Heat Transfer*, 7:59–75, 1984.

[8] R.S. Amano, M.K. Jensen, and P. Goel. A numerical and experimental investigation of turbulent heat transport downstream from an abrupt pipe expansion. *J. Heat Transfer*, 105:862–869, 1983.

[9] J. Antoniou and G. Bergeles. Development of the reattached flow behind surface-mounted two-dimensional prisms. *J. Fluids Engineering*, 110:127–1336, 1988.

[10] J. Bardina, J.H. Ferziger, and R.S. Rogallo. Effect of rotation on isotropic turbulence: computation and modelling. *J. Fluid Mechanics*, 154:321–336, 1985.

[11] W. Bauer, O. Haag, and D.K. Hennecke. Accuracy and robustness of nonlinear eddy viscosity models. *Int. J. Heat and Fluid Flow*, 21:312–319, 2000.

[12] J.W. Baughn and X. Yan. Local heat transfer measurements in square ducts with transverse ribs. In *National Heat Transfer Conference*, 1992.

[13] D.L. Besserman and S. Tanrikut. Comparison of heat transfer measurements with computations for turbulent flow around 180 deg bend. *J. Turbomachinery*, 114:865–871, 1992.

[14] B. Bonhoff, T. Schneider, B. Johnson, and I. Jennions. Prediction for turbulent flow in rotating and non rotating coolant channels. In *2:nd Int. Symp. on Turbulence, Heat and Mass Transfer*, 1997.

[15] B. Bonhoff, U. Tomm, B.V. Johnson, and I. Jennions. Heat transfer predictions for rotating u-shaped coolant channels with skewed ribs and with smooth walls. In *Int. Gas Turbine & Aeroengine Congress and Exhibition*, 1997.

[16] J.P. Bons and J.L. Kerrebrock. Complementary velocity and heat transfer measurements in a rotating cooling passage with smooth walls. *J. Turbomachinery*, 121:651–662, 1999.

[17] T.V. Boussinesq. Mém. pres Acad. Sci.,3rd ed Paris XXIII p. 46, 1877.

[18] P. Bradshaw. The analogy between streamline curvature and buoyancy in turbulent shear flow. *J. Fluid Mechanics*, 36:177–191, 1969.

[19] J. Bredberg. Prediction of flow and heat transfer inside turbine blades using EARSM, $k-\varepsilon$ and $k-\omega$ turbulence models. Thesis for the Degree of Licentiate of Engineering, Dept. of Thermo and Fluid Dynamics, Chalmers University of Technology, Gothenburg, 1999. Also available at www.tfd.chalmers.se/˜bredberg.

[20] J. Bredberg. On the wall boundary condition for turbulence model. Report 00/4, Dept. of Thermo and Fluid Dynamics, Chalmers University of Technology, Gothenburg, 2000. Also available at www.tfd.chalmers.se/~bredberg.

[21] J. Bredberg. On two-equation eddy-viscosity models. Report 01/8, Dept. of Thermo and Fluid Dynamics, Chalmers University of Technology, Gothenburg, 2001. Also available at www.tfd.chalmers.se/~bredberg.

[22] J. Bredberg and L. Davidson. Case 7.2: Two-dimensional flow and heat transfer over a smooth wall roughened with squared ribs. In *7th ERCOFTAC/IAHR workshop on refined turbulence modeling*, Manchester, 1998.

[23] J. Bredberg and L. Davidson. Prediction of flow and heat transfer in a stationary 2-D rib roughened passage using low-Re turbulent models. In *3:rd European Conference on Turbomachinery*, pages 963–972, London, 1999. IMechE.

[24] J. Bredberg and L. Davidson. Low-Reynolds number turbulence models: An approach for reducing mesh sensitivity. Submitted for Journal publication, 2002.

[25] J. Bredberg and L. Davidson. Prediction of turbulent heat transfer in stationary and rotating U-ducts with rib roughened walls. Accepted to 5th Int. Symp. on Engineering Turbulence Modelling and Measurements, 2002.

[26] J. Bredberg, L. Davidson, and H. Iacovides. Comparison of near-wall behavior and its effect on heat transfer for $k-\omega$ and $k-\varepsilon$ turbulence models in rib-roughened 2D channels. In Y. Nagano, K. Hanjalić, and T. Tsuji, editors, *3:rd Int. Symp. on Turbulence, Heat and Mass Transfer*, pages 381–388, Nagoya, 2000. Aichi Shuppan.

[27] J. Bredberg, S-H. Peng, and L. Davidson. On the wall boundary condition for computing heat transfer with $k-\omega$ models. In J.H. Kim, editor, *HTD-Vol. 366-5, ASME Heat Transfer Divison - 2000*, volume 5, pages 243–250, Orlando, 2000. The American Society of Mechanical Engineers.

[28] J. Bredberg, S-H. Peng, and L. Davidson. An improved $k-\omega$ turbulence model applied to recirculating flows. Accepted for publication in Int. J. Heat and Fluid Flow, 2002.

[29] M. Breuer and W. Rodi. Large-Eddy Simulation of turbulent flow through a straight square duct and a 180 deg bend. In *1st ERCOFTAC workshop on DNS and LES*, Guildford, UK, 1994.

[30] I.P. Castro. Relaxing wakes behind surface-mounted obstacles in rough wall boundary layers. *J. Fluid Mechanics*, 93:631–659, 1979.

[31] S.C. Cheah, H. Iacovides, D.C. Jackson, H. Ji, and B.E. Launder. LDA investigation of the flow development through rotating U-duct. *J. Turbomachinery*, 118:590–596, 1996.

[32] H.C. Chen and V.C. Patel. Near-wall turbulence models for complex flows including separation. *AIAA Journal*, 26:641–649, 1988.

[33] C.C. Chieng and B.E. Launder. On the calculation of turbulent heat transfer transport downstream an abrupt pipe expansion. *Numerical Heat Transfer*, 3:189–207, 1980.

[34] Y.D. Choi, H. Iacovides, and B.E. Launder. Numerical computation of turbulent flow in a square-sectioned 180 deg bend. *J. Fluid Engineering*, 111:59–68, 1989.

[35] M. Ciofalo and M. W. Collins. $k-\varepsilon$ predictions of heat transfer in turbulent recirculating flows using an improved wall treatment. *Numerical Heat Transfer, Part B*, 15:21–47, 1989.

[36] M. Ciofalo and M. W. Collins. Large-eddy simulation of turbulent flow and heat transfer in a plane and rib-roughened channel. *Int. J. Numerical Methods in Fluids*, 15:453–489, 1992.

[37] T.J. Craft and B.E. Launder. A Reynolds stress closure designed for complex geometries. *Int. J. Heat and Fluid Flow*, 17:245–254, 1996.

[38] T.J. Craft, B.E. Launder, and K. Suga. Development and application of a cubic eddy-viscosity model of turbulence. *Int. J. Heat and Fluid Flow*, 17:108–115, 1996.

[39] T.J. Craft, B.E. Launder, and K. Suga. Prediction of turbulent transitional phenomena with a nonlinear eddy-viscosity model. *Int. J. Heat and Fluid Flow*, 18:15–28, 1997.

[40] B.J. Daly and F.H. Harlow. Transport equation in turbulence. *Physics of Fluids*, 13:2634–2649, 1970.

[41] L. Davidson and B. Farhanieh. CALC-BFC. Report 95/11, Dept. of Thermo and Fluid Dynamics, Chalmers University of Technology, Gothenburg, 1995.

[42] A.O. Demuren and W. rodi. Calculation of turbulence-driven secondary motion in non-circular ducts. *J. Fluid Mechanics*, 140:189–222, 1984.

[43] F.W. Dittus and L.M.K. Boelter. Heat transfer in automobile radiators of the tubular type. *Univ. of Calif. Pubs. Eng.*, 2:443–461, 1930.

[44] H.S. Dol, K. Hanjalić, and S. Kenjeres. A comparative assessment of the second-moment differential and algebraic models in turbulent natural convection. *Int. J. Heat Fluid Flow*, 18:4–14, 1997.

[45] J.P. Van Doormal and G.D. Raithby. Enhancement of the simple method for predicting incompressible fluid flows. *Numerical Heat Transfer*, 7:147–163, 1984.

[46] L.D. Drain and S. Martin. Two-component velocity measurements of turbulent flow in a ribbed-wall flow channel. In *Int. Conf. on Laser Anenometry - Advances and Application*, 1985.

[47] P.A. Durbin. Near-wall turbulence closure modeling without damping functions. *Theoretical Computational Fluid Dynamics*, 3:1–13, 1991.

[48] P.A. Durbin. A Reynold stress model for near-wall turbulence. *J. Fluid Mechanics*, 249:465–498, 1993.

[49] S. Dutta, M.J. Andrews, and J-C. Han. Prediction of turbulent heat transfer in rotating smooth square ducts. *Int. J. Heat and Mass Transfer*, 39:2505–2514, 1996.

[50] S. Dutta and J-C. Han. Local heat transfer in rotating smooth and ribbed two-pass square channels with three channel orientation. *J. Heat Transfer*, 118:578–584, 1996.

[51] S. Dutta, J-C. Han, Y. Zhang, and C.P. Lee. Local heat transfer in a rotating two-pass triangular duct with smooth walls. *J. Turbomachinery*, 118:435–443, 1996.

[52] S.V. Ekkad and J-C. Han. Detailed heat transfer distributions in two-pass square channels with rib turbulators. *Int. J. Heat and Mass Transfer*, 40:2525–2537, 1997.

[53] D.K. Gartling. A test problem for outflow boundary condition – flow over a backward-facing step. *Int. J. Numerical Methods in Fluids*, 11:953–967, 1990.

[54] T.B. Gatski and C.G. Speziale. On explicit algebraic stress models for complex turbulent flows. *J. Fluid Mechanics*, 254:59–78, 1993.

[55] S. Gavrilakis. Numerical simulation of low-Reynolds-number turbulent flow through a straight square duct. *J. Fluid Mechanics*, 244:101–129, 1992.

[56] W.B. George. Lecture notes, turbulence theory. Report, Dept. Thermo and Fluid Dynamics, Chalmers University of Technology, Gothenburg, 2001.

[57] M.M. Gibson and B.E. Launder. On the calculation of horizontal nonequilibrium turbulent free shear flows under gravitational influence. *J. Heat Transfer*, 98:81–87, 1976.

[58] M.M. Gibson and B.E. Launder. Ground effects on pressure fluctuations in the atmospheric boundary layer. *J. Fluid Mechanics*, 86:491–511, 1978.

[59] H.P. Greenspan. *The Theory of Rotating Fluids*. Cambridge University Press, Cambridge, 1968.

[60] H. Grotjans and F.R. Menter. Wall functions for general application CFD codes. In *CD-ROM Proceedings of ECCOMAS*, pages 1112–1117, Athens, 1998.

[61] Z. Guo and D.L. Rhode. Assessment of two- and three-scale $k - \epsilon$ models for rotating cavity flows. *J. Turbomachinery*, 118:826–834, 1996.

[62] J.C. Han. Heat transfer and friction characteristics in rectangular channels with rib turbulators. *J. Heat Transfer*, 110:321–328, 1988.

[63] J.C. Han, L.R. Glicksman, and W.M. Rohsenow. Turbulent heat and mass transfer from a wall with parallel roughness ridges. *Int. J. Heat and Mass Transfer*, 21:1143–1156, 1978.

[64] J.C. Han and J.S. Park. Developing heat transfer in a rectangular channels with rib turbulators. *Int. J. Heat and Mass Transfer*, 31:183–195, 1988.

[65] J.C. Han, J.S. Park, and C.K. Lei. Heat transfer enhancement in channels with promoters. *J. Eng. Gas Turbines and Power*, 107:628–635, 1985.

[66] J.C. Han and Y.M. Zhang. High performance heat transfer ducts with parallel broken and v-shaped ribs. *Int. J. Heat and Mass Transfer*, 35:513–523, 1992.

[67] J.C. Han, Y.M. Zhang, and C.P. Lee. Augmented heat transfer in square channels with parallel, crossed, and V-shaped angled ribs. *J. Heat Transfer*, 113:590–596, 1991.

[68] J.C. Han, Y.M. Zhang, and C.P. Lee. Influence of surface heating condition on local heat transfer in a rotating square channel with smooth walls and radial outward flow. *J. Turbomachinery*, 116:149–158, 1994.

[69] K. Hanjalić. Second-moment turbulence closure for CFD: Needs and prospects. *IJCFD*, 12:67–97, 1999.

[70] K. Hanjalić and B.E. Launder. A Reynolds stress model of turbulence and its application to thin shear flows. *J. Fluid Mechanics*, 52:609–638, 1972.

[71] K. Hanjalić and B.E. Launder. Contribution towards a Reynolds-stress closure for low-Reynolds-number turbulence. *J. Fluid Mechanics*, 74:593–610, 1976.

[72] K. Hanjalić, B.E. Launder, and R. Schiestel. Multiple-time-scale concepts in turbulent transport modeling. In *2:nd Int. Symp. on Turbulent Shear Flows*, 1980.

[73] K. Hanjalić and S. Vasic. Computation of turbulent natural convection in rectangular enclosures with an algebraic flux model. *Int. J. Heat and Mass Transfer*, 36:3603–3624, 1993.

[74] A. Hellsten. Some improvements in Menters $k-\omega$ SST turbulence model. 29th AIAA Fluid Dynamics Conference, AIAA 98-2554, 1998.

[75] J.O. Hinze. *Turbulence*. McGraw-Hill, Inc, 1975.

[76] M. Hirota, H. Yokosawa, and H.M. Fujita. Turbulence kinetic energy in turbulent flows through square ducts with rib-roughened walls. *Int. J. Heat and Fluid Flow*, 13:22–29, 1992.

[77] J.H.G. Howard, S.V. Patankar, and R.M. Bordynuik. Flow prediction in rotating ducts using Coriolis modified turbulence models. *J. Fluids Engineering*, 102:456–461, 1980.

[78] S-S. Hsieh and Y-J. Hong. Heat transfer coefficients in an orthogonally rotating duct with turbulators. *J. Turbomachinery*, 117:69–78, 1995.

[79] S-S. Hsieh and W-J. Liu. Uneven wall heat flux effects on local heat transfer in rotating two-pass channels with two opposite ribbed channels. *J. Heat Transfer*, 118:864–876, 1996.

[80] A. Huser and S. Biringen. Direct numerical simulation of turbulent flow in a square duct. *J. Fluid Mechanics*, 257:65–95, 1993.

[81] A. Huser, S. Biringen, and F.F. Hatay. Direct simulation of turbulent flow in a square duct: Reynolds-stress budget. *Physics of Fluids*, 6:3144–3152, 1994.

[82] C.B. Hwang and C.A. Lin. A low Reynolds number two-equation $k_\theta - \varepsilon_\theta$ model to predict thermal fields. *Int. J. Heat and Mass Transfer*, 42:3217–3230, 1999.

[83] G.J. Hwang and C.R. Kuo. Experimental studies and correlations of convective heat transfer in a radially rotating serpentine passage. *J. Heat Transfer*, 119:460–466, 1997.

[84] H. Iacovides. Computation of flow and heat transfer through rotating ribbed passages. *Int. J. Heat and Fluid Flow*, 19:393–400, 1998.

[85] H. Iacovides. The computation of turbulent flow through stationary and rotating U-bend with rib-roughened surfaces. *Int. J. Numerical Methods in Fluids*, 29:865–876, 1999.

[86] H. Iacovides, D.C. Jackson, H. Ji, G. Kelemenis, and B.E. Launder. LDA study of flow development through an orthogonally rotating U-bend of strong curvature and rib-roughened walls. Paper ASME-96-GT-476, Int. Gas-Turbine and Aero Congress, Birmingham, 1996.

[87] H. Iacovides, D.C. Jackson, H. Ji, G. Kelemenis, B.E. Launder, and K. Nikas. LDA study of flow development through an orthogonally rotating U-bend of strong curvature and rib-roughened walls. *J. Turbomachinery*, 120:386–391, 1998.

[88] H. Iacovides, D.C. Jackson, G. Kelemenis, and B.E. Launder. The measurement of local wall heat transfer is stationary U-ducts of strong curvature, with smooth and rib roughened walls. In W. Rodi and D. Laurence, editors, *4:th Engineering Turbulence Modelling and Experiments*, pages 773–782. Elsevier Science Ltd, 1999.

[89] H. Iacovides, D.C. Jackson, G. Kelemenis, B.E. Launder, and Y.M. Yuan. Experiments on local heat transfer in rotating square-ended U-bend. *Int. J. Heat and Fluid Flow*, 20:302–310, 1999.

[90] H. Iacovides, D.C. Jackson, G. Kelemenis, B.E. Launder, and Y.M. Yuan. Flow and heat transfer in rotating U-bend with 45 degree ribs. *Int. J. of Heat and Fluid Flow*, 22:308–314, 2001.

[91] H. Iacovides and B.E. Launder. PSL - an economical approach to the numerical analysis of near-wall, elliptic flow. *J. Fluid Engineering*, 106:241–242, 1984.

[92] H. Iacovides, B.E. Launder, and H-Y. Li. Application of a reflection-free DSM to turbulent flow and heat transfer in a square-sectioned U-bend. *Exp. Thermal and Fluid Science*, 13:419–429, 1996.

[93] H. Iacovides, B.E. Launder, and H-Y. Li. The computation of flow development through stationary and rotating U-duct of strong curvature. *Int. J. Heat and Fluid Flow*, 17:22–33, 1996.

[94] H. Iacovides and M. Raisee. Computation of flow and heat transfer in 2-D rib roughened passages. In K. Hanjalić and T.W.J. Peeters, editors, *2:nd Int. Symp. on Turbulence Heat and Mass Transfer (Addendum)*, pages 21–30, Delft, 1997. Delft University Press.

[95] H. Iacovides and M. Raisee. Recent progress in the computation of flow and heat transfer in internal cooling passages of turbine blades. *Int. J. Heat and Fluid Flow*, 20:320–328, 1999.

[96] Y-J. Jang, H-C. Chen, and J-C. Han. Flow and heat transfer in a rotating square channel with 45 deg angled ribs by Reynolds stress turbulence model. *J. Turbomachinery*, 123:124–132, 2001.

[97] A.V. Johansson and M. Hallbäck. Modelling of rapid pressure strain in Reynolds-stress closures. *J. Fluid Mechanics*, 269:143–168, 1994.

[98] B.V. Johnson, J.H. Wagner, G.D. Steuber, and F.C. Yeh. Heat transfer in rotating serpentine passages with trips skewed to the flow. *J. Turbomachinery*, 116:113–123, 1994.

[99] R.W. Johnson and B.E. Launder. Discussion of: On the calculation of turbulent heat transfer transport downstream an abrupt pipe expansion. *Numerical Heat Transfer*, 5:493–496, 1982.

[100] J.P. Johnston, R.M. Halleen, and D.K. Lezius. Effects of spanwise rotation on the structure of two-dimensional fully developed turbulent channel flow. *J. Fluid Mechanics*, 56:533–557, 1972.

[101] W.P. Jones and B.E. Launder. The prediction of laminarization with a two-equation model of turbulence. *Int. J. Heat and Mass Transfer*, 15:301–314, 1972.

[102] B.A. Kader and A.M. Yaglom. Turbulent heat and mass transfer from a wall with parallel roughness ridges. *Int. J. Heat and Mass Transfer*, 20:345–357, 1977.

[103] H. Kawamura, H. Abe, and Y. Matsuo. DNS of turbulent heat transfer in channel flow with respect to Reynolds and Prandtl number effects. *Int. J. Heat and Fluid Flow*, 20:196–207, 1999.

[104] W.M. Kays. Turbulent Prandtl number - where are we? *J. Heat Transfer*, 116:284–295, 1994.

[105] W.M. Kays and M.E. Crawford. *Convective Heat and Mass Transfer*. McGraw-Hill, Inc, 1993.

[106] A. Khodak and C. Hirsch. Second order non-linear $k - \varepsilon$ models with explicit effect of curvature and rotation. In *Proceedings of the Third ECCOMAS Computational Fluid Dynamics Conference*, Paris, 1996.

[107] J. Kim, P. Moin, and R. Moser. Turbulence statistics in fully developed channel flow at low Reynolds number. *J. Fluid Mechanics*, 177:133–166, 1987.

[108] S.H Ko and D.L. Rhode. Derivation and testing of a new multiscale $k - \varepsilon$ turbulence model. AIAA Paper 90-0243, 1990.

[109] R. Kristoffersen and H.I. Andersson. Direct simulation of low-Reynolds-number turbulent flow in a rotating channel. *J. Fluid Mechanics*, 256:163–197, 1993.

[110] R.T. Kukreja, S.C. Lau, and R.D. McMillin. Local heat/mass transfer distribution in a square channel with full and V-shaped ribs. *Int. J. Heat and Mass Transfer*, 36:2013–2020, 1993.

[111] C.R. Kuo and G.J. Hwang. Experimental studies and correlations of radially outward and inward air-flow heat transfer in a rotating square duct. *J. Heat Transfer*, 118:23–30, 1996.

[112] Y.G. Lai and R.M.C. So. Near-wall modeling of turbulent heat flux. *Int. J. Heat and Mass Transfer*, 33:1429–1440, 1990.

[113] J. Larsson. *Numerical Simulation of Turbulent Flows for Turbine Blade Heat Transfer Applications*. PhD thesis, Dept. of Thermo and Fluid Dynamics, Chalmers University of Technology, Gothenburg, 1998.

[114] B.E. Launder. Heat and mass transfer. In P. Bradshaw, editor, *Turbulence-Topics in Applied Physics, vol 12*, pages 232–287. Springer-Verlag, 1976.

[115] B.E. Launder. Numerical computation of convective heat transfer in complex turbulent flows: Time to abandon wall functions? *Int. J. Heat and Mass Transfer*, 27:1485–1491, 1984.

[116] B.E. Launder. Introduction to the modelling of turbulence. Report, von Karman Institute for Fluid Dynamics, 1985.

[117] B.E. Launder. On the computation of convective heat transfer in complex turbulent flows. *J. Heat Transfer*, 110:1112–1128, 1988.

[118] B.E. Launder. Second-moment closure: present .. and future? *Int. J. Heat and Fluid Flow*, 10:282–300, 1989.

[119] B.E. Launder, C.H. Priddin, and B.I. Sharma. The calculation of turbulent boundary layers on spinning and curved surfaces. *J. Fluids Engineering*, 99:231–239, 1977.

[120] B.E. Launder, G.J. Reece, and W. Rodi. Progress in the development of a Reynolds-stress turbulence closure. *J. Fluid Mechanics*, 68:537–566, 1975.

[121] B.E. Launder and B.I. Sharma. Application of the energy-dissipation model of turbulence to the calculation of flow near a spinning disc. *Letters in Heat and Mass Transfer*, 1:131–138, 1974.

[122] B.E. Launder and D.B. Spalding. The numerical computation of turbulent flows. *Computational Methods Appl. Mech. Eng.*, 3:269–289, 1974.

[123] B.E. Launder, D.P. Tselepidakis, and B.A. Younis. A second-moment closure study of rotating channel flow. *J. Fluid Mechanics*, 183:63–75, 1987.

[124] H. Le, P. Moin, and J. Kim. Direct numerical simulation of turbulent flow over a backward-facing step. *J. Fluid Mechanics*, 330:349–374, 1997.

[125] B.P. Leonard. A stable and accurate convective modelling procedure based on quadratic upstream interpolation. *Computational Methods Appl. Mech. Eng.*, 19:59–, 1979.

[126] Y.-L. Lin, T.I.-P. Shih, M.A. Stephens, and M.K. Chyu. A numerical study of flow and heat transfer in a smooth and ribbed U-duct with and without rotation. *J. Heat Transfer*, 123:219–232, 2001.

[127] T.-M. Liou and C.-C. Chen. LDV study of developing flows through a smooth duct with a 180 deg straight-corner turn. *J. Turbomachinery*, 121:167–174, 1999.

[128] T.-M. Liou and J.-J. Hwang. Turbulent heat transfer augmentation and friction in periodic fully developed channel flows. *J. Heat Transfer*, 114:56–64, 1992.

[129] T-M. Liou, J-J. Hwang, and S-H. Chen. Simulation and measurement of enhanced turbulent heat transfer in a channel with periodic ribs on one principal wall. *Int. J. Heat and Mass Transfer*, 36:507–517, 1993.

[130] T.-M. Liou and C.-F. Kao. Symmetric and asymmetric turbulent flows in a rectangular duct with a pair of ribs. *J. Fluids Engineering*, 110:373–379, 1988.

[131] T.-M. Liou, Y.Y. Wu, and Y. Chang. LDV-measurements of periodic fully developed main and secondary flows in a channel with rib-disturbed walls. *J. Fluids Engineering*, 115:109–114, 1993.

[132] J. Luo and B. Lakshminarayana. Analysis of streamline curvature effects on wall-bounded turbulent flows. *AIAA Journal*, 35:1273–1279, 1997.

[133] J. Luo and B. Lakshminarayana. Prediction of strongly curved turbulent duct flows with Reynolds stress model. *AIAA Journal*, 35:91–98, 1997.

[134] R. Manceau, S. Parnexi, and D. Laurence. Turbulent heat transfer predictions using the $v^2 - f$ model on unstrcutured meshes. *Int. J. Heat and Fluid Flow*, 21:320–328, 2000.

[135] W.H. McAdams. *Heat Transmission*. McGraw-Hill, New York, 2nd edition, 1942.

[136] F.R. Menter. Two-equation eddy-viscosity turbulence models for engineering applications. *AIAA Journal*, 32:1598–1605, 1994.

[137] Y. Miyake, K. Tsujimoto, and M. Nakaji. Direct numerical simulation of rough-wall heat transfer in a turbulent channel flow. *Int. J. Heat and Fluid Flow*, 22:237–244, 2001.

[138] S. Mochizuki, J. Takamura, S. Yamawaki, and W-J. Yang. Heat transfer in serpentine flow passages with rotation. *J. Turbomachinery*, 116:133–140, 1994.

[139] W.D. Morris and K. Farhadi Rahmat-Abadi. Convective heat transfer in rotating ribbed tubes. *Int. J. Heat and Mass Transfer*, 39:2253–2266, 1996.

[140] R.D. Moser, J. Kim, and N.N. Mansour. Direct numerical simulation of turbulent channel flow up to Re=590. *Physics of Fluids*, 11:943–945, 1999. Data available at www.tam.uiuc.edu/Faculty/Moser/.

[141] A. Murata and S. Mochizuki. Large eddy simulation applied to internal forced-convection cooling of gas-turbine blades. In *11:th IHTC*, pages 565–570, 1998.

[142] Y. Nagano and M. Shimada. Developments of a two-equation heat transfer model based on direct simulations of turbulent flows with different prandtl number. *Physics of Fluids*, 12:3379–3402, 1996.

[143] D. Naot, A Shavit, and M Wolfshtein. Interactions between components of the turbulent velocity correlation tensor. *Israel J. Tech.*, 9:259–, 1970.

[144] G. J. E. Nicklin. Augmented heat transfer in a square channel with asymmetrical turbulence promotion. Final year project report, Dept. of Mech. Eng., UMIST, Manchester, 1998.

[145] K-S. Nikas and H. Iacovides. The computation of flow and heat transfer through square-ended U-bends, using low-Reynolds-number models. In *2:nd Int. Symp. on Turbulent Shear Flows Phenomena*, pages 229–234, Stockholm, 2001.

[146] J. Nikuradse. Strömungsgesetze in rauhen rohren. VDI Forschungsh. 361, 1933.

[147] S. Nisizima and A. Yoshizawa. Turbulent channel and couette flows using an anisotropic $k - \varepsilon$ model. *AIAA Journal*, 25:414–420, 1987.

[148] Y. Okita and H. Iacovides. Comparisons of high-Reynolds-number EVM and DSM models in prediction of flow and heat transfer in internal cooling passages of turbine bladess. In *CD-ROM Proceedings of ECCOMAS*, pages 1–19, Swansea, 2001.

[149] A. Ooi, G. Iaccarino, and M. Behnia. Heat transfer predictions in cavaties. In *Centre for Turbulence Research Summer Program 1998*, 1998.

[150] A. Ooi, B.A. Petterson-Reif, G. Iaccarino, and P.A. Durbin. Evaluation of RANS for rotating flows. In *Centre for Turbulence Research Summer Program 2000*, 2000.

[151] J. Pallares and L. Davidson. Large eddy simulation of a rotating 3D duct. Private communication, Dept. of Thermo and Fluid Dynamics, Chalmers University of Technology, Gothenburg, 1999.

[152] J. Pallares and L. Davidson. Large eddy simulation of turbulent flow in a rotating square duct. *Physics of Fluids*, 12:2878–2894, 2000.

[153] P.K. Panigrahi and S. Acharya. Mechanisms of turbulence transport in a turbine blade coolant passage with a rib turbulator. *J. Turbomachinery*, 121:152–159, 1999.

[154] R.L. Panton. *Incompressible flow*. John Wiley and Sons, Inc, 1995.

[155] C.W. Park. *Local Heat/Mass Transfer Distribution in Rotating Two-pass Square Channels*. PhD thesis, Dept. of Mechanical Engineering, Texas A&M University, College Station, TX, 1996.

[156] T.S. Park and H.J. Sung. A nonlinear low-Reynolds-number $k$ – $\varepsilon$ model for turbulent separated and reattaching flows – I. flow field computations. *Int. J. Heat and Mass Transfer*, 38:2657–2666, 1995.

[157] J.A. Parsons, J-C. Han, and Y. Zhang. Wall heating effects on local heat transfer in a rib rotating two-pass square channel with 90 deg rib turbulators. *Int. J. Heat and Mass Transfer*, 37:1411–1420, 1994.

[158] J.A. Parsons, J-C. Han, and Y. Zhang. Effect of model orientation and wall heating condition on local heat transfer in a rotating two-pass square channel with rib turbulators. *Int. J. Heat and Mass Transfer*, 38:1151–1159, 1995.

[159] S.V. Patankar, C.H. Liu, and E.M. Sparrow. Fully developed flow and heat transfer in ducts having streamwise-periodic variations of cross-sectional area. *J. Heat Transfer*, 99:180–186, 1977.

[160] S.V. Patankar and D.B. Spalding. *Heat and Mass Transfer in Boundary Layers*. Intertext Books, London, 1970.

[161] V.C. Patel, W. Rodi, and G. Scheuerer. Turbulence models for near-wall and low Reynolds number flows: A review. *AIAA Journal*, 23:1308–1319, 1985.

[162] S-H. Peng, L. Davidson, and S. Holmberg. A modified low-Reynolds-number $k - \omega$ model for recirculating flows. *J. Fluid Engineering*, 119:867–875, 1997.

[163] B.A. Pettersson-Reif and H.I Andersson. Second-moment closure prediction of turbulent-induced secondary flow in a straight square duct. In W. Rodi and D. Laurence, editors, *4:th Engineering Turbulence Modelling and Experiments*, pages 349–359. Elsevier Science Ltd, 1999.

[164] S.B. Pope. A more general effective-viscosity hypothesis. *J. Fluid Mechanics*, 72:331–340, 1975.

[165] C. Prakash and R. Zerkle. Prediction of turbulent flow and heat transfer in a radially rotating square duct. *J. Turbomachinery*, 114:835–846, 1992.

[166] C. Prakash and R. Zerkle. Prediction of turbulent flow and heat transfer in a ribbed rectangular duct with and without rotation. *J. Turbomachinery*, 117:255–264, 1995.

[167] L. Prandtl. Bericht über die ausgebildete turbulenz. *ZAMM*, 5:136–139, 1925.

[168] L. Prandtl. Verhandlung des 2. internationalen kongresses für technische mechanik. Zürich, 1926.

[169] L. Prandtl. Report. NACA TM-625, 1929.

[170] M. Raisee. Heat transfer models in rib roughened passages. Private communication Dept. of Mechanical Engineering, UMIST, 1998.

[171] G. Rau, M. Cakan, D. Moeller, and T. Arts. The effect of periodic ribs on the local aerodynamic and heat transfer performance of a straight cooling channel. *J. Turbomachinery*, 120:368–375, 1998.

[172] P. Rautaheimo and T. Siikonen. Improved solid-wall boundary treatment in low-Reynolds number turbulent models. AIAA Paper 2000-0136, Reno, NV, USA, 2000.

[173] O. Reynolds. On the dynamical theory of incompressible viscous fluids and the determination of the criterion. *Ph. Trans. Royal Soc. London, Series A*, 186:123–, 1895.

[174] W.C. Reynolds, S.C. Kassinos, C.A. Langer, and S.L. Haire. New directions in turbulence modeling. Keynote lecture at 3:rd Int. Symp. on Turbulence, Heat and Mass Transfer, 2000. Also available at http://asbm.stanford.edu.

[175] C.M. Rhie and W.L. Chow. Numerical study of the turbulent flow past an airfoil with trailing edge separation. *AIAA Journal*, 21:1525–1532, 1983.

[176] P.D. Richardson. Heat and mass transfer in turbulent separated flows. *Chemical Eng. Sci*, 18:149–155, 1963.

[177] D.L. Rigby. Prediction of heat and mass transfer in a rotating ribbed coolant passage with a 180 degree turn. Report, NASA/TM-1999-208501, 1999. Also available from ftp://ftp-letrs.lerc.nasa.gov/LeTRS/reports/1999/TM-1999-208501.pdf.

[178] D.L. Rigby, A.A. Ameri, and E. Steinthorsson. Internal passage heat transfer prediction using multiblock grids and a $k-\omega$ turbulence model. Paper ASME-96-GT-188, Int. Gas-Turbine and Aero Congress, Birmingham, 1996.

[179] J.C. Rotta. Statistische theori nichthomogener turbulenz. *Z. Phys.*, 129:547–572, 1951.

[180] A. Saidi and B. Sunden. On prediction of turbulent convective heat transfer in rib-roughened rectangular cooling ducts. In W. Rodi and D. Laurence, editors, *4:th Engineering Turbulence Modelling and Experiments*, pages 763–772. Elsevier Science Ltd, 1999.

[181] V. Scherer and S. Wittig. The influence of the recirculation region: A comparison of the convective heat transfer downstream of a backward-facing step and behind a jet in a crossflow. *J. Eng. for Gas Turbines and Power*, 113:126–134, 1991.

[182] T.-S. Shih, W.W. Liou, A. Shabbir, Z. Yang, and J. Zhu. A new $k - \varepsilon$ eddy viscosity model for high Reynolds number turbulent flows. *Computers Fluids*, 24:227–238, 1995.

[183] T.-S. Shih, J. Zhu, and J.L. Lumley. A new Reynolds stress algebraic equation model. *Computer Methods Appl. Mech. Eng.*, 125:287–302, 1995.

[184] J. Smagorinsky. General circulation experiments with the primitive equations I. the basic experiment. *Monthly Weather Review*, 91:99–165, 1963.

[185] R.M.C. So, Y.G. Lai, H.S. Zhang, and B.C. Hwang. Second-order near-wall turbulence closures: A review. *AIAA Journal*, 29:1819–1835, 1991.

[186] R.M.C. So and T.P. Sommer. A near-wall eddy conductivity model for fluids with different Prandtl numbers. *J. Heat Transfer*, 116:844–854, 1994.

[187] R.M.C So and T.P. Sommer. An explicit algebraic heat-flux model for the temperature field. *Int. J. Heat and Mass Transfer*, 39:455–465, 1996.

[188] H.H. Sogin. A summary of experiments on local heat transfer from the rear of bluff obstacles to a low speed airstream. *Trans AMSE*, 86:200–202, 1964.

[189] T.P. Sommer and R.M.C So. Wall-bounded buoyant turbulent flow and its modeling. *Int. J. Heat and Mass Transfer*, 39:3595–3606, 1996.

[190] T.P. Sommer, R.M.C. So, and Y.G. Lai. A near-wall two-equation model for turbulent heat fluxes. *Int. J. Heat and Mass Transfer*, 35:3375–3387, 1992.

[191] D.B. Spalding. A novel finite difference formulation for differeential expressions involving both the first and second derivates. *J. Numerical Methods Eng.*, 4:551–559, 1972.

[192] C.G. Speziale. On nonlinear $k - l$ and $k - \varepsilon$ models of turbulence. *J. Fluid Mechanics*, 178:459–475, 1987.

[193] C.G. Speziale, S. Sarkar, and T.B. Gatski. Modeling the pressure-strain correlation of turbulence: an invariant dynamical systems approach. *J. Fluid Mechanics*, 227:245–472, 1991.

[194] M.A Stephens and T. I-P. Shih. Computation of compressible flow and heat transfer in a rotating duct with inclined ribs and a $180^o$ bend. In *Int. Gas Turbine & Aeroengine Congress and Exhibition*, 1997.

[195] M.A Stephens and T. I-P. Shih. Flow and heat transfer in a smooth U-bend with and without rotation. *J. of Propulsion and Power*, 15:272–279, 1999.

[196] M.E. Taslim. Aero-thermal performance of internal cooling systems in turbomachines. VKI Lecture Series 2000-03, 2000.

[197] M.E. Taslim, T. Li, and D.M. Kercher. Experimental heat transfer and friction in channels roughened with angled, V-shaped and discrete ribs on two opposite walls. *J. Turbomachinery*, 118:20–28, 1996.

[198] E.R. van Driest. On turbulent flow near a wall. *Aeronautical Sciences*, 23:1007–, 1956.

[199] B. van Leer. Towards the ultimate conservative difference monotonicity and conservation combined in a second-order scheme. *J. Computational Physics*, 14:361–370, 1974.

[200] J.C. Vogel and J.K. Eaton. Combined heat transfer and fluid dynamic measurements downstream of a backward-facing step. *J. Heat Transfer*, 107:922–929, 1985.

[201] J.H. Wagner, B.V. Johnson, and T.J. Hajek. Heat transfer in rotating passages with smooth walls and radial outward flow. *J. Turbomachinery*, 113:42–51, 1991.

[202] J.H. Wagner, B.V. Johnson, and F.C. Kopper. Heat transfer in rotating serpentine passages with smooth walls. *J. Turbomachinery*, 113:321–330, 1991.

[203] S. Wallin and A.V. Johansson. An explicit algebraic Reynolds stress model for incompressible and compressible turbulent flows. *J. Fluid Mechanics*, 403:89–132, 2000.

[204] R.L. Webb, E.R.G. Eckert, and J. Goldstein. Heat transfer and firction in tubes with roughness. *Int. J. Heat and Mass Transfer*, 14:601–617, 1971.

[205] P.M. Wikström and A.V. Johansson. On the modelling of transport equation for the passive scalar dissipation rate. In W. Rodi and D. Laurence, editors, *4:th Engineering Turbulence Modelling and Experiments*, pages 175–184. Elsevier Science Ltd, 1999.

[206] P.M. Wikström, S. Wallin, and A.V. Johansson. Derivation and investigation of a new explicit algebraic model for the passive scalar flux. *Physcis of Fluids*, 12:688–702, 2000.

[207] D.C. Wilcox. Reassessment of the scale-determining equation for advanced turbulence models. *AIAA Journal*, 26:1299–1310, 1988.

[208] D.C. Wilcox. Comparison of two-equation turbulence models for boundary layers with pressure gradient. *AIAA Journal*, 31:1414–1421, 1993.

[209] D.C. Wilcox. *Turbulence Modeling for CFD*. DCW Industries, Inc., 1993.

[210] D.C. Wilcox and T.L. Chambers. Streamline curvature effects on turbulent boundary layers. *AIAA Journal*, 15:574–580, 1977.

[211] M. Wolfshtein. The velocity and temperature distribution in one-dimensional flow with turbulence augmentation and pressure gradient. *Int. J. Heat and Mass Transfer*, 12:301–318, 1969.

[212] C.R. Yap. *Turbulent heat and momentum transfer in recirculation and impinging flows*. PhD thesis, Dept. of Mech. Eng., Faculty of Technology, Univ. of Manchester, 1987.

[213] A. Yoshizawa. Statistical modeling of a transport equation for the kinetic energy dissipation rate. *Physics of Fluids*, 30:628–631, 1987.

[214] A. Yoshizawa. Bridging between eddy-viscosity-type and second-order turbulence models through a two-scale turbulence theory. *Physcial review E*, 48:273–281, 1993.

[215] M.S. Youssef, Y. Nagano, and M. Tagawa. A two-equation heat transfer model for predicting turbulent thermal fields under arbitrary wall thermal conditions. *Int. J. Heat and Mass Transfer*, 35:3095–3104, 1992.

[216] Y.M. Zhang, J-C. Han, J.A. Parsons, and C.P. Lee. Surface heating effects on local heat transfer in a rotating two-pass square channel with $60^o$ angled rib turbulators. *J. Turbomachinery*, 117:272–280, 1995.

# Paper I

# Paper II

# Paper III

# Paper IV

# Paper V

# Paper VI

# Paper VII

# Paper VIII